

3D PRINTED, CELL CARRYING GELMA HYDROGELS
IN CORNEAL STROMA ENGINEERING

A THESIS SUBMITTED TO
THE GRADUATE SCHOOL OF NATURAL AND APPLIED SCIENCES
OF
MIDDLE EAST TECHNICAL UNIVERSITY

BY

CEMİLE BEKTAŞ

IN PARTIAL FULFILLMENT OF THE REQUIREMENTS
FOR
THE DEGREE OF DOCTOR OF PHILOSOPHY
IN
BIOTECHNOLOGY

DECEMBER 2018

Approval of the thesis:

**3D PRINTED, CELL CARRYING GELMA HYDROGELS
IN CORNEAL STROMA ENGINEERING**

submitted by **CEMİLE BEKTAŞ** in partial fulfillment of the requirements for the degree of **Doctor of Philosophy in Biotechnology Department, Middle East Technical University** by,

Prof. Dr. Halil Kalıpçılar
Dean, Graduate School of **Natural and Applied Sciences** _____

Prof. Dr. Can Özen
Head of Department, **Biotechnology** _____

Prof. Dr. Vasıf Hasırcı
Supervisor, **Dept. of Biological Sciences, METU** _____

Prof. Dr. Ayşe Burcu
Co-Supervisor, **Dept. of Eye Diseases,
University of Health Sciences** _____

Examining Committee Members:

Prof. Dr. Aykut Özkul
Dept. of Virology, Ankara University _____

Prof. Dr. Vasıf Hasırcı
Dept. of Biological Sciences, METU _____

Prof. Dr. Ayşe Elif Erson Bensean
Dept. of Biological Sciences, METU _____

Prof. Dr. Sreeparna Banerjee
Dept. of Biological Sciences, METU _____

Assoc. Prof. Dr. Halime Kenar
Arslanbey Vocational School, Kocaeli University _____

Date: 06.12.2018

I hereby declare that all information in this document has been obtained and presented in accordance with academic rules and ethical conduct. I also declare that, as required by these rules and conduct, I have fully cited and referenced all material and results that are not original to this work.

Name, Last name : Cemile Bektaş

Signature :

ABSTRACT

3D PRINTED, CELL CARRYING GELMA HYDROGELS IN CORNEAL STROMA ENGINEERING

Bektaş, Cemile
Ph.D., Department of Biotechnology
Supervisor: Prof. Dr. Vasıf Hasırcı
Co-Supervisor: Prof. Dr. Ayşe Burcu

December 2018, 150 pages

Tissue engineering is an emerging field which aims to replace missing or damaged tissues and restore their functions. Three dimensional (3D) printing has recently been in the heart of tissue engineering which enables design and production cell loaded or cell carrying scaffolds with shapes, sizes, and porosities specific for the patients.

Corneal damages and diseases are the third major cause for blindness after cataract and glaucoma. Transplantation and keratoprotheses are the only acceptable treatments for severe corneal damages despite their limitations.

In the current study a 3D bioprinted stromal equivalent was designed to mimic the ultrastructure of the native tissue. The construct was produced by bioprinting a keratocyte loaded GelMA solution, using a model created by Sketchup program resulting in a stable, highly transparent, cell loaded hydrogels to serve as a corneal stroma.

In order to carry on physical characterization and study the *in vitro* and *in vivo* performance of the constructs “slab” equivalents of the 3D printed constructs were used.

GelMA slabs prepared from solutions with different concentrations (5, 8, 10 and 15%, w/v in PBS) showed that water content of the hydrogels decreased with increasing concentration and UV duration. Stability of the hydrogels studied by incubation in PBS and collagenase type II was also enhanced with increased hydrogel concentration. Transparency of the hydrogels was over 90% at 700 nm and comparable with the native cornea. Transparency of the constructs did not change during enzymatic degradation tests.

Human keratocytes in the native stroma are elongated and interact with each other. Optimum concentration of the cells in the hydrogels was 1×10^6 cells/mL enabled interactions between the cells. Live-Dead cell viability assay showed that over 90% of the cells were alive and homogeneously distributed in the hydrogels. Alamar Blue cell proliferation assay showed continuous cell proliferation, Draq5 Phalloidin stained cells illustrated network like structures, and immunofluorescence studies showed synthesis of representative collagens (Collagen types I and V) and proteoglycans (decorin and biglycan) of the cells in the hydrogels.

HEMA, another hydrogel forming polymer widely used as a biomaterial in contact lenses, was incorporated into the GelMA structure to enhance the mechanical properties of the constructs. Compressive modulus of the constructs significantly increased in the presence of HEMA but number of cells loaded in the hydrogels decreased. Collagen types I and V synthesis by the cells in GelMA-HEMA hydrogels were also lower than in GelMA hydrogels. Pure GelMA hydrogels, therefore, were used in 3D bioprinting and *in vivo* studies.

In order to have pattern reproducibility in 3D printing, the printing conditions were optimized by changing movement speed of the nozzle in x-y direction (Fxy, mm/min) and the spindle speed (R/S, Dots/min). 3D printed hydrogels were very stable in PBS during three weeks of incubation (92% remained). Live-Dead cell viability assay showed 98% cell viability on Day 21 indicating that printing conditions did not harm the cells. Mechanical properties of the cell loaded 3D printed hydrogel increased significantly during three weeks of incubation. Transparency of cell loaded and cell free hydrogels was studied for three weeks and

was over 80% (at 700 nm) at all time points which is comparable to that of the native cornea (90% at 700 nm). The *in situ* and *in vitro* performances of the three selected 3D printed hydrogels were similar.

In vivo performance of the GelMA15-Slab (Cell free) hydrogel was tested on rabbits. It was implanted into a mid-stromal pocket without suture fixation and observed for 8 weeks under slit lamp. No edema, ulcer formation, inflammation or infection was detected in both control (sham) and hydrogel implanted corneas. Slight vascularization on week 3 was treated with one dose of anti-VEGF application. Hematoxylin and Eosin staining showed that the hydrogel was integrated with the host tissue and there was only a minimal foreign body reaction. Moreover, results demonstrated some degradation of the construct in 8 weeks as evidenced by the decrease of its diameter from 4 mm to 2.6 mm.

Thus, the 3D printed cell loaded GelMA hydrogels could mimic the native ultrastructure of the corneal stroma with excellent transparency, adequate mechanical strength, high cell viability and proliferation. *In vivo* studies with cell-free slabs further demonstrated that the hydrogels could be used in corneal tissue engineering applications.

Keywords: Corneal Stroma, Tissue Engineering, 3D Bioprinting, GelMA, HEMA.

ÖZ

3B BASILI HÜCRE TAŞIYAN GELMA HİDROJELLERİ İLE KORNEA STROMA MÜHENDİSLİĞİ

Bektaş, Cemile
Doktora, Biyoteknoloji Bölümü
Tez Yöneticisi: Prof. Dr. Vasıf Hasırcı
Ortak Tez Yöneticisi: Prof. Dr. Ayşe Burcu

Aralık 2018, 150 sayfa

Doku mühendisliği olmayan veya zarar görmüş organları değiştirerek fonksiyonlarını eski haline getirmeyi amaçlayan gelişmekte olan bir alandır. Üç boyutlu basım (3B) hastaya özel kontrol edilebilir boyutta, şekilde, ve gözeneklilikte hücre taşıyan iskelelerin üretimine olanak sağlayan son zamanlarda doku mühendisliği alanında çok yaygın kullanılmaya başlayan bir yöntemdir.

Kornea'da meydana gelen hasarlar ve hastalıklar katarakt ve glokomdan sonra en yaygın üçüncü körlük sebebidir. Günümüzde transplantasyon ve yapay kornea (keratoprotez) kısıtlamalara karşın tek kabul edilen tedavi yöntemleridir.

Bu çalışmada doğal korneanın mikro yapısını taklit eden 3B biyobasım yöntemiyle basılan kornea stroma eşlenikleri tasarlanmıştır. Sketchup programı ile oluşturulan modele göre keratosit yüklenmiş GelMA çözeltisinden 3B basılmış hidrojel oluşturulmuştur. Elde edilen kornea stroma eşleniği görevi görece hücre taşıyan yapılar oldukça yüksek ışık geçirgenliğine sahip ve dayanıklıdır.

Hidrojellerin karakterizasyonu ve *in vitro* ve *in vivo* performanslarının test edilmesi için 3B basılmış hidrojellerin eşleniği olarak “slab (desensiz plaklar)” hidrojeller kullanılmıştır.

Farklı konsantrasyonlarda (%5, 8, 10, ve 15 w/v, PBS içinde) hazırlanan GelMA hidrojel slablarının su içerikleri artan GelMA konsantrasyonu ve UV süresi ile azalmıştır. Hidrojellerin dayanıklılığı fosfat tampon çözeltisi (PBS) ve kollajenaz tip II enzimi içerisinde bekletilerek test edilmiş ve artan GelMA konsantrasyonunun sağlamlığı da arttırdığı görülmüştür. Hidrojellerin ışık geçirgenliği 700 nm’de %90’ın üzerindedir ve değerler doğal korneanın ışık geçirgenliği ile örtüşmektedir. Hidrojellerin ışık geçirgenlikleri enzimatik bozunma sırasında da değişmemiştir.

İnsan keratosit hücreleri doğal kornea içinde uzamış ve birbirleriyle etkileşim içerisinde bulunurlar. Bu çalışmada hücrelerin hidrojel içinde birbirleri ile etkileşimlerini sağlayan en uygun konsantrasyon 1×10^6 hücre/mL olarak belirlenmiştir. Canlı-Ölü hücre canlılığı testi hidrojel içerisindeki hücrelerin %90’ından fazlasının canlı olduğunu ve hidrojel içinde homojen olarak dağıldığını göstermiştir. Alamar Mavisi hücre çoğalmasında hücre sayılarının sürekli olarak arttığı gözlenmiş, Draq5-Falloidin (çekirdek ve sitoplazma boyaları) boyamaları hücrelerin ağ benzeri yapılar oluşturduğunu göstermiş ve immün boyamalar hidrojel içindeki hücrelerin kornea hücrelerine özel kollajenleri (Kollajen tip I ve V) ve proteoglikanları (decorin ve biglikan) sentezlendiğini göstermiştir.

HEMA, diğer bir hidrojel oluşturan polimer, kontak lenslerin yapımında sıkça kullanılan bir biyomalzemedir ve bu çalışmada hidrojellerin mekanik sağlamlıklarını arttırmak amacıyla GelMA’nın yapısına katılmıştır. Hidrojellerin basma modülü HEMA varlığında önemli ölçüde artmış fakat hidrojel içindeki hücre sayısı düşmüştür. HEMA içeren hidrojellerin kollajen tip I ve V sentezlerinin de GelMA hidrojellerine kıyasla düşük olduğu görülmüştür. Bu sebeple, 3B biyobasım ve *in vivo* çalışmalar için sadece GelMA içeren hidrojeller kullanılmıştır.

3B basımda desenlerin düzgün bir şekilde elde edilebilmesi için basım koşulları iğnenin x-y yönündeki hızı (F_{xy} , mm/min) ve enjeksiyon hızı (R/S, Dots/min)

değiştirilerek optimize edilmiştir. 3B basılan hidrojeller PBS içinde üç hafta inkübe edilmiş ve oldukça sağlam oldukları görülmüştür (21 gün sonunda %92'si kalmıştır). Canlı-Ölü hücre canlılığı testine göre 21. günde 3B basılan hidrojellerin içindeki hücrelerin %98'inin canlı olduğu görülmüş ve basım koşullarının hücrelere zarar vermediği sonucuna ulaşılmıştır. Hücre taşıyan 3B basılan hidrojellerin basma modülleri üç hafta içinde önemli ölçüde artmıştır. Hücre taşıyan ve hücreless 3B basılan hidrojellerin ışık geçirgenlikleri 3 hafta boyunca incelenmiş ve 700 nm'de %80'in üzerinde olduğu görülmüştür. Bu değer doğal korneanın ışık geçirgenliği (700 nm'de %90) ile karşılaştırılabilecek düzeydedir. Optimizasyon sırasında seçilen üç 3B basılı hidrojelin *in situ* ve *in vitro* performansları benzerdir.

GelMA15-Slab (hücreless) hidrojel *in vivo*'da tavşanda denenmiştir. Hidrojel stromanın ortasına açılan cebe yerleştirilmiş ve 8 hafta boyunca slit lambası altında gözlenmiştir. Kontrol (sham) ve hidrojel yerleştirilen kornealarda herhangi bir ödem, ülser oluşumu, enfeksiyon ya da inflamasyon gözlenmemiştir. Üçüncü haftada meydana gelen hafif damarlaşma tek doz anti-VEGF uygulaması ile önlenmiştir. Hematoksilen-eozin boyaması hidrojelin ana doku ile birleştiğini göstermiş ve yalnızca minimal bir yabancı cisim reaksiyonu gözlenmiştir. Ayrıca implant edilen hidrojelin çapının 8 haftada 4 mm'den 2.6 mm'e düşmesi hidrojelin bozunduğunu da göstermektedir.

Elde edilen sonuçlara göre, 3B basılı hücre taşıyan GelMA hidrojelleri oldukça yüksek ışık geçirgenliği, yeterli mekanik özellikleri, iyi düzeyde hücre canlılığı ve çoğalması sağlamasıyla doğal korneanın mikro yapısını taklit edebilir. Ayrıca hücreless slabla yapılan *in vivo* çalışma da hidrojellerin kornea doku mühendisliği uygulamalarında kullanılabileceğini göstermektedir.

Anahtar Kelimeler: Korneal Stroma, Doku Mühendisliği, 3B Basım, GelMA, HEMA.

Dedicated to my beloved family, Özgür and Deniz..

ACKNOWLEDGMENTS

I would like to express my special endless thanks, gratitude and respect to my thesis advisor, Prof. Dr. Vasif Hasırcı who has been supervising me for almost 10 years including my undergraduate and graduate education. I am very grateful for his support, motivation and encouragement during all the stages of my research. I feel obviously very lucky to have had opportunity to do my thesis under his guidance.

I would like to thank to my co-supervisor, Prof. Dr. Ayşe Burcu, for her valuable contribution to this work through *in vivo* studies and by kindly giving me a chance to join all the stages of implantation and observations. I would also like to thank Prof. Dr. Gökhan Gedikoğlu, Dr. Hande H. Telek, and Dr. Firdevs Örnek for their advices and time and efforts they had spent during *in vivo* studies.

I would like to express my special thanks to Prof. Dr. A. Elif Erson Bensen and Prof. Dr. Aykut Özkul, my thesis monitoring committee members, for their advices, discussions and contributions to this study, and for their effort and time they had spent throughout this work.

I am also grateful to Prof. Dr. Nesrin Hasırcı for her advices, comments and patience especially during 1002 project. She has always been a role model for all of us in this long journey. I have learned much from her but the most important one was never giving up.

I am deeply thankful to my beloved husband, my partner in life, my best friend, the best gift of my life Özgür Bektaş for his endless love, patience, support, and understanding. I would also like to thank to my little baby girl, Deniz Bektaş, to whom I do not know how to write and express my deepest love. Without them this work would not have any meaning.

I am indebted to my family Arzı Kılıç, Ali İhsan Kılıç, my little sister Eylül Kılıç, Ahmet Kılıç and his family for their endless support, love and understanding. I am

very thankful to my big family in Ankara Elif Bektaş, Veysel Bektaş, Nuri Bektaş and his family, Seyfi and Çetinkaya families for their friendship, love and great moments we have shared with.

I am also deeply grateful to my lovely friends especially Emine Kurt Ulutaş, Sadiye Mehmetođlu, Fatma Demir Kanarya, Derya Özhava and my cousin Tuğçe Çelik for their presence in my life.

I am very thankful to my lab mates for their friendship and support during this long term journey. I present my thanks especially to my roommates Gökhan Bahçeciođlu, Ezgi Antmen and Menekşe Ermiş Şen for their comments, support and friendship. I would like to thank to all members of BIOMATEN especially Gözde Eke, Aylin Kömez, Senem Büyüksungur, Arda Büyüksungur, Funda Can, M. Ayça Tuncel, Dilara Tamay A. Selcen Alagöz, and Tuğba Dursun. I would also like to thank to Deniz Atilla for her help in the mechanical testing. I present my thanks to Zeynel Akın, Yüksel Güneş and Ramazan Kavak for their help and patience throughout these years.

I would like to acknowledge to TÜBİTAK for their support through BİDEB 2211-E and 2211-C Scholarships.

TABLE OF CONTENTS

ABSTRACT.....	v
ÖZ	ix
ACKNOWLEDGMENTS	xiii
TABLE OF CONTENTS.....	xv
LIST OF TABLES	xxi
LIST OF FIGURES	xxiii
LIST OF ABBREVIATIONS	xxvii
1 INTRODUCTION	1
1.1 Cornea and Its Structure.....	2
1.1.1 Function of the Stroma.....	4
1.2 Corneal Diseases	6
1.3 Current Treatment Approaches and Their Limitations	8
1.3.1 Tissue Engineering.....	13
1.3.1.1 Corneal Tissue Engineering.....	13
1.3.1.1.1 Cell Sources.....	13
1.3.1.1.2 The Scaffold Materials	15
1.3.1.1.2.1 Natural Materials.....	15
1.3.1.1.2.2 Synthetic Materials.....	18
1.3.1.1.3 Scaffolds.....	18
1.3.1.1.3.1 3D Printing	20

1.3.1.1.3.1.1	Hydrogels	21
1.3.1.1.3.1.2	3D Bioprinting.....	22
1.3.1.1.3.1.2.1	Laser based systems	23
1.3.1.1.3.1.2.2	Inkjet Based Systems	23
1.3.1.1.3.1.2.3	Extrusion Based Systems	24
1.4	Novelty of the Study	25
2	MATERIALS AND METHODS.....	27
2.1	Materials	27
2.2	Methods.....	28
2.2.1	Synthesis of Methacrylated Gelatin	28
2.2.2	¹ H Nucleic Magnetic Resonance (¹ H-NMR) of GelMA.....	28
2.2.3	Preparation of GelMA Hydrogel Slabs.....	28
2.2.4	Preparation of GelMA-HEMA Hydrogel Slabs.....	29
2.2.5	Preparation of HEMA Hydrogel Slabs	30
2.2.6	Preparation of 3D Printed GelMA Hydrogels	30
2.2.7	Characterization of the Hydrogels	31
2.2.7.1	Stereomicroscopy	31
2.2.7.2	FTIR-ATR	31
2.2.7.3	Equilibrium Water Content (EWC) of GelMA Hydrogels.....	31
2.2.7.4	In Situ Degradation in PBS	32
2.2.7.5	In Situ Enzymatic Degradation with Collagenase Type II.....	32
2.2.8	<i>In vitro</i> Studies.....	33
2.2.8.1	Human Keratocyte Cell Culture	33
2.2.8.2	Flow Cytometry of Human Keratocytes.....	33
2.2.8.3	Preparation of Cell Loaded Hydrogel Slabs	34

2.2.8.4	Preparation of Cell Loaded HEMA and GelMA-HEMA Hydrogels	34
2.2.8.5	Preparation of Cell Loaded 3D Bioprinted Hydrogels	34
2.2.8.6	Microscopical Studies	35
2.2.8.6.1	Live-Dead Cell Viability/Cytotoxicity Assay	35
2.2.8.6.2	Live Cell Imaging	36
2.2.8.6.3	DRAQ5, DAPI and Phalloidin Staining	37
2.2.8.6.4	Immunofluorescence Staining	37
2.2.8.6.5	Scanning Electron Microscopy (SEM)	38
2.2.8.7	Mechanical Properties of Cell Loaded and Cell Free Hydrogels	38
2.2.8.8	Transparency of the Hydrogels	39
2.2.8.9	MMP Activity of the Cell Loaded Hydrogels	39
2.2.9	In vivo Studies	40
2.2.9.1	Schirmer's Test	42
2.2.9.2	Sodium Fluorescein Staining	42
2.2.9.3	Histological Examination	42
2.2.10	Statistical Analysis	43
3	RESULTS AND DISCUSSION	45
3.1	GelMA Hydrogels	45
3.1.1	¹ HNMR of GelMA	45
3.1.2	Equilibrium Water Content of Hydrogels	47
3.1.3	In Situ Degradation of GelMA Hydrogels	48
3.1.4	Enzymatic Degradation of GelMA Hydrogels	49
3.1.5	In Vitro Studies	51
3.1.5.1	Flow Cytometry of Human Keratocytes	51

3.1.5.2	Optimization of Cell Number in Hydrogels	53
3.1.5.3	Live Cell Imaging	57
3.1.5.4	Cell Proliferation in the Hydrogels with Different Stiffness	59
3.1.5.5	Cell Morphology Analysis with DAPI/Draq5-Phalloidin Staining and SEM	60
3.1.5.6	Immunofluorescence Staining: Extracellular Matrix Synthesis by the Human Keratocytes in the GelMA Hydrogels	62
3.1.5.7	Transparency of the Cell Loaded Hydrogels	64
3.1.5.8	Compressive Mechanical Properties of Hydrogels	66
3.1.5.9	Mechanical Strength Testing of GelMA Hydrogel with Artificial Anterior Chamber	68
3.2	GelMA-HEMA Hydrogels.....	69
3.2.1	Characterization of the GelMA-HEMA Hydrogels.....	69
3.2.2	FTIR-ATR Spectra of GelMA-HEMA Hydrogels	69
3.2.3	Compressive Mechanical Tests.....	70
3.2.4	Equilibrium Water Contents (EWC) of the GelMA-HEMA Hydrogels	71
3.2.5	In Situ Degradation of GelMA-HEMA Hydrogels.....	72
3.2.6	Enzymatic Degradation with Collagenase	72
3.2.6.1	Transparency of Hydrogels during Collagenase Assay	73
3.2.7	In vitro Studies	75
3.2.7.1	Live-Dead Assay and Draq5-Phalloidin Staining of Hydrogels ..	75
3.2.7.2	Cell Proliferation in the Hydrogels.....	78
3.2.7.3	Immunofluorescence Staining: Extracellular Matrix Synthesis by the Human Keratocytes in the GelMA, GelMA-HEMA and HEMA Hydrogels	79
3.2.7.4	Light Transmission of the GelMA-HEMA Hydrogels.....	81

3.3	3D Printed GelMA15 Hydrogels	83
3.3.1	Optimization of Printing Conditions.....	84
3.3.2	Equilibrium Water Content (EWC) of Printed Hydrogels.....	86
3.3.3	<i>In Situ</i> Degradation of Hydrogels	87
3.3.4	<i>In vitro</i> Studies	89
3.3.4.1	Viability of Keratocytes in 3D Printed Hydrogels.....	89
3.3.4.2	Cell Proliferation in 3D Printed Hydrogels	93
3.3.4.3	Mechanical Properties of Cell Loaded Hydrogels under Compression.....	94
3.3.4.4	Immunofluorescence Staining: Extracellular Matrix Synthesis of the Human Keratocytes in the 3D Printed Hydrogels and Hydrogel Slabs ...	95
3.3.4.5	MMP Activity of the Keratocytes Loaded into 3D Printed Hydrogels and Hydrogel Slabs	98
3.3.4.6	Transparency of Cell Loaded, 3D Printed Hydrogels.....	100
3.4	<i>In Vivo</i> Studies	103
3.4.1	Implantation and Examination in Rabbits.....	103
3.4.2	Histological Examination of the Constructs	109
	CONCLUSION.....	113
	REFERENCES	115
	APPENDIX A	135
	APPENDIX B	137
	APPENDIX C	139
	APPENDIX D	141
	APPENDIX E	143
	CURRICULUM VITAE.....	145

LIST OF TABLES

Table 2.1: Dimensions of the PDMS Discs for different applications.....	29
Tabel 2. 2: 3D bioprinting parameters chosen after optimization studies.....	31
Table 2.3: Sum of the abbreviations, operation type, GelMA dimensions, and observation period.....	42
Table 3.1: Compressive modulus and EWC of the hydrogels.	72
Table 3.2: Transmittance (%) of GelMA and GelMA-HEMA (8:2) at 300 and 700 nm, after incubation in PBS and 4 different collagenase concentrations.....	75
Table 3.3: Printability of the GelMA hydrogels as a function of movement speed of the nozzle in x-y direction (F _{xy} , mm/min) and spindle speed (R/S, Dots/min)..	86
Table 3.4: Equilibrium Water Content (EWC) of the hydrogels.	87
Table 3.5: Transmittance (%) of cell loaded (w cells) and cell free (w/o cells) 3D printed and hydrogels slabs at 300 and 700 nm during 21 days of incubation.....	102

LIST OF FIGURES

Figure 1.1: The eye and cross section of the cornea.	2
Figure 1.2: Figures showing orientation of lamellae in the structure of the cornea.....	6
Figure 1.3: Types of keratoplasties	10
Figure 1.4: Boston Type I and Osteo-odonto Keratoprosthesis (OOKP)	12
Figure 1.5: Corneal tissue section showing the transition zone between sclera and cornea, named as limbus.	14
Figure 1.6: 3D Bioprinting methods.	24
Figure 2.1: Schematic representation of preparation of human keratocytes (HK) loaded hydrogels	35
Figure 2.2: Live cell imaging setup.....	37
Figure 2.3: Labeling protocol of the rabbits used in pre-clinical studies.....	41
Figure 2.4: Workflow for <i>in vivo</i> studies.	43
Figure 3.1: ¹ H-NMR spectra of gelatin and gelatin methacrylamide prepared (in D ₂ O, RT.	46
Figure 3.2: Effect of uncrosslinked GelMA concentration and UV exposure duration on the water content of the GelMA hydrogels.	47
Figure 3.3: Degradation of GelMA hydrogels for up to three weeks in PBS (pH 7.4, 10 mM) at 37°C.....	49
Figure 3.4: Enzymatic degradation and resultant changes in the appearance and transparency of the GelMA hydrogels	51
Figure 3.5: Histograms of unstained samples, isotype controls, negative markers (CD34 and CD45, hematopoietic stem/progenitor cell and lymphocyte cell markers, respectively), and positive markers (CD73 and CD90, mesenchymal stem cell markers) after flow cytometry analysis.....	52
Figure 3.6: CSLM images of Live-Dead assay of keratocytes in GelMA hydrogel on Day 1 and Day 7.....	54

Figure 3.7: CLSM images showing results of Live Dead Cell Viability Assay of GelMA hydrogels on Days 1 and 2.....	55
Figure 3.8: CLSM images showing results of Live Dead Cell Viability Assay of GelMA hydrogels on Days 7 and 21.....	56
Figure 3.9: CLSM images showing results of Live Dead Cell Viability Assay of GelMA10 hydrogels on Day 1 and 21	57
Figure 3.10: Live cell imaging of the HK in GelMA hydrogels on Days 3 and 14...	58
Figure 3.11: Proliferation (as indicated by Reduction % obtained with Alamar Blue test) of human keratocytes in GelMA10 and GelMA15 hydrogels over 3 weeks	59
Figure 3.12: Fluorescence micrographs of DAPI (nucleus, blue) –Phalloidin (cytoskeleton, green) stained human keratocytes	60
Figure 3.13: CLSM and SEM micrographs of keratocyte seeded GelMA hydrogels after 21 days of culture.	61
Figure 3.14: Immunocytochemistry of GelMA hydrogels	63
Figure 3.15: Transparency of hydrogels	65
Figure 3.16: Change of compressive moduli change of cell loaded GelMA10 and GelMA15 hydrogels over 3 weeks	67
Figure 3.17: Scheme of artificial anterior chamber.	68
Figure 3.18: FTIR-ATR spectra of GelMA, HEMA and GelMA-HEMA hydrogels.	70
Figure 3.19: Stability of GelMA and GelMA-HEMA hydrogels	73
Figure 3.20 Transparency of GelMA and GelMA-HEMA hydrogels.....	74
Figure 3.22: SEM images of cell loaded hydrogels. Arrow heads point to cells on day 21	77
Figure 3.21: Live-Dead Assay and Draq5-Phalloidin staining of hydrogels on Day 3, studied by CSLM	77
Figure 3.23: Proliferation (as indicated by Reduction %) of human keratocytes in GelMA, GelMA-HEMA and HEMA hydrogels over 3 weeks.....	78
Figure 3.24: Immunocytochemistry of GelMA-15, GelMA-HEMA and HEMA hydrogels.....	80

Figure 3.25: Change of transparency of the hydrogels with and without keratocytes in the hydrogel bulk in 21 days	82
Figure 3.26: Stereomicrographs of 3D printed GelMA hydrogels.	84
Figure 3.27: Stereomicrographs of 3D printed GelMA hydrogels	85
Figure 3.28: <i>In situ</i> stability test of 3D printed hydrogels (in PBS, pH 7.4, 10 mM) for 1 week)	88
Figure 3.29: CLSM images showing results of Live Dead Cell Viability Assay of 3D printed GelMA hydrogels on Day 21	91
Figure 3.30: CLSM images showing results of Live Dead Cell Viability Assay of 3D printed GelMA hydrogels on Day 21	92
Figure 3.31: Proliferation of human keratocytes in 3D Printed and GelMA15-Slab hydrogels over 3 weeks.	93
Figure 3.32: Compressive moduli change of cell loaded 3D Printed, unloaded 3D printed, cell loaded GelMA15-Slab and unloaded GelMA15-Slab hydrogels over 3 weeks.....	95
Figure 3.33: Immunocytochemistry of 3D printed hydrogels and hydrogel slabs.....	97
Figure 3.34: MMPs activity of the keratocytes in the 3D printed hydrogels and hydrogel slabs during 21 days of culture	99
Figure 3.35: Transparency of the 3D printed hydrogels	101
Figure 3.36: Implantation of GelMA15-Slab hydrogel in one eye of a New Zealand white rabbit.....	104
Figure 3.37: Examination of control and test eye on Day 7 with Schirmer’s test and sodium fluorescein staining.....	105
Figure 3.38: Examination of control eye.....	105
Figure 3.39: Implantation of GelMA15-Slab hydrogel on one eye of one rabbit....	106
Figure 3.40: Operation of left cornea of the rabbit to serve as Sham control	107
Figure 3.41: Examination of control and test eye on Day 7 with Schirmer’s test and sodium fluorescein staining.....	107
Figure 3.42: Corneas removed at the end of the test period.....	109
Figure 3.43: Hematoxlin and Eosin (H&E) staining of sections of the rabbit cornea after implantation	111

Figure A.1: A typical stress strain curve for viscoelastic materials.....	135
Figure A.2: Alamar Blue Assay calibration curve for human corneal keratocytes .	137
Figure A.3: 5-FAM-Pro-Leu-OH Calibration Curve for MMP Activity.....	139
Figure A.4: Coomassie Plus (Bradford) Assay calibration curve for total protein determination.	141
Figure A.5: Ethical permission was granted by Ankara Education and Research Hospital, Animal Experiments Local Ethics Committee.	143

LIST OF ABBREVIATIONS

µm	micrometer
2D	Two Dimensional
3D	Three Dimensional
Ab	Antibody
ADSC	Adipose Derived Stem Cells
ALK	Anterior Lamellar Keratoplasty
ANOVA	Two-way Analysis of Variance
APS	Ammonium Persulfate
BSA	Bovine Serum Albumin
CAD	Computer Aided Design
CLSM	Confocal Laser Scanning Microscopy
CO ₂	Carbon Dioxide
CT	Computer Tomography
D	Diameter
DAPI	4', 6-diamidino-2-phenylindole
DALK	Deep Anterior Lamellar Keratoplasty
DMEM–HAM's F12	Dulbecco's Modified Eagle Medium–Ham's nutrient mixture F12
DMSO	Dimethyl Sulfoxide
ECM	Extracellular Matrix
EGDMA	Ethyleneglycol Dimethacrylate
EK	Endothelial Keratoplasty
EWC	Equilibrium Water Content
FDM	Fused Deposition Modeling
FITC	Fluorescein Isothiocyanate

g	gram
GelMA	Methacrylated Gelatin
h	hour
HIV	Human Immunodeficiency Virus
HK	Human Corneal Keratocytes
¹ H-NMR	¹ H Nucleic Magnetic Resonance
IP	Inkjet Printing
Irgacure 2959	2-(Hydroxyl)-4-(2-hydroxyethoxy)-2-methylpropiophenone
kPa	Kilo Pascal
KPro	Keratoprotheses
LAB	Laser-assisted Bioprinting
M	Molarity
MA	Methacrylic Anhydride
mg	milligram
min	minute
mL	milliliter
mm	millimeter
MMP	Matrix Metalloproteinase
Mpa	Mega Pascal
MRI	Magnetic Resonance Imaging
MSCs	Mesenchymal Stem Cells
OCT	Optimal Cutting Temperature Compound
OOKP	Osteo-odonto Keratoprosthesis
P	Passage
PBS	Phosphate Buffered Saline
PDMS	Poly(dimethylsiloxane)
Pen/Strep	Penicillin/Streptomycin
PGA	Polyglycolic acid
PGMA	Poly(glycerol monomethacrylate)
PHB	Poly(3-hydroxybutyric acid)

PHBV	poly(3-hydroxyvaleric acid)
pHEMA	Poly(2-hydroxyethyl methacrylate)
PLGA	Poly(lactic acid-co-glycolic acid)
PMMA	Poly(methyl methacrylate)
PVA	Poly(vinyl alcohol)
RGD	arginine-glycine-aspartic acid
RT	Room Temperature
SEM	Scanning Electron Microscopy
SLA	Stereolithography
SLS	Selective Laser Sintering
TCPs	Tissue Culture Polystyrene
TEMED	<i>N,N,N',N'</i> -tetramethylethylenediamine
UV	Ultraviolet
VEGF	Vascular Endothelial Growth Factor
w	weight
WHO	World Health Organization
w/v	Weight/volume
W _d	Dry Weight
W _w	Wet Weight

CHAPTER 1

INTRODUCTION

Cornea, the outermost surface of the eye, transmits the outside world information although it only accounts for the 0.1% of the body. Under normal conditions the integrity and the transparency of the cornea is maintained but due to its position on the eye it is highly vulnerable to the infections and trauma (Chirila *et al.*, 1998). Today, corneal damages are the second major cause of the blindness worldwide after cataract. Transplantation is the most common treatment but the number of the available donor corneas and also the quality of them falls far behind the demand (Connon, 2015). Keratoprotheses (KPro) is currently the only acceptable treatment if there is a high rejection risk or there is a graft failure history after transplantation. However, development of glaucoma, increased intraocular pressure and lamina degradation are several problems associated with the use of KPros (Viitala *et al.*, 2009; Laattala *et al.*, 2011; Ghezzi, Rnjak-Kovacina and Kaplan, 2015).

Tissue engineering is highly promising and aims to replace and/or regenerate the damaged tissues and organs in order to restore their functions. The concept includes isolation of cells from the patient himself, expand in cell culture, seed on a scaffold (a cell carrier) and graft back to the patient (Yang *et al.*, 2001). Up to date various synthetic and/or natural biomaterials were used to construct scaffolds for corneal tissue engineering in a wide range of forms like meshes, films, foams, fibers, and cell sheets. Although some of the scaffolds mimicked well the ultrastructure of the cornea, only a few could pass to Phase I clinical stages (Fagerholm *et al.*, 2010), and at present there is no available artificial corneal construct available for routine use. Transplantation of allografts, therefore, still remains the major and long term treatment for corneal damages despite its drawbacks. All these urge the need for an

alternative and efficient treatment method to meet the demand and overcome the limitations of current methods.

Moreover, a viable corneal construct that mimics the native tissue is also needed in the field of pharmaceuticals and cosmetic products to decrease animal testing (eye irritation or toxicity) (Ghezzi, Rnjak-Kovacina and Kaplan, 2015).

1.1 Cornea and Its Structure

Cornea is the outermost, transparent tissue that covers iris, lens and anterior chamber of the eye (Figure 1.1A). Diameter of the cornea is about 11-12 mm horizontally and 9-11 mm vertically. The center of the adult cornea is 520 μm in thickness and increases to 650 μm near the limbus (Ruberti and Zieske, 2008; Jacob and Naveen, 2016). Cornea is avascular and has immune privilege that makes it unique. Two main functions of the cornea are to act as a barrier against external objects and UV radiation, and to serve as the principal optical element; refracts about 65-75% of the light passing through the eye. Tear is the main nutrition source of the cornea due to its mucin, lipid and aqueous nature. With the aid of blinking process, a tear film is formed on the surface of the eye by keeping the cornea clean and moist (Ludwig and Dulebohn, 2017). Oxygen is supplied by the tear film and perilimbal capillaries

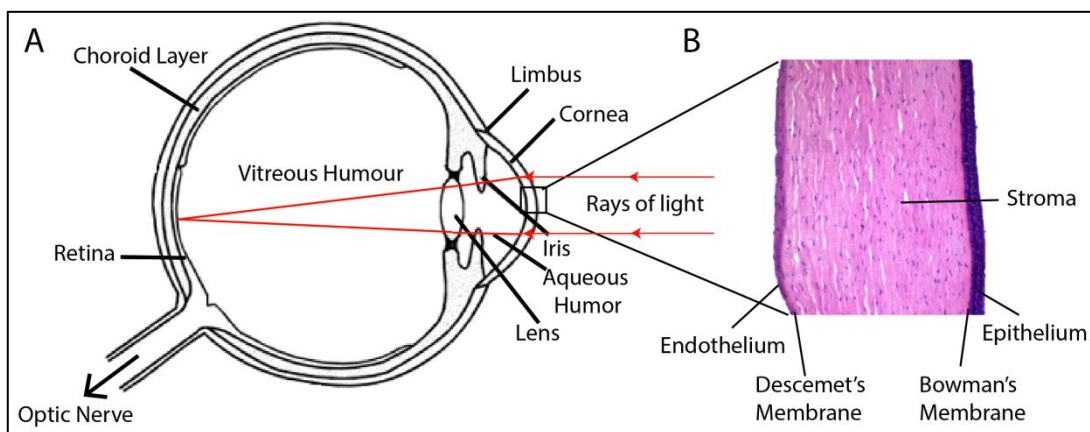


Figure 1.1: The eye and cross section of the cornea. A) The eye, and B) Hematoxylin Eosin (H&E) staining is showing five layers of the cornea; epithelium, Bowman's membrane, stroma, Descemet's membrane and endothelium from exterior to interior. Red lines shows the incoming light and refraction power of the cornea.

while glucose is obtained from aqueous humor (Jacob and Naveen, 2016). Five distinct layers make up the microstructure of the cornea; epithelium, acellular Bowman's membrane, the stroma, acellular Descemet's membrane and endothelium (Figure 1.1B).

Nonkeratinized, squamous and stratified epithelial cells form the 50 μm thick (in humans) epithelium layer. Tight junctions between the cells protect the cornea from external objects and pathogens. However, it is permeable to compounds like sodium, glucose, O_2 , and CO_2 needed by eye. Epithelium also has a significant role in refraction. Epithelial cells forming this layer are in a continuous movement due to regular apoptosis and desquamation where the lifetime is around 7-10 days. These cells are renewed by the stem cells coming from the limbus (Eghrari, Riazuddin and Gottsch, 2015; Ludwig and Dulebohn, 2017).

Beneath the epithelium layer, a thin (about 8-12 μm), transparent, and acellular Bowman's membrane is located which is made up of collagen (Jacobsen et al. 1984; Eghrari et al. 2015). Although it may have a protection role of the sub-epithelial nerve plexus, its absence is not associated to vision loss or significant change in the overall structure of the cornea (Eghrari, Riazuddin and Gottsch, 2015).

The stroma is the thickest part of the cornea; 90% of its thickness. Collagen is the main structural protein of the stroma (70% of its dry weight) and the rest is water, glycoproteins, proteoglycans, and inorganic salts. These molecules contribute to the typical spherical shape of the cornea which is essential for suitable light transmission and scattering (Eghrari, Riazuddin and Gottsch, 2015; Ludwig and Dulebohn, 2017). Aligned nature of the collagen fibrils is vital for both transparency and mechanical properties of the cornea (Torbet *et al.*, 2007). Mesenchyme-derived fibroblasts, keratocytes, are sparsely distributed in the stroma and form an interconnected cellular network (West-Mays and Dwivedi, 2006).

Collagen types IV and VIII, and proteoglycans form the thin acellular Descemet's membrane (10 μm in thick). This membrane supports the endothelial layer and helps

maintain corneal hydration together with corneal endothelium which is essential for clarity (Eghrari, Riazuddin and Gottsch, 2015; Meek and Knupp, 2015).

A single layer of flat and polygonal cells with 5 μm in thickness and 20 μm in diameter form the innermost endothelial layer of the cornea (Eghrari, Riazuddin and Gottsch, 2015). Endothelium acts as a leaky barrier between the aqueous humor and stroma and allows the transfer of nutrients, metabolites and water. Cornea is maintained in hydrated state with the aid of tight junctions between the endothelial cells and pumping mechanism of this layer through Na^+/K^+ -ATPase and bicarbonate dependent Mg^{2+} -ATPase (Waring *et al.*, 1982; Bourne and McLaren, 2004). Aqueous fluid income is seen due to endothelial failure which results in corneal edema. Unlike the epithelial cells, in the case of a damage and cell death endothelial cells do not go into mitosis but are substituted by the migration of the adjacent cells to maintain barrier and pump functions (Eghrari, Riazuddin and Gottsch, 2015).

Structure and function of the stroma is explained in detail in the following section.

1.1.1 Function of the Stroma

As was stated in Section 1.1 the stroma is about 500 μm in thickness, sparsely populated by corneal keratocytes (3-10% by volume) and consists mainly of collagen (70% of its dry weight). Central cornea is composed of about 200-400 lamellae where collagen fibrils are aligned parallel to each other within the lamella but nearly at right angles to adjacent lamellae similar to plywood (Fullwood, 2004) (Figure 1.2 A and C).

Small diameter hybrids of collagen types I and V fibrils (ranging from 25 to 33 nm) (Figure 1.2 B) form the lamellae together with significant amounts of other collagens like XII, XIV and VI (Meek and Fullwood, 2001; Ghezzi, Rnjak-Kovacina and Kaplan, 2015). Glycoproteins and proteoglycans form a hydrated matrix in which the collagen fibrils are embedded. Corneal transparency and hydration is sustained by the small leucine rich proteoglycans including biglycan, decorin, keratocan, and lumican through maintaining the space between the fibers. Any alteration in the

content of the proteoglycans and structure in the collagens may lead to corneal opacity (Funderburgh *et al.*, 1998; Ghezzi, Rnjak-Kovacina and Kaplan, 2015).

The integrity of the stroma layer is maintained by the mesenchyme derived corneal fibroblasts, called as keratocytes through continuous production of collagens, glycosaminoglycans, and matrix metalloproteinases (West-Mays and Dwivedi, 2006; Ruberti, Zieske and Trinkaus-Randall, 2007; Eghrari, Riazuddin and Gottsch, 2015). Scattering of light due to keratocytes is overcome by the water soluble crystallins like aldehyde dehydrogenase, alpha-enolase and transketolase (Hassell and Birk 2010; Eghrari *et al.* 2015) expressed by them. In case of injury, keratocytes are stimulated to undergo apoptosis or to change their quiescent state into repair phenotypes which results in either regeneration or fibrotic scar formation. Regeneration occurs when epithelium layer is swapped where cells close to basement membrane undergo apoptosis and are then replaced by the mitosis of adjacent cells. This harmless response is believed to protect cornea from loss of clarity and inflammation (West-Mays and Dwivedi, 2006). In pathological corneas, however, phenotype of the cells change and stroma accumulates fibrotic deposits which are detrimental for corneal clarity due to decreased expression levels of crystallins (Funderburgh, Mann and Funderburgh, 2003; Muthusubramaniam *et al.*, 2012).

Avascularity of the stroma is essential for its transparency and is achieved by anti-angiogenic factors like soluble vascular endothelial growth factor receptor-1 (sVEGFR-1 or sflt-1) which nullifies angiogenic VEGF (Ambati *et al.*, 2006).

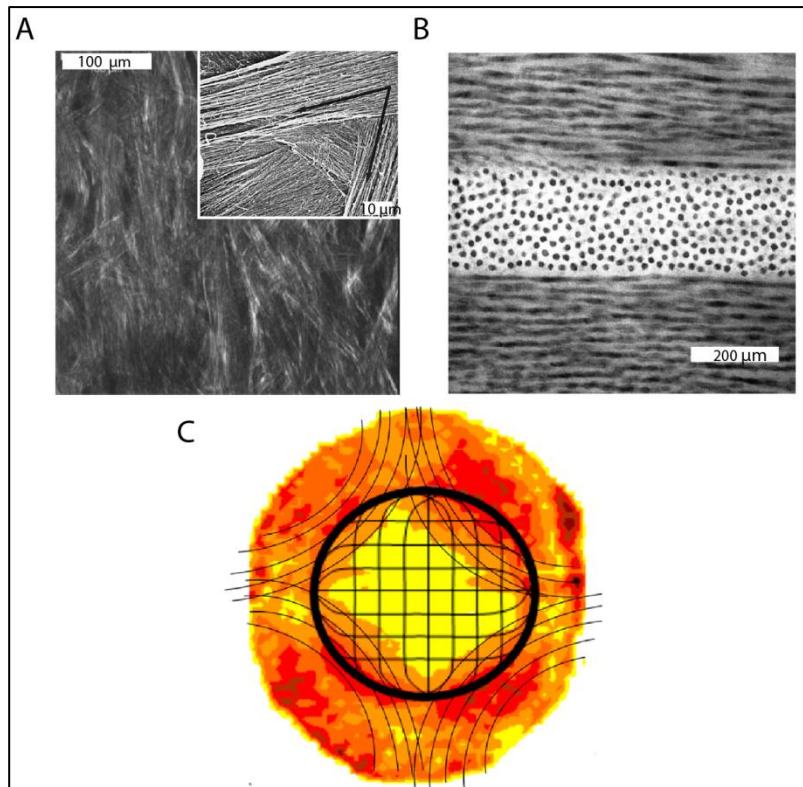


Figure 1.2: Figures showing orientation of lamellae in the structure of the cornea. A) SEM showing the directions of the adjacent lamellae. (Adapted from Meek and Knupp, 2015. Inset is adapted from Meek and Fullwood, 2004). B) TEM showing orientation of collagen fibrils in adjacent lamellae. Regular diameter and spacing of the fibers are clearly seen in the mid-lamellae (fibers directed out of the page). (Adapted from Fullwood, 2004). C) Simplified model based on X-Ray Data showing fibril orientation in the cornea. (Adapted from Meek and Knupp, 2015). Scale bars are: (A) 100 μm and inset is 10 μm, and (B) 200 nm.

1.2 Corneal Diseases

After cataract and glaucoma, corneal diseases and wounds are the third leading cause of blindness affecting millions of people including 10 million patients with bilateral corneal blindness. It is estimated that about 12.7 million people are waiting for corneal transplantation and only 1 in 70 is successful in getting one (Gain *et al.*,

2016). Infections, nutrient deficiency, inflammatory diseases, hereditary diseases, degenerative diseases, and traumas are among the causes of corneal blindness (Burton, 2009). Trachoma, ocular trauma, corneal ulcerations and childhood blindness are the major reasons.

Trachoma is a corneal disease caused by infection with *Chlamydia trachomatis* that leads to corneal opacification and blindness. Once established, treatment is quite difficult and corneal grafts are usually unsuccessful due to the dry and damaged surface of the eye (Burton, 2009). Trachoma is associated poor hygienic conditions because limited access to water increases the risk of infection. Infection is easily transmitted from eye to eye through contaminated fingers, flies, and clothing. Today, trachoma can be treated and the blindness due to trachoma can be prevented through a group of measures called the SAFE (S: Surgery for trichiasis, A: Antibiotic treatment, F: Facial cleanliness, E: Environmental changes and improvements) strategy of the World Health Organization (WHO) otherwise it leads to corneal opacification (Whitcher, Srinivasan and Upadhyay, 2001; Oliva, Gulati and Schottman, 2012).

Ocular trauma is the most important cause for unilateral blindness in the developing countries and makes up 5% of the bilateral blindness cases (Whitcher, Srinivasan and Upadhyay, 2001; Pradhan, 2017). Home and work accidents, sport activities, traffic accidents, burns, and foreign bodies are the common causes where the damage can range from a small epithelial abrasion to ruptured globe. Children are more prone to such injuries and the damage can be much more serious. However, visual loss seen in children due to injuries can be prevented significantly by parental education and supervision (Pradhan, 2017).

Corneal ulceration is another leading cause of corneal blindness and 6 million new people are recorded every year with corneal ulcers in the ten countries of South East Asia (Srinivasan, 2017). Corneal ulcer is diagnosed by clinical examination using a slit-lamp and characterized by a break in epithelium continuity and stromal infiltrate. When the integrity of the epithelium is damaged or there is a problem with lids and tear film, any organism can attack corneal stroma leading to infections. In the

developed countries viruses are the major causes for the infections while bacteria, *Acanthamoebae*, and fungi are the main causes in the developing nations. Drugs administered locally or orally can relieve pain and prevent synechiae formation. Public education of risk factors and early recognition may prevent disease occurrence otherwise cause blindness (Garg and Rao, 1999).

It is estimated that there are about 1.5 million blind children worldwide and half a million new cases are reported every year (Whitcher, Srinivasan and Upadhyay, 2001). The causes vary with the socioeconomic status of the countries. For example optic nerve lesions and damages in complex visual pathways are the major causes in high-income countries while corneal scarring, vitamin A deficiency, use of traditional eye drugs, and ophthalmia neonatorum are the main ones in low-income countries (Gilbert and Foster, 2001). Among them, vitamin A deficiency makes up 70% of the cases leading to xerophthalmia which can be severe enough to cause perforation, bilateral corneal melting and blindness. This disease can be prevented by education of the families about nutrition, distribution of vitamin A capsules, and immunizations (Whitcher, Srinivasan and Upadhyay, 2001).

1.3 Current Treatment Approaches and Their Limitations

Damaged eye due to corneal diseases like trachoma, corneal trauma, ulceration or childhood diseases usually remains blind throughout the life of the person. Surgical procedures after blindness is rarely successful unless high quality equipment, well trained doctors and nurses, and clean operating rooms are supplied (Whitcher, Srinivasan and Upadhyay, 2001). Corneal transplantation (penetrating keratoplasty, and lamellar keratoplasty), ocular surface reconstruction and keratoprosthesis are the current treatment options of the damaged corneas. Cornea is the most successful and mostly transplanted tissue worldwide among other solid organ transplantations (In 2010, 42,642 corneal transplantations were done compared to total 12,623 transplantations of kidney, liver, intestine, and pancreas in 2008) (Tan *et al.*, 2012) due to immune privilege and avascular nature of it. Storage (in eye-banks) and transplantation is also easier than other transplantations (Gain *et al.*, 2016).

Penetrating keratoplasty (PK) is the replacement of the full-thickness corneal tissue (all five layers) which has treated many affected corneas for many decades (Wong *et al.*, 2017) (Figure 1.3 B). However, the success rate is significantly decreased when there is deep vascularization, and when the cornea is scarred because of altered tear film production or glaucoma. Severe chemical burns, trachoma, severe dry eye syndrome, Stevens-Johnson syndrome, and severe traumas also result in poor outcome (Chirila *et al.*, 1998).

With the development of lamellar keratoplasty, replacement of only affected layers of the cornea, and ocular surface reconstruction, the success rate significantly increased. Lamellar keratoplasty can be done in several ways; anterior lamellar keratoplasty (ALK) replaces only epithelium and stroma layers with donor Bowman's membrane (Figure 1.3 C) (when all stroma is removed called as Deep anterior lamellar keratoplasty, DALK), and endothelial keratoplasty (EK) includes only Descemet's membrane and endothelium layer (Figure 1.3 D) with or without stroma. Corneal surface reconstruction is another viable option for the treatment of affected cornea when the damage is not deep; Limbal epithelial transplantation replaces only the epithelial layer by using donor tissue. Cultivated mucosal epithelial transplantation, on the other hand, replaces epithelial layer by ex-vivo cultivation of epithelium on amniotic membrane (Tan *et al.*, 2012; Gain *et al.*, 2016). Although keratoplasty is the main solution for the corneal damages, there are, unfortunately, clinical, social and logistical barriers to achieve successful results. Clinically, not all the blindness cases are treatable because of the severity of the damages resulted from diseases like deep corneal vascularization, glaucoma, ocular surface diseases and adherent leukemia. Social and economic status of the person also affects access of the patients to the services, and drugs like steroids and antibiotics (Oliva, Gulati and Schottman, 2012). Lack of trained doctors for surgeries or lack of access to surgical equipment are also other barriers for the treatment. However, the most significant limitation is the number of the available donor tissue; it is far from the demand worldwide and long waiting lists exist in eye banks. In addition, 10% of the transplanted corneas are rejected in the first year of implantation and graft survival rate decreases significantly in the repeated transplantations. Tissue rejection is very

painful for the patient and can result in permanent blindness. Religious and cultural factors because of low education or lack of eye banks limit the cadaveric cornea donation (Tan *et al.*, 2012; Wong *et al.*, 2017). Number of suitable corneas for transplantation also decreases because of transmissible diseases (like HIV virus), refractive surgeries and age of the donor (Ghezzi, Rnjak-Kovacina and Kaplan, 2015).

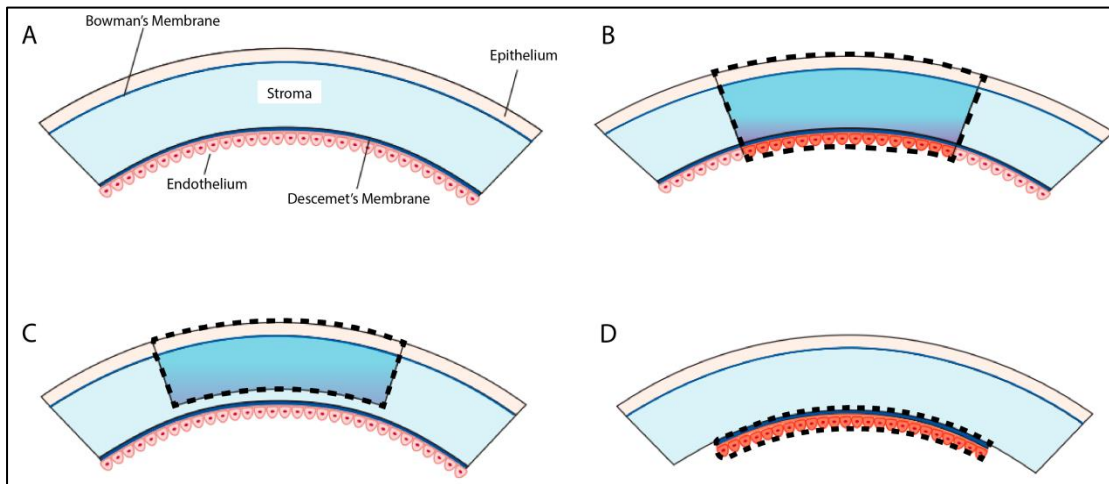


Figure 1.3: Types of keratoplasties. A) Structure of cornea, showing five distinct layers. B) Penetrating keratoplasty, C) Anterior lamellar keratoplasty (ALK), and D) Descemet's membrane endothelial keratoplasty (DMEK). Transplanted regions are highlighted with dotted lines in each case. Adapted from Tan *et al.*, 2012.

Artificial corneas, known as keratoprostheses (KPro), are synthetic substitutes for full thickness corneas. The history of the first KPro attempts goes back to 19th century where De Quengsy firstly implanted a glass substitute to the rabbits. However, unsuccessful results with glass because of risk of removal led to the use of synthetic materials. Poly(methyl methacrylate) (PMMA) was the first keratoprosthetic material and was followed by other polymers including poly(2-hydroxyethyl methacrylate) (PHEMA), poly(vinyl alcohol) (PVA), and poly(glyceryl monomethacrylate) (PGMA) (Chirila *et al.*, 1998).

An ideal KPro should be biocompatible, transparent with an appropriate curvature and refractive index, flexible, and should prevent infection and epithelium

downgrowth (Ghezzi, Rnjak-Kovacina and Kaplan, 2015). Although there is no ideal keratoprosthesis today, with the development of “core-and-skirt” model a good integration between the host tissue and the material is achieved through the porous skirt around the central core material. Today, this model forms the basis of most of the keratoprosthesis devices where anchorage of the cornea occurs through the ingrowth of the fibroblasts on the porous and elastic skirt. Boston KPro and Osteo-odonto Kpro (OOKP) are the most commonly used types (Salvador-Culla and Kolovou, 2016).

Boston type I keratoprosthesis consists of two main parts: PMMA anterior plate and titanium back plate (Figure 1.4 A). Titanium part has 16 holes to achieve access to the aqueous humor. Donor cornea is placed between the PMMA and titanium plates and the whole complex then sutured to host eye (Salvador-Culla and Kolovou, 2016) (Figure 1.4 B). Although vision repair is good in short term, complications like glaucoma and endophthalmitis are still problems which decrease the chance of long term use (Ghezzi, Rnjak-Kovacina and Kaplan, 2015).

Osteo-odonto keratoprosthesis (OOKP) was developed in 1963 by Strampelli. In this model, an optical PMMA cylinder has two distinct anterior and posterior segments with different diameters which allow anchorage to the tooth (Figure 1.4 C) (tooth is taken from the patient with its root and jaw bone and a hole is made to place the PMMA cylinder) (Falcinelli *et al.*, 2005; Liu *et al.*, 2005; Salvador-Culla and Kolovou, 2016). Surgery includes removal of the entire iris and lens to place the KPro (Figure 1.4 D) and it is only used as the last option of the patient where the eye is not suitable for PK. Today OOKP is the most common treatment for Stevens-Johnson syndrome and chemical burns by offering a long term use (Ghezzi, Rnjak-Kovacina and Kaplan, 2015). Despite the success of this model, several problems reported in the literature including bone bioresorption, increased intraocular pressure (IOP), and lamina degradation due to chronic inflammations. In addition, the whole procedure is quite complex and long; it consists of two or three stages and each takes about 3-5 months (Viitala *et al.*, 2009; Laattala *et al.*, 2011).

Currently, transplantation remains the major and long-term treatment for corneal damages, despite its limitations. This indicates that an alternative, efficient approach is needed to meet the demand and overcome the limitations of the current treatment methods.

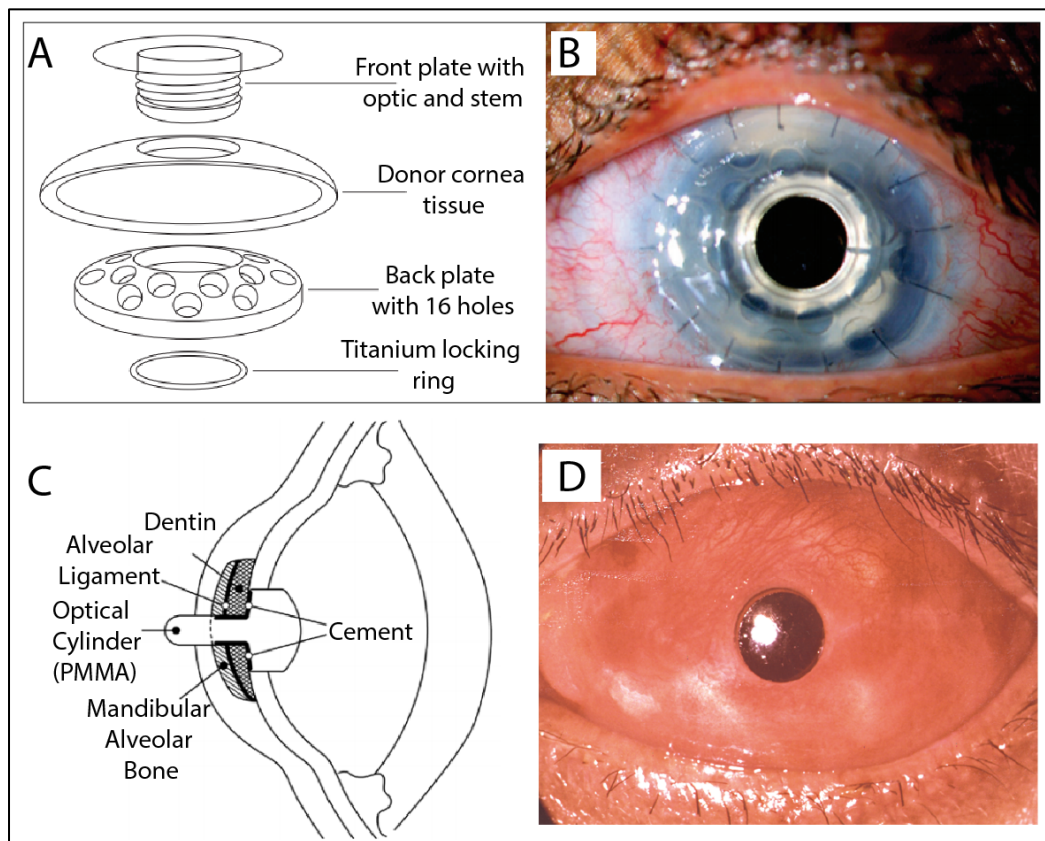


Figure 1.4: Boston Type I and Osteo-odonto Keratoprosthesis (OOKP). A) Components of Boston KPro (Adapted from Tan et al., 2012), B) Boston KPro sutured in place (Adapted from Tan et al., 2012), C) OOKP drawn in place (Adapted from Laattala et al., 2011), D) Appearance of the eye after 3 months of OOKP surgery (Adapted from Falcinelli et al., 2005).

1.3.1 Tissue Engineering

In case of severe diseases, injury and trauma, transplantation of patient's own tissue is the main treatment approach (autograft), and the other is transferring tissues from another individual (allograft). Although these treatment techniques are lifesaving, there are serious problems and limitations associated with them. Treatment with autografts is painful and causes donor site morbidity. Allografts, similarly, can be rejected by the immune system of the patient, or the host can be infected. Tissue engineering is a viable alternative to auto or allografts and aims to regenerate tissues by replacing, restoring and improving the function of the tissue by employing biomaterials, cells and growth factors (Langer and Vacanti, 1993).

Tissue engineering requires porous, 3D scaffolds as the ideal surroundings for the cells for their attachment, proliferation and secretion of extracellular matrix (ECM) thus mimicking the natural tissue (O'Brien, 2011). Damaged tissue is regenerated by the deposition and organization of the newly synthesized ECM on the scaffolds which provide the initial mechanical support needed. During this process the scaffold eventually is degraded or metabolized and is replaced by the fresh and viable organ or tissue (Stock and Vacanti, 2001). An ideal scaffold should be biocompatible, biodegradable, have appropriate mechanical strength, and interconnected pores to allow penetration of cells, nutrients and removal of waste products (O'Brien, 2011).

1.3.1.1 Corneal Tissue Engineering

1.3.1.1.1 Cell Sources

The first step in constructing a viable 3D cornea by tissue engineering is using the right kind of cells. Isolation of the primary cells or stem cells from the host (animal or patient) which have potential to differentiate into desired lineage in the presence of right factors is the main step finding the cell source (Germain *et al.*, 2000).

Corneal keratocytes (Figure 1.5) can be isolated from the stromal layer following dispase digestion and removal of epithelium layer. Another option for keratocyte isolation is use of a mixture of cells containing stromal cells and epithelial cells. With the aid of keratocyte specific growth medium epithelial cells are lost and keratocytes can be harvested (Germain *et al.*, 2000). A small portion of the cell population of the stroma consists of mesenchymal stem cells which exhibit multipotent differentiation capability, clonal growth and express stem cell markers. They are potential candidates for corneal tissue engineering applications. These cells are located in the limbal stroma near the corneal epithelium stem cells (Figure 1.5) suggesting their interaction *in vivo* (Pinnamaneni and Funderburgh, 2012). Adipose derived stem cells (ADSC) (Du *et al.*, 2010), human embryonic stem cells (hESC) (Chan *et al.*, 2013), and bone marrow mesenchymal stem cells (BMSC) (Hongshan *et al.*, 2011) are also known to differentiate into keratocyte lineage which can be used as alternative cell sources in engineering stroma.

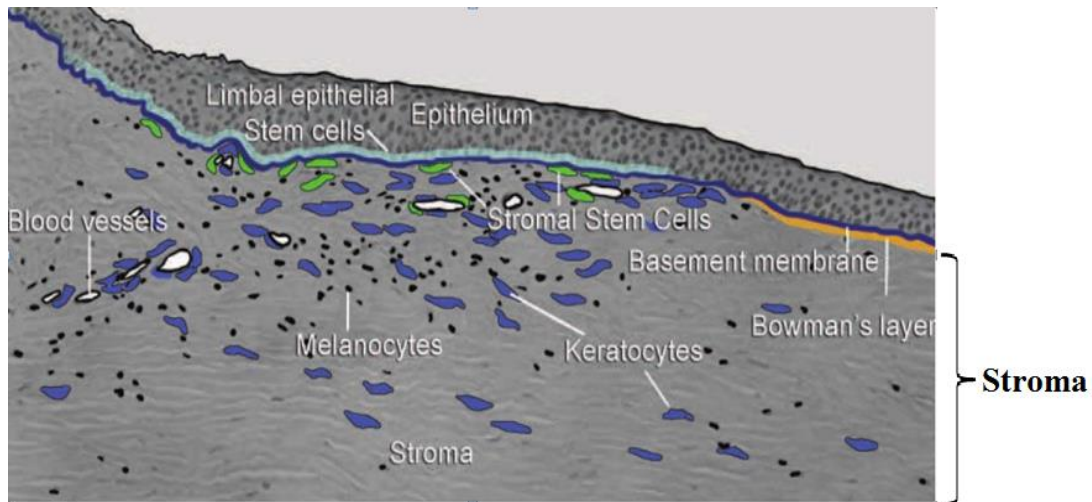


Figure 1.5: Corneal tissue section showing the transition zone between sclera and cornea, named as limbus. Limbal epithelial stem cells are found in limbal basal epithelium and corneal stromal stem cells (green) are localized near the epithelial stem cells. Different from central part of the cornea, limbal part is vascularized (white holes) and have melanocytes (black). Mesenchymal keratocytes are shown in blue in the figure. Adopted from (Pinnamaneni and Funderburgh, 2012).

1.3.1.1.2 The Scaffold Materials

The choice of biomaterials is highly critical in the design of a tissue engineered substitute which should fulfill the minimum requirements of the desired tissue. At present a variety of different biomaterials with natural and/or synthetic origin are used for corneal stroma reconstruction.

1.3.1.1.2.1 Natural Materials

Natural materials are highly attractive in corneal stroma engineering and some of them are highly biocompatible, have gelation ability, biodegradability, and high water binding capacity. Moreover, modification of the natural origin materials chemically or enzymatically is possible to obtain materials with additional functional properties. However, batch to batch variability, immune responses, and limited availability are some of the disadvantages of the natural polymers (Malafaya, Silva and Reis, 2007; Correlo *et al.*, 2011). Polyhydroxyalkanoates, polysaccharides and protein-origin polymers are the three major classes employed in corneal stroma engineering applications. These polymers are obtained from various sources like plants, algae, animals and microorganisms through enzymatic reactions or fermentation (Hasirci *et al.*, 2001).

Polyhydroxyalkanoates are generally biodegradable, thermoprocessable, and biocompatible biomaterials produced by microorganisms. Poly(3-hydroxybutyric acid) (PHB) and copolymers of it with hydroxyalkanoates (like poly(3-hydroxyvaleric acid) (PHBV)) are highly attractive due to their mechanical strengths, fiber forming ability, biocompatibility and biodegradability. Polyhydroxyalkanoates and its composites are employed in various applications including sutures, stents, nerve guides, and wound dressing (Hasirci *et al.*, 2001; Chen and Wu, 2005). In corneal stroma engineering PHBV was used in the production of micropatterned films to guide the keratocytes along the patterns which mimic the natural organization of the stroma (Zorlutuna *et al.*, 2006, 2007).

Polysaccharides are other class of natural origin biomaterials made up of monosaccharides that are linked to each other through O-glycosidic linkages. Their physical properties like solubility, gelation ability, and viscosity vary depending on their monosaccharide composition, chain shapes and molecular weights. They are obtained from various sources including plants, animals, and microorganisms (Mano *et al.*, 2007). They have been widely used in tissue engineering applications as well as corneal stroma engineering due to their non-toxicity, low cost in production, tunable mechanical properties, and biocompatibility (Nair and Laurencin, 2007). Chondroitin sulfate is an example for polysaccharides which is found in the structure of native cornea provide viscoelasticity and enhance water binding capacity to the tissue. In several studies it is blended with collagen and these scaffolds successfully supported growth of corneal keratocytes (Vrana *et al.*, 2008; Acun and Hasirci, 2014). Scaffolds containing chitosan blended with natural materials like collagen and gelatin resulted in mechanically strong, transparent, biocompatible and elastic corneal tissue equivalents (Rafat *et al.*, 2008). Hyaluronic acid is another example for polysaccharides used in cornea tissue engineering. Films produced from the blend of collagen, gelatin and hyaluronic acid were reported to have adequate mechanical strength, appropriate hydrophilicity and transparency (Liu, Ren and Wang, 2013).

Proteins are the main components of the extracellular matrices and have active role tissue regeneration, wound healing mechanisms, and regulation pathways. They are highly popular in the construction of scaffolds, sutures, and in the studies of drug delivery systems. They are removed from the body through natural mechanisms of the host body via degradation hydrolytically (Nair and Laurencin, 2007). Scaffolds produced from proteins present excellent cell support, mimic the ECM well, and are highly biocompatible. Collagen is the most common ECM component in mammalian tissues and is widely employed in corneal stroma reconstruction in various forms including films (Vrana *et al.*, 2007; Kilic *et al.*, 2014), foams (Vrana *et al.*, 2008; Acun and Hasirci, 2014), and fibers (Phu *et al.*, 2010; Acun and Hasirci, 2014). Extracted and purified collagen, however, lacks the mechanical strength and elasticity, and degrades rapidly compared to intact collagen due to dissociation of the

natural crosslinks in the course of the purification process (Friess, 1998). Additionally, batch to batch variability of the purified collagens and limited natural sources to extract them are other limitations. Recombinant human collagens, therefore, avoid these limitations by making production of proteins with pre-defined properties possible (Liu *et al.*, 2008). Silk fibroin is another protein-origin polymer used extensively in corneal tissue engineering due to its good tensile strength, high availability, transparency, biocompatibility, and fast processing (Hazra *et al.*, 2016). Gil *et al.*, (2010) were used RGD-functionalized silk fibroin films to mimic the natural lamellar structure of the corneal stroma. The constructs have been shown to support cell attachment, alignment, and proliferation.

Gelatin, another protein-origin polymer, was employed in this study because it is inexpensive, does not possess any antigenicity and a range of different sources are available. Gelatin is also suitable for the cells since it is a natural polymer obtained by denaturation of collagen and thus contains natural cell binding motifs like arginine-glycine-aspartic acid (RGD) (Van Den Bulcke *et al.*, 2000). Gelatin needs to be crosslinked in order to make it stable at room temperature. In the literature gelatin has been reported to be used in corneal tissue engineering through crosslinking chemically with glutaraldehyde, carbodiimide, and NHS (Mimura *et al.* 2008; Luo *et al.* 2018, respectively). However, long processing durations, inability to load cells, and use of toxic crosslinking agents are some disadvantages of these approaches. Methacrylated gelatin (GelMA) is a photopolymerizable hydrogel obtained by modification of gelatin by addition of methacrylate groups to the amine containing side groups and enables gelatin to crosslink upon UV exposure to form an irreversible hydrogel. The degree of methacrylation allows the control of crosslinking extent which in turn allows control of swelling and mechanical properties. Very short UV exposures and absence of organic solvents are several advantages of this method (Nichol *et al.*, 2010; Kilic Bektas and Hasirci, 2018).

1.3.1.1.2.2 Synthetic Materials

Synthetic polymers are also very attractive in corneal stroma engineering applications for several reasons. Some of the biodegradable synthetic polymers are biocompatible and do not cause any immune response, their mechanical properties and degradation rates can be controlled changing the processing conditions, and they can be functionalized to increase cell attachment and proliferation. Polyglycolic acid (PGA) (Hu *et al.*, 2005) and poly (lactic acid-co-glycolic acid) (PLGA) (Hong *et al.*, 2018) are commonly used in corneal tissue engineering because of their biocompatibility and biodegradability. Their degradation occurs through hydrolysis of the ester linkages and are removed from the body by natural metabolic pathways (Gunatillake, Adhikari and Gadegaard, 2003). Poly(ester urethane) is another synthetic material used in corneal stroma engineering (Wu *et al.*, 2013). Constructs were reported to have poor transparency but human stromal stem cells differentiated successfully into keratocyte lineage when seeded on them. The main problem of the synthetic materials is poor transparency and limited biological responses which are overcome by combining them with natural-derived materials for corneal tissue engineering applications (Ozcelik *et al.*, 2013; Ghezzi, Rnjak-Kovacina and Kaplan, 2015).

Poly(2-hydroxyethyl methacrylate) (HEMA) is one of the most widely used synthetic materials used in ophthalmic applications like soft contact lenses and intraocular lenses. pHEMA is chemically stable (non-degradable), biocompatible and its permeability, transparency and hydrophilicity can be adjusted by changing crosslinking conditions. Since their first use by Wichterle and Lím (1960), it was reported to be used in many fields including tissue engineering (Madden *et al.*, 2010; Dragusin *et al.*, 2012). pHEMA was used in this study in combination with GelMA to enhance the mechanical strength of the hydrogels.

1.3.1.1.3 Scaffolds

An ideal scaffold for corneal stroma replacement should be optically transparent, sufficiently strong, biocompatible and should allow cell adhesion, migration and

proliferation (Lin and Jin, 2018). Up to date a number of scaffolds were developed for corneal tissue engineering by either mimicking only one layer (epithelium, stroma, or endothelium; (Wu *et al.*, 2013; Kilic *et al.*, 2014; Kilic Bektas and Hasirci, 2018), two layers (hemi-cornea epithelium and stroma; (Zorlutuna *et al.*, 2006; Acun and Hasirci, 2014; Wang *et al.*, 2017), or all three layers (Vrana *et al.*, 2008).

The choice of processing technique for scaffold production is as crucial as the material selection and researcher should decide on the technique according to the needs of the material. For instance, while some materials withstand high pressure, heat, and acid/base treatments, others may require mild conditions to be processed. The most widely used processing techniques include freeze drying, electrospinning, solvent casting and particulate leaching, lithography, and 3D printing.

Freeze drying is one of the most commonly employed methods that yield highly porous sponges or foams. In this method a phase separation occurs between the polymer and solvent when the solution is frozen. Finally solvent is sublimed under high vacuum and very low temperature leaving pores behind. A homogenously prepared polymer solution, therefore, results in interconnected pores with various dimensions (Hasirci *et al.*, 2016). Freeze drying is widely used for corneal tissue engineering applications (Vrana *et al.*, 2008; Acun and Hasirci, 2014; Takeda and Xu, 2014).

Electrospinning is another commonly used method by which micro and nano fibers are produced. The polymer solution loaded into a syringe and is pumped to expel the solution towards the collector where the polymer fibers are collected with the aid of electric field created. Due to high voltage created by the electric field, the solvent evaporates before the fibers are collected which results in polymer mats at the side of the collector. Diameter and structure of the fibers are affected from many parameters including applied voltage, nozzle diameter, distance between the needle tip and the collector, and type of the solvent (Doshi and Reneker, 1995). This technique has been used to produce scaffolds for many tissues as well as corneal tissue (Wray and Orwin, 2009; Tonsomboon and Oyen, 2013; Kong *et al.*, 2017)

Solvent casting and particulate leaching are two techniques used together to produce scaffolds. In this method polymer solution containing particulates like porogen or salt is cast in a mold and after solidification the particulates are removed from the scaffold by dissolving them away with the aid of a liquid. Interconnected pores are obtained in the places of particulates. This technique is quite simple and the sizes of the pores can be controlled by the amount and the size of the added particulate (Liao *et al.*, 2001). Several studies on cornea engineering have been used this technique in the literature (Gil *et al.*, 2010; Wang *et al.*, 2017).

Lithography is an advance scaffold fabrication technique which allows shape control with the aid of a mask or a mold. Poly(dimethylsiloxane) (PDMS) and poly(methylmethacrylate) (PMMA) are the most commonly used hydrophobic molds in soft lithography which allow removal of the films on their surface. In corneal tissue engineering studies micro or nano patterns created on the surface of the films have been used to guide the cells to align along the patterns that mimics the natural organization of the tissue (Vrana *et al.*, 2007; Gil *et al.*, 2010; Kilic *et al.*, 2014).

1.3.1.1.3.1 3D Printing

Three dimensional printing (3D) (also known as additive manufacturing) is used to build complex scaffolds by layer-by-layer deposition of a biomaterial by using computer aided design (CAD) data sets. The production process involves three major steps: Images are acquired from computer tomography (CT) or magnetic resonance imaging (MRI) scans, raw data of the images are converted into a CAD model, and rapid prototyping machines generate 3D solid structure by layer-by-layer deposition of the biomaterial. The main advantage of the 3D printed technology is its ability to create structures with quite high complexity which can mimic the natural organization of the tissues in detail (Rengier *et al.*, 2010; Hasirci *et al.*, 2016). 3D printing technology is a growing field and currently there are a variety of different approaches like selective laser sintering (SLS), fused deposition modeling (FDM), stereolithography (SLA), inkjet printing (IP) and 3D bioprinting (Guvendiren *et al.*, 2016). Among them, 3D bioprinting is the most suitable technique for the

construction of corneal tissue equivalents because of transparency, high water content and elasticity requirements of the tissue. These requirements of the tissue are provided by the hydrogels and complex organization of the tissue is mimicked by 3D bioprinting. In the following section hydrogels and 3D bioprinting approaches are detailed.

1.3.1.1.3.1.1 Hydrogels

Hydrogels, which are also employed in this study, have a significant potential in cornea and other tissue engineering applications due to their significant similarity to the natural micro environment of the tissues. Hydrogels are hydrophilic polymeric networks that absorb and retain large amounts of water and they introduce compositional similarity to extracellular matrix of the tissues, biocompatibility and structural integrity (Hasirci *et al.*, 2016). Hydrogel forms of gelatin (Liu, Ren and Wang, 2013; Kawakita *et al.*, 2014), chitosan (Ozcelik *et al.*, 2013; Tang *et al.*, 2017) and collagen (Rafat *et al.*, 2008; Mirazul Islam *et al.*, 2015) were used for corneal tissue reconstruction. For example, in one of the studies gelatin hydrogels were prepared by crosslinking with glutaraldehyde, seeded with corneal fibroblasts and *in vitro* and *in vivo* studies were conducted (Mimura *et al.*, 2008). Implanted gelatin hydrogels carrying fibroblasts showed an intense collagen type I expression and did not lead to any opacity when tested *in vivo*.

Hydrogels prepared with different biofabrication methods were also studied. Production of cryogels is one of the newer techniques employed in various tissues including cornea. Cryogels are obtained when the solution temperature is decreased below the freezing temperature of the solvent and crosslinking is carried out in a small portion of gel solution. By increasing temperature gradually macro-pores are formed when solvent crystals melt (Lozinsky *et al.*, 2003; Henderson *et al.*, 2013). In a recent study, cryogels were used to host corneal keratocytes (Luo *et al.*, 2018). Gelatin/ascorbic acid cryogels crosslinked with carbodiimide created by this method were shown to favor growth of the keratocytes. However, low cell penetration into the structure due to cell seeding after construct is formed is a disadvantage of this

method. Moreover, restricted working conditions like temperature and pH, use of organic solvents and toxic crosslinking agents for polymerization are other limiting factors.

Polymerization via photocrosslinking through UV or visible light is a viable alternative to other hydrogel forming methods due to the fast and controllable polymerization at ambient temperatures, and ease of loading cells and/or other biological factors during polymerization. Photopolymerization is also popular in other fields including dentistry, coatings, and production of electronic materials (Nguyen and West, 2002). In tissue engineering applications cell loading into the hydrogel is desired for homogenous cell distribution in the constructs which is only possible with the water soluble photoinitiators that do not damage the cells during polymerization. Irgacure 2959 (I2959, 2-(Hydroxyl)-4-(2-hydroxyethoxy)-2-methylpropiophenone) is one of the widely used water soluble photoinitiator which is activated at low UV intensity to initiate radical polymerization reaction (Komez *et al.*, 2016; Kilic Bektas and Hasirci, 2018). Presence of unreacted monomers are also a question in these reactions but due to the aqueous nature of the hydrogels a high conversion is obtained (Ifkovits and Burdick, 2007).

1.3.1.1.3.1.2 3D Bioprinting

3D bioprinting is a growing and highly promising hydrogel forming method which involves positioning of cells, growth factors and biological materials in a layer-by-layer fashion to obtain highly organized 3D scaffolds. With the use of CAD technology, one can attempt to mimic the organization of natural tissues. The limitations of other methods like lack of organization and/or the ability to load cells in the structure homogeneously are overcome (Marco, Javier and P., 2018).

Laser, inkjet and extrusion based systems are three different type of 3D hydrogel bioprinting methods.

1.3.1.1.3.1.2.1 Laser based systems

Laser-assisted bioprinting (LAB) is based on the assembly and patterning of single cell deposits with the aid of laser beam. The set-up basically composed of three units: a pulsed laser source (at UV or near-UV wavelength), a ribbon which is coated with the liquid material (bioink) to be printed, and a receiving substrate. The ribbon is irradiated with the laser pulse which evaporates the bioink and the bioink is deposited on the receiving substrate in droplet form (Figure 1.6 A). The receiving substrate is usually a cell culture medium or a biopolymer which supports adhesion and growth of the cells in the droplets following printing. The resolution of the printed constructs depends on many factors including the complexity of the model, printing speed, the thickness of the bioink on the ribbon, and the wettability of the receiving substrate (Barron *et al.*, 2004; Guillemot *et al.*, 2010; Li *et al.*, 2016).

Compared to inkjet and extrusion systems, materials with higher viscosity can be printed with this method (Billiet *et al.*, 2012; Xu *et al.*, 2014). However, optimization of working conditions of new materials is time consuming. Non-homogenous cell distribution, use of cytotoxic photoinitiators and necessity of post-curing are also reported in some types of laser based systems (for example stereolithography (SLA)) (Billiet *et al.*, 2012). The only 3D printed corneal construct by using this method was recently reported (Sorkio *et al.*, 2018). Researchers used collagen type I bioink, human embryonic stem cells derived epithelial stem cells (hESC) for epithelial layer, and human adipose derived stem cells (hASCs) for stromal layer. These cell loaded split-thickness constructs showed the feasibility of this method to create a 3D bioprinted corneal tissue.

1.3.1.1.3.1.2.2 Inkjet Based Systems

Inkjet based systems are another class for 3D bioprinting systems which are commonly used due to the availability of the parts and ease in optimizations. In this method desired volumes of bioink are deposited on predefined locations in droplets generated by thermal or piezoelectric actuators (Figure 1.6 B) (Murphy and Atala, 2014; Li *et al.*, 2016; Mandrycky *et al.*, 2016). Rapid build-up, flexible patterning on

a large printing area and ease of printing of different materials are several advantages of this method (Xu *et al.*, 2014; Mandrycky *et al.*, 2016). However, difficulty in printing of highly viscous materials, aggregation of the cells, problem at the reproducibility level, and clogging of the nozzle are several limitations associated with this method (Billiet *et al.*, 2012). Up to date, no 3D bioprinted cornea construct was reported with this technique.

1.3.1.1.3.1.2.3 Extrusion Based Systems

An extrusion based system, which is used in this study, is a combination of an automated robotic and a fluid dispensing system for bioprinting and extrusion, respectively. Dispensing of the bioink, cell suspension in biomaterial solution, is done through a pneumatic or mechanical (screw-driven or piston) system under computer control to deposit the bioink in a desired 3D structures (Figure 1.6 C). Continuous printing of the bioink results in rapid and precise fabrication of the products. The desired 3D shapes can be created by CAD software and printed directly. Researcher can create his own CAD file or can obtain data from MRI or CT scans which makes this technique quite convenient for printing 3D cell loaded constructs (Dababneh and Ozbolat, 2014; Ozbolat and Hospodiuk, 2016). Although for highly viscous bioink solutions screw-driven systems can be beneficial, pressure created in the nozzle may harm the cells. Piston-driven deposition, therefore, provide a better control of bioink deposition. Printed structure is stabilized by crosslinking via light, chemicals or thermal changes. The limitations of this method are short list

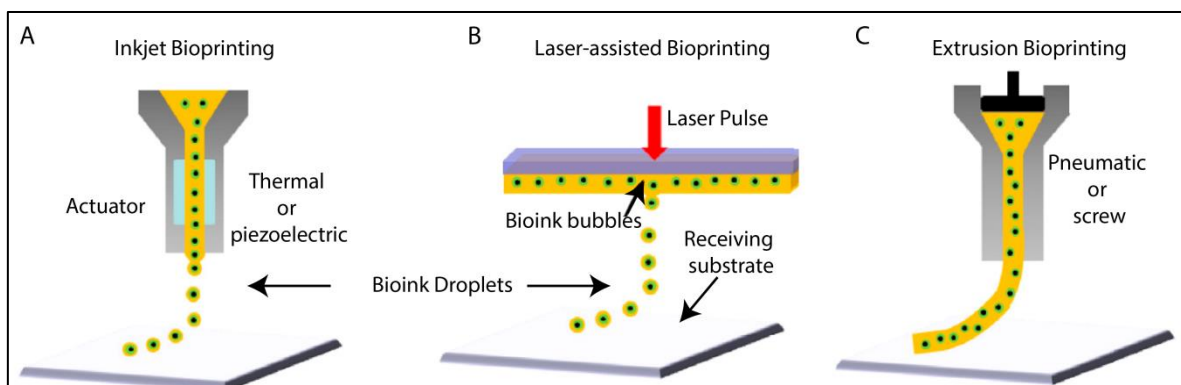


Figure 1.6: 3D Bioprinting methods. A) Inkjet bioprinting, B) Laser-assisted bioprinting, and C) Extrusion bioprinting. (Adapted from Mandrycky *et al.*, 2016)

of materials for bioink preparation due to the need for rapid cell loading prior to gel formation and shear stress. However, these limitations can be overcome by optimizing the conditions like diameter of the nozzle, concentration of the material, pressure and flow rate (Dababneh and Ozbolat, 2014; Xu *et al.*, 2014).

Extrusion based printing has been employed to print various tissues including vasculature (Suntornnond *et al.*, 2017), liver (Lee *et al.*, 2017), cardiovascular tissue (Duan, 2016), and bone (Byambaa *et al.*, 2017). The only 3D printed corneal tissue with extruder-based system was recently reported (Isaacson, Swioklo and Connon, 2018). It used a pneumatic dual extruder 3D bioprinter and printing was done based on the data from 3D digital human corneal model. High viability of the corneal keratocytes showed the feasibility of the extrusion-based bioprinting technique for corneal tissue engineering. Although a digital human cornea model was the starting point of this 3D printed structure, its organization is different than the native tissue: Concentric circles were printed starting from the center to the upwards of the rim in the 3D printed model. However, collagen bundles are aligned and formed plywood like structure in native corneal stroma.

1.4 Novelty of the Study

The micro-structure of the native corneal stroma is highly organized, consists of multilayered collagen fibers aligned parallel to each other and nearly 90° to the subsequent layers as in plywood. In this study, highly transparent GelMA hydrogel was produced, working conditions were optimized and hydrogels loaded with stromal keratocytes were printed by pneumatic extrusion based bioprinter. The model consisted of parallel fibers and the subsequent layers located as the fibers are at 90° to each other in the native structure of the stroma. In this study, the organization of the stroma was constructed for the first time with cell loaded 3D printed GelMA hydrogels which mimics the natural organization of native corneal stroma. High cell viability, transparency and adequate mechanical strength of the hydrogels make the construct a strong alternative for the allografts which are in short supply.

CHAPTER 2

MATERIALS AND METHODS

2.1 Materials

Irgacure 2959 (2-(Hydroxyl)-4-(2-hydroxyethoxy)-2-methylpropiophenone), methacrylic anhydride, Type A gelatin from porcine skin (70–100 bloom), amphotericin B, trypsin–EDTA (0.25%), penicillin/streptomycin, sodium cacodylate trihydrate, bovine serum albumin (BSA), paraformaldehyde, sodium azide, Coomassie brilliant blue, D-glucose, 1.25% *N,N,N',N'*-tetramethylethylenediamine (TEMED), ethyleneglycol dimethacrylate (EGDMA), 2-hydroxyethyl methacrylate (HEMA), collagenase Type II from *Clostridium histolyticum*, and 4,6-diamidino-2-phenylindole dihydrochloride (DAPI) were purchased from Sigma-Aldrich (USA). Sodium dihydrogen phosphate dihydrate, disodium hydrogen phosphate heptahydrate and sodium chloride were bought from Merck (Germany). Optimal Cutting Temperature compound (OCT) was from Miles Scientific, USA. Sylgard 184 polydimethylsiloxane elastomer and curing agent were from Dow Corning, USA. Live–Dead cell viability/cytotoxicity kit, Actin phalloidin (532 and FITC labelled), DRAQ5, Dulbecco's Modified Eagle Medium–Ham's nutrient mixture F12 (DMEM–HAM's F12, 1:1) with and without phenol red, newborn calf serum, and Coomassie Plus Bradford Assay Kit were from Thermo Fisher Scientific (USA). Human basic fibroblast growth factor (hFGF basic/FGF2) without carrier was purchased from Cell Signaling Technology, Inc. (USA). NucleoCassettes were from ChemoMetec (Denmark). SnakeSkin dialysis tubing was purchased from HyClone, Thermo Scientific (USA). Dimethyl sulfoxide (DMSO), Triton X-100 and ammonium persulfate (APS) were from AppliChem (USA). CellTracker green CMFDA and Live Cell Imaging solution were from Molecular Probes, USA. Alexa Fluor 488 CD34, CD45 and IgGI mouse isotype, APC CD73, and Alexa Fluor 647 CD90 were purchased from Biolegend, USA. Alamar Blue and Alexa Fluor 488 (goat anti-mouse and anti-rabbit) were from Invitrogen Inc. (USA). Primary

antibodies for collagen Type I (mouse), collagen Type V (rabbit), decorin (mouse), biglycan (rabbit), α -smooth muscle actin (α -SMA) (rabbit) were from Abcam Inc. (Cambridge, MA). Sensolyte® 520 Generic MMP Assay Kit (Fluorimetric) was brought from AnaSpec Inc., USA. Ketamine base (Ketalar®) was purchased from Pfizer, USA. Schimer's and fluorescein papers were from EastPharma, Turkey. Maxidex® was purchased from Novartis, Australia. Netildex™ was bought from SIFI, Italy. Eyelea was from Regeneron Inc., USA.

2.2 Methods

2.2.1 Synthesis of Methacrylated Gelatin

Methacrylated gelatin (GelMA) was synthesized according to protocol of Nichol *et al.*, (2010). Briefly, 5 g of type A porcine skin gelatin was dissolved in 40 mL phosphate buffered saline (PBS, pH 7.4, 10 mM) at 60°C. Methacrylic anhydride (MA) (10 mL) was added to this solution at a rate of 0.5 mL/min at 50°C to yield a MA concentration of 20% (v/v). The reaction was stopped after 1 h by 5x dilution with warm (40°C) PBS, and the solution was dialyzed (CO 10,000) against distilled water for 7 days at 40°C to remove the excess methacrylic acid and salts. The resultant solution was lyophilized (Labconco Freezone 6, USA) and stored at +4°C until further use.

2.2.2 ¹H Nucleic Magnetic Resonance (¹H-NMR) of GelMA

Gelatin and lyophilized GelMA were dissolved in D₂O (30 mg/mL) at 40°C. Bruker DPX 400 spectrometer was used to obtain ¹H NMR spectra at ¹H resonance frequency of 400 MHz. For averaging signal-to-noise ratio, sixteen scans were made.

2.2.3 Preparation of GelMA Hydrogel Slabs

To prepare hydrogels slabs from GelMA solution, a PDMS template was created. Briefly, PDMS prepolymer was mixed with catalyst, poured into glass petri dishes and cured at 70°C for 3 h. Resulting PDMS film was peeled off. Small discs with different dimensions were prepared from PDMS films (Table 2.1). Solutions with 5, 8, 10 and 15% GelMA (w/v) (labeled GelMA5, GelMA8, GelMA10, and GelMA15, respectively) in PBS containing 0.5% Irgacure 2959 photoinitiator (w/v) were

poured into PDMS molds and exposed to UV (365 nm, 0.120 Joule/cm²) for 1 min in a UV crosslinker chamber (BIO-LINK™ UV Crosslinker DLX-365, Germany). After 1 min, the reverse side of the hydrogel was exposed to UV for 1 more min.

To serve as a control of printed hydrogels, GelMA15 solution was prepared in PBS in the presence of 0.5% photoinitiator (w/v), poured into the PDMS molds, incubated for 15 min at 4°C, and crosslinked for 5 s with OmniCure (S1500, Lumen Dynamics, Canada) (15 mW/cm², at 365 nm) at a distance of 3 cm.

Table 2.1: Dimensions of the PDMS Discs for different applications.

Application	PDMS Disc Dimensions (D: diameter, h: height)
In situ and <i>in vitro</i> studies	D = 1 cm, h = 0.5 mm
Mechanical Tests	D = 1 cm, h = 2 mm
Transparency Tests	D = 0.5 cm, h = 0.5 mm
Control for 3D Printing Part- in situ and in vitro studies and Transparency Tests	D = 0.6 cm, h = 0.5 mm
Control for 3D Printing Part-Mechanical Tests	D = 0.6 cm, h = 2 mm
<i>In vivo</i> Studies	D = 0.5 cm, h = 0.30 mm D = 0.4 cm, h = 0.15 mm

2.2.4 Preparation of GelMA-HEMA Hydrogel Slabs

GelMA15 was prepared according to Section 2.2.3. HEMA solution was prepared as follows: 98% HEMA, 1.25% TEMED and 1% EGDMA. GelMA and HEMA (8:2, v/v) were mixed and freshly prepared APS in PBS (10%, w/v) was added to this solution to make 5% final solution (v/v). Final solution was vortexed and immediately put into PDMS molds. After waiting 1 min to allow HEMA to crosslink, hydrogels were crosslinked under UV for 1 min, each side. Resultant hydrogels were washed three times with PBS before characterization.

2.2.5 Preparation of HEMA Hydrogel Slabs

HEMA solution was prepared as mentioned above (Section 2.2.4), mixed with APS, put onto templates and after 1 min, both sides of hydrogels were crosslinked under UV for 1 min/each side. Hydrogels were washed three times with PBS before characterization studies.

2.2.6 Preparation of 3D Printed GelMA Hydrogels

GelMA (15%, w/v) (GelMA15) was dissolved in PBS in the presence of Irgacure (0.5%, w/v). This solution was loaded into 3 mL Luer lock syringe compatible with Bioscaffolder® (SYS-ENG, Salzgitter-Bad, Germany) 3D Printer low temperature dispense head. GelMA is liquid at temperatures above RT and in gel form at lower temperatures. In order to be able to print the GelMA, the syringe loaded with solution was put in refrigerator (+4°C) for 15 min before printing. Bioscaffolder® prints 3D products by coordinated motion of pneumatic syringe dispenser onto a stationary platform. GelMA was printed at a movement speed of the nozzle in x-y direction (Fxy) of 100, 200, or 300 mm/min, a spindle speed (R/S) of 0.01, 0.02, or 0.03 Dots/mm, and from a nozzle with diameter of 0.26 mm (25 ga x ½ Luer stubs, Instech, USA). Layer thickness and the distance between two strands were set as 0.14 mm and 1 mm, respectively.

After observation under stereomicroscope following parameters were chosen for further studies: 1) Fxy 200 and R/S 0.01 (GelMA15-001), 2) Fxy 200 and R/S 0.2 (GelMA15-002), and 3) Fxy 300 and R/S 0.03 (GelMA15-003). Rectangular prism GelMA hydrogels (14x14x2 mm³ for mechanical tests (15 layers printed for GelMA15-001 and 10 layers for others) and 14x14x0.5 mm³ for other studies (5 Layers for GelMA15-001 and 3 Layers for others)) were plotted according to a model prepared using Sketchup (Google Inc, USA) and loaded to the CAM (Computer Aided Manufacturing) software (Prim-CAM, Einsiedeln, Switzerland) of the Bioscaffolder® (Table 2.2). Two dimensional (2D) layers were deposited perpendicular to each other at every layer. Obtained 3D printed hydrogels were crosslinked for 5 s with OmniCure (15 mW/cm², at 365 nm) at 3 cm distance, punched with 6 mm diameter punches and stored in PBS until characterization.

Tabel 2. 2: 3D bioprinting parameters chosen after optimization studies.

R/S (Dots/min)	Fxy (mm/min)	Total Number of Layers	Abbreviation
0.01	200	15 -Mechanical Tests 5 - In situ and In vitro Tests	GelMA15-001
0.02	200	10 Layers-Mechanical Tests 3 Layers- In situ and In vitro Tests	GelMA15-002
0.03	300	10 Layers-Mechanical Tests 3 Layers- In situ and In vitro Tests	GelMA15-003

2.2.7 Characterization of the Hydrogels

2.2.7.1 Stereomicroscopy

3D printed hydrogels were examined under a Nikon SMZ1500 stereomicroscope (USA) to study pattern fidelity. Hydrogels were stained with Coomassie blue (0.1% w/v in PBS) to ease the observation.

2.2.7.2 FTIR-ATR

GelMA, GelMA-HEMA and HEMA Hydrogels were air dried and their FTIR spectra were obtained in the region 4000–400 cm^{-1} using Perkin Elmer FTIR Spectrometer (USA) to study integration of HEMA in the structure of GelMA.

2.2.7.3 Equilibrium Water Content (EWC) of GelMA Hydrogels

GelMA discs were incubated in PBS at 37°C for 24 h in a shaking incubator. After gently removing the excess water with filter paper, wet weights (W_w) were recorded. Hydrogels were then rinsed with distilled water to remove salts coming from PBS and then lyophilized and weighed (W_d). Equilibrium water content (%) was calculated from the following equation:

$$EWC (\%) = \frac{W_w - W_d}{W_w} \times 100 \quad (1)$$

where

EWC (%): Equilibrium Water Content (% , w/w)

W_d : Weight of dry samples

W_w : Weight of wet samples

2.2.7.4 In Situ Degradation in PBS

Hydrogels were washed with distilled water and lyophilized to determine their initial weights (n=3). Samples were then incubated in PBS (pH 7.4, 10 mM) at 37°C in a shaking incubator for three weeks. On days 1, 7, 14, and 21 samples were rinsed with distilled water, lyophilized and weighed. Weight loss (%) was determined gravimetrically according to following equation:

$$\text{Remaining weight (\%)} = \frac{W_d}{W_0} \times 100 \quad (2)$$

where

W_0 : Initial dry weight of the samples

W_d : Dry weight of samples after incubation.

2.2.7.5 In Situ Enzymatic Degradation with Collagenase Type II

The stability of the hydrogels against enzymatic degradation was determined using collagenase type II. Initial wet weight of the hydrogels were recorded (W_0) and then they were incubated in collagenase type II solutions at different concentrations (1, 2.5, 5, and 10 U collagenase type II/mL in PBS, pH 7.4) for 4 h. The remaining wet weight was determined every hour and extent of degradation was calculated according to following equation.

$$\text{Remaining weight (\%)} = \frac{W_w}{W_0} \times 100 \quad (3)$$

where

W_0 : Initial wet weight of the samples

W_w : Wet weight of samples after incubation.

2.2.8 *In vitro* Studies

2.2.8.1 Human Keratocyte Cell Culture

Isolated human corneal keratocytes (passages 5-15) which were kindly provided by Prof. Odile Damour (Banque de Cornées des Hospices Civils de Lyon, Lyon, France) were stored frozen in their medium supplemented with 15% DMSO in liquid nitrogen. Following thawing, cell suspension was centrifuged and the cell pellet was suspended in a medium containing Dulbecco's Modified Eagle Medium–Ham's nutrient mixture F12 (DMEM–HAM's F12, 1:1), newborn calf serum (10%), amphotericin B (1 µg/mL), penicillin (100 UI/mL), and streptomycin (100 µg/mL), and bFGF (10 ng/mL). Cells were cultured in tissue culture polystyrene (TCPS) flasks in a CO₂ incubator (SanyoMCO-17 AIC, Japan) at 37°C. Growth medium was changed every two days.

2.2.8.2 Flow Cytometry of Human Keratocytes

Surface markers (CD34, CD45, CD73, and CD90) of human keratocytes were analyzed with BD Accuri C6 flow cytometer (BD Biosciences, USA) in order to study whether they preserve their keratocyte phenotype or not. Cells were trypsinized and centrifuged (3000 rpm, 5 min). The pellet was washed with FACS buffer (PBS containing 1% BSA and 0.1% sodium azide) and after centrifugation, PFA (750 µL, 4% (w/v) in PBS) was added on the pellet to fix of cells for 15 min at room temperature. After fixation, cells were centrifuged and the pellet was washed twice with FACS buffer. Pellet was resuspended in FACS buffer and was divided into eppendorfs as 100 µL in each. One µL of Alexa Fluor 488, Alexa Fluor 647, or APC conjugated antibodies from 1 µg/mL stock was added in each tube and incubated for 30 min at room temperature. After incubation, 1 mL of PBS was added to each tube and centrifuged. The pellet was resuspended in 400 µL PBS and examined with flow cytometry through 4 channels: 1) forward scatter channel (FSC), 2) side scatter channel (SSC), 3) fluorescence channel (FL1 filter, laser 488 nm), and 4) fluorescence channel (FL4 filter, laser 647 nm). CFlow®Plus software was used to analyze the data after gating the samples from debris and dead cells by using

forward and side scatter profiles. An isotype control was employed in each experiment to calculate specific staining.

2.2.8.3 Preparation of Cell Loaded Hydrogel Slabs

Cultured human keratocytes were detached from TCPS surface by using trypsin-EDTA at 37°C for 5 min. After centrifugation (3000 g, 5 min), cells were suspended in the medium and the number of cells was determined with a NucleoCounter (Chemo-Metec, Denmark). Initially, four different cell densities (5×10^5 , 1×10^6 , 5×10^6 , and 2.5×10^6 cells/mL) were used to optimize the cell number in the hydrogel for both optimum cell-to-cell contact and extent of gel formation. For this purpose, determined number of cells was taken in a separate falcon tube, centrifuged and suspended directly with GelMA solution prepared with growth medium. As a control for 3D printed samples cell pellet containing 1×10^6 cells/mL was suspended with GelMA15 solution. The gel precursors were exposed to UV as in Section 2.2.4 (Figure 2.1 A). Hydrogel prepared was washed several times with growth medium and incubated in the same medium at 37°C in a CO₂ incubator. The growth medium was changed every two days for 21 days. At predetermined time points (Days 1, 7, 14 and 21) hydrogels were used for microscopical analysis, mechanical tests, and transparency studies.

2.2.8.4 Preparation of Cell Loaded HEMA and GelMA-HEMA Hydrogels

GelMA-HEMA and HEMA solutions were prepared as mentioned in section 2.2.4 and 2.2.5, respectively (growth medium was used instead of PBS). Cell pellet containing 1×10^6 cells/mL was suspended in these solutions and processed as in respective sections (Figure 2.1 B). Crosslinked hydrogels were washed twice with growth medium and incubated in the same medium in a CO₂ incubator at 37°C for *in vitro* studies.

2.2.8.5 Preparation of Cell Loaded 3D Bioprinted Hydrogels

GelMA15 bioink containing 1×10^6 cells/mL was prepared as mentioned in Section 2.2.8.3. Bioink was loaded into the syringe and incubated for 15 min at 4°C. Printing process was carried out as in Section 2.2.6. After crosslinking, 6mm diameter

hydrogels were punched, washed twice with growth medium, and incubated in a CO₂ incubator at 37°C (Figure 2.1 C).

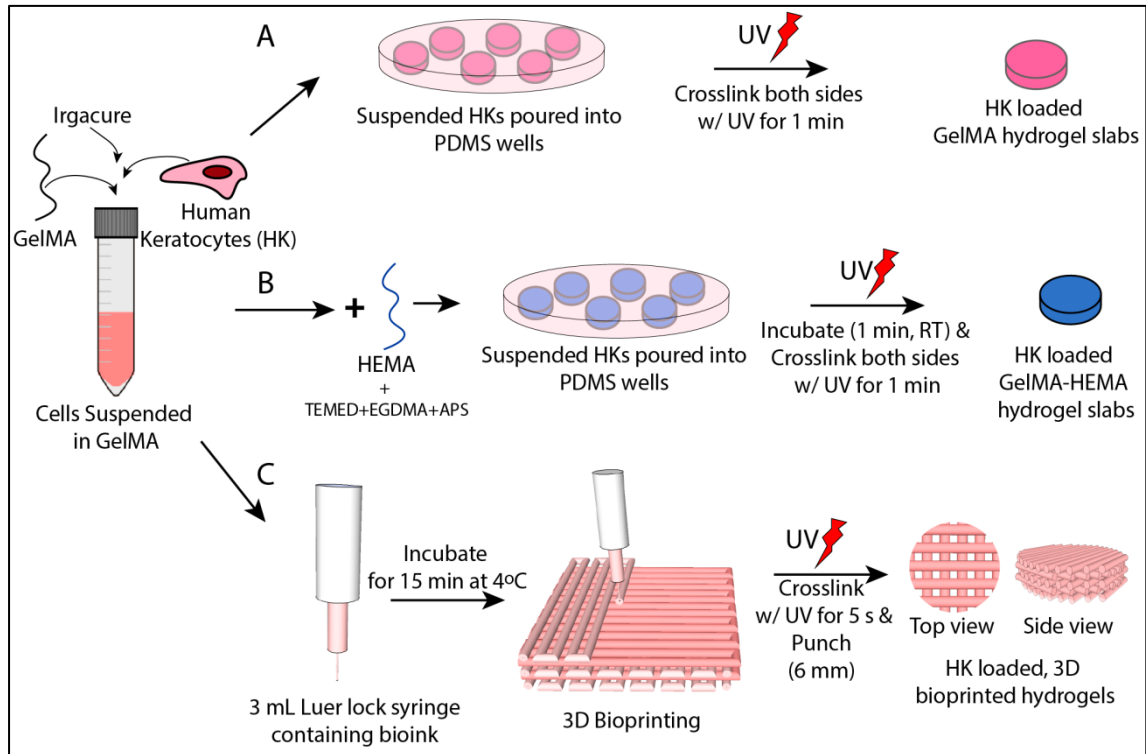


Figure 2.1: Schematic representation of preparation of human keratocytes (HK) loaded hydrogels. A) GelMA, B) GelMA-HEMA, and C) 3D bioprinted GelMA hydrogels.

2.2.8.6 Microscopical Studies

2.2.8.6.1 Live-Dead Cell Viability/Cytotoxicity Assay

Live-Dead Viability Assay was conducted to determine the viability of the cells (%) in the GelMA hydrogels on Days 1, 2, 7, 14, and 21. Briefly, after the medium was discarded samples were double stained with calcein AM (2 μ M in PBS), ethidium homodimer-1 (4 μ M in PBS) for 30 min at room temperature (RT). After incubation, samples were washed with PBS and examined under Zeiss LSM 800 or Leica DM 2500 (Germany) Confocal Laser Scanning Microscopies (CSLM). Live and dead cells were counted on the micrographs (n=3) by using ImageJ NIH software to

determine the viability of keratocytes (%) in the hydrogels according to following equation:

$$\text{Viability of cells (\%)} = \frac{\text{Live Cells (Green)}}{\text{Total Cells (Green+Red)}} \times 100 \quad (4)$$

2.2.8.6.2 Live Cell Imaging

GelMA15 hydrogels loaded with 1×10^6 cells/mL were incubated in growth medium until analysis. CellTracker green CMFDA was prepared in growth medium (15 mM) with all ingredients except serum. On Days 3 and 14 growth medium of the hydrogels were discarded and cells were incubated in the staining solution for 1 h. Then, staining solution was removed and hydrogels were incubated for 30 min in keratocyte growth medium. Finally, hydrogels were washed twice with PBS and put on small glass of live cell imaging setup and incubated in Live Cell Imaging solution containing amphotericin B (1 $\mu\text{g/mL}$), penicillin (100 UI/mL), streptomycin (100 $\mu\text{g/mL}$), and 4.5 g/L D-glucose. After placing an o-ring around the hydrogel, bigger glass of the setup was put closed tightly to ensure sterility (Setup components were purchased from H. Saur Laborbedarf, Germany) (Figure 2.2). Setup was connected to the temperature control device (Warner Instruments, USA) in order to keep the temperature at 37 °C. Samples were studied using Leica DM 2500 CLSM. Images were acquired at every 15 s for 5 h and avi. video was obtained at the end by using the software of the microscope.

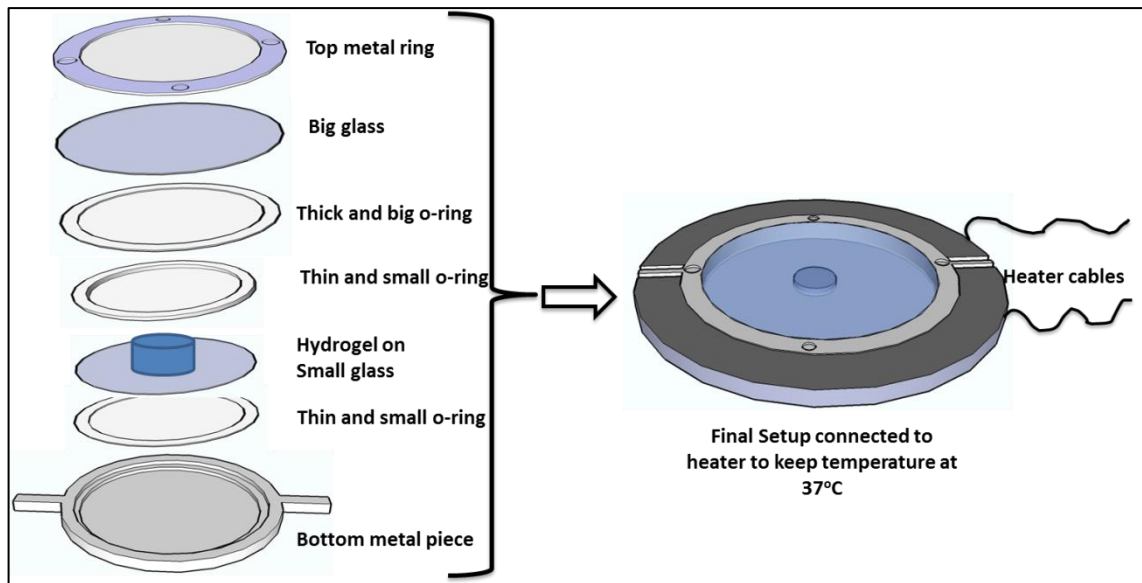


Figure 2.2: Live cell imaging setup. To ensure viability of the cells, a live cell imaging solution was used and the temperature of the setup was controlled by connecting to heating at 37 °C.

2.2.8.6.3 DRAQ5, DAPI and Phalloidin Staining

The growth medium in which the hydrogels were incubated was discarded and hydrogels were fixed directly with 4% (w/v) PFA for 30 min at RT. Membrane of the cells were permeabilized with 1% Triton X-100 (v/v, in PBS) for 5 min. For blocking, samples were incubated in 1% BSA (w/v, in PBS) at 37°C for 1 h. After blocking step, samples were incubated with solution containing FITC-labeled Phalloidin (1:200 v/v, in 0.1% w/v BSA in PBS) for 1 h at 37 °C to stain cytoskeleton. Samples were washed three times with 0.1% BSA and the nucleus of the cells were stained with DRAQ5 (1:1000 v/v in 0.1% BSA) for 1 h, at RT or with DAPI (1:1000 v/v in 0.1% BSA) for 10 min, at RT. Stained hydrogels were rinsed and stored in PBS until examination with CLSM.

2.2.8.6.4 Immunofluorescence Staining

Samples were treated as in section 2.2.8.6.3 until the blocking step. Primary antibodies of Collagen type I (1:100 v/v in 0.1% BSA), collagen type V (1:100 v/v in 0.1% BSA), Decorin (4.8 µg/mL in 0.1% BSA), biglycan (10 µg/mL in 0.1% BSA),

and α -SMA (1:100 v/v in 0.1% BSA) were prepared and after blocking steps hydrogels were incubated with these primary antibodies overnight at 4°C. Next day, samples were washed and incubated with either anti-rabbit or anti-mouse Alexafluor 488 secondary antibody (1:100 v/v in 0.1% BSA) (37°C, 1 h). Hydrogels were rinsed twice and incubated with DRAQ5 (1:1000 v/v in 0.1% BSA) for 1 h, at RT. Hydrogels were washed twice and stored in PBS until examination with CLSM.

Same gain value of the photomultiplier tube (PMT detector) was used to obtain all of the CLSM images. Images from each channel were obtained and intensities were measured without any threshold. To measure the intensities of the micrographs (n=3) Mean Gray Value function of NIH ImageJ program according to Lam *et al.*, (2010) was used. Intensity of the interested antibody was normalized to the signal intensity coming from DNA of the same image according to the following equation.

$$\text{Normalized Fluorescence Intensity} = \frac{I_{Ab}}{I_{DNA}} \quad (5)$$

where

I_{Ab} = Intensity of antibody

I_{DNA} = Intensity of DNA (from Draq5 stained image)

2.2.8.6.5 Scanning Electron Microscopy (SEM)

Cell free hydrogels were frozen at -80°C and lyophilized. Cell loaded hydrogels were fixed with 4% PFA at RT for 30 min, washed with cacodylate buffer (pH 7.4), frozen at -80°C and lyophilized. Dry samples were coated with Au–Pd under vacuum and examined with a scanning electron microscope (SEM) (JEOL, JSM-6400, USA) at 5–20 kV.

2.2.8.7 Mechanical Properties of Cell Loaded and Cell Free Hydrogels

Cell loaded (1×10^6 cells/mL) and cell free hydrogels were prepared and tested mechanically under compression (n=5) by using 10 N load cell (Univert, Canada) at a displacement rate of 1 mm/min speed at room temperature. Hydrogels were tested on Days 1, 7, 14 and 21 and kept in growth medium until testing. For characterization of GelMA, GelMA-HEMA and HEMA hydrogels, they were tested

under compression (n=5) by using 50 N load cell (Shimadzu AGS-X, Japan) at a displacement rate of 1 mm/min speed at RT.

Compressive moduli of the scaffolds were calculated according to Harley et al. (2007) from the slope of the very first linear region of the stress strain curve according to the following equations:

$$\text{Stress: } \sigma = \frac{F}{A} \quad (6)$$

$$\text{Strain: } \varepsilon = \frac{\Delta l}{l} \quad (7)$$

$$\text{Compressive Modulus: } \frac{\sigma}{\varepsilon} \quad (8)$$

where

F: Applied force, A: Cross-sectional area, l: Initial sample length, and Δl : Displacement

2.2.8.8 Transparency of the Hydrogels

Cell loaded (1×10^6 cells/mL) and cell free hydrogels were transferred to 96 well plates on Days 0, 1, 7, 14, and 21. Fresh medium was added on the hydrogels and wells containing only growth medium served as the blank. Samples were scanned in the 250-700 nm range by using a Multiscan UV Visible spectrophotometer (Thermo Scientific, USA). Average value of blanks was deducted from the sample readings and transmittance values were obtained. By using the same settings, transparency of the hydrogels after enzymatic treatment was also measured every 2 h. The UV-Vis spectrum of natural cornea was used as the positive control (Mallet and Rochette, 2013).

2.2.8.9 MMP Activity of the Cell Loaded Hydrogels

SensoLyte[®] 520 Generic MMP Assay Kit (Fluorimetric) was used to detect MMP activity in supernatant of cell culture media. Assay was performed according to the manufacturer instructions. Briefly, cell culture media was collected at every media change, centrifuged for 15 min at 1000X g, +4°C, and stored at -80°C until use. At

the end of 21 days of incubation, collected culture media was thawed and incubated in 1 mM 4-aminophenylmercuric acetate (APMA, Component C of the kit that is diluted with Component D) for 3h at 37°C to activate the MMPs. 50 µL/well of sample was loaded into 96 well plates, 50 µL/well MMP substrate solution (Component A of the kit that is diluted with Component D) was added on them and incubated for 1 h, at RT. Component E was added (50 µL/well) on the wells to stop the reaction and then fluorescence intensity was measured at E_x and $E_m = 490$ nm and 520 nm. Assay buffer containing wells (Component D) served as substrate control. Relative fluorescence units (RFU) were obtained by subtracting control substrate reading from all readings. MMPs activity in µM was calculated according to a calibration curve plotted by using 5-FAM-Pro-Leu-OH standard (Component B) (Appendix C). Calculated MMPs activity was divided into total protein concentration of each sample at each time point to normalize the results.

Total protein in the supernatant of cell culture media was detected by Coomassie Plus (Bradford) Assay Kit. Briefly, 10 µL of culture media was mixed with 300 µL of Coomassie Plus Reagent in a 96 well plate, incubated for 10 min at RT and absorbance was measured at 595 nm. Absorbance of the blanks was subtracted from the readings. Total protein concentration (µg/mL) was calculated according to a calibration curve plotted by using BSA standard (Appendix D).

2.2.9 In vivo Studies

GelMA (15%, w/v) (GelMA15) was dissolved in growth medium in the presence of Irgacure (0.5%, w/v) and resultant mixture was added on the PDMS template (16 mm in diameter and 300 µm or 150 µm in thickness). Solution was crosslinked for 5 s with a UV source (OmniCure) (15 mW/cm², at 365 nm) at 3 cm distance. Hydrogel was punched with 5 mm or 4 mm diameter punches and put in medium until implantation (Table 2.2).

The following *in vivo* studies were performed by Prof. Dr. Ayşe Burcu, Dr. Hande H. Telek, and Dr. Firdevs Örnek in compliance with the ethical committee report (No: 0045) granted by Ankara Education and Research Hospital, Animal Experiments Local Ethics Committee (Appendix E, Figure A.5) . Two healthy 20 week-old New Zealand Rabbits weighing 3 kg were used as a pre-clinical test to

evaluate the in vivo performance of the hydrogel. Protocol for the labeling of the rabbits was according to Figure 2.3. For implantation, rabbits were anesthetized with 50 mg/mL ketamine base and a lamellar dissection was made in three eyes of the rabbits and one eye was used as blank control. GelMA15 hydrogels were implanted into a mid-stroma cornea pocket (Figure 2.4) with or without suture fixation (Table 2.2). Netildex™ anti-infective and anti-inflammatory eye drop was started following implantation and used for 1 week as 5 times a day. On Day 7, rabbits were anesthetized with ketamine and examined with slit lamp to ensure clarity of the cornea.

On Day 7 Maxidex® eye drop was started as 4 times a day to reduce the redness and the foreign body reaction of the eye and used until the end of the observations. Upon vascularization, one sub-conjunctival dose of anti-VEGF (Eyelea) was used in the 3rd week.

Right eye of the first rabbit was used as blank for 7 weeks and then operated to implant anti-VEGF absorbed GelMA hydrogel (2r=4 mm, h= 150 μm) with no suture fixation. However, rabbits removed the construct and this type, therefore, is not given in Figure 2.3 and Table 2.2.

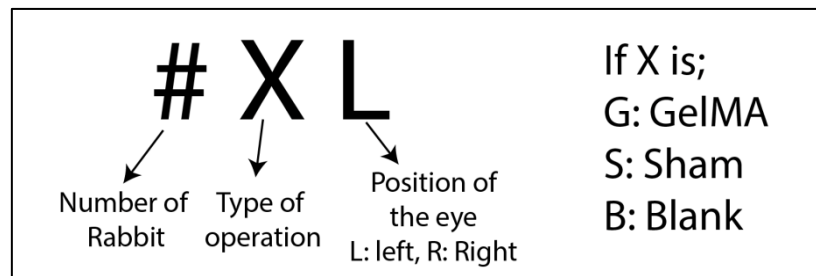


Figure 2.3: Labeling protocol of the rabbits used in pre-clinical studies.

Table 2.3: Sum of the abbreviations, operation type, GelMA dimensions, and observation period.

Rabbit #	Abbreviation	GelMA Implantation D: diameter, h: height	Observation Duration
Rabbit 1, Left Eye	1GL, Suture fixed	Yes, D = 5 mm, h = 300 μ m	15 weeks
Rabbit 1, Right Eye	1BR, No operation	No	7 weeks
Rabbit 2, Left Eye	2SL, No suture fixation	No	8 weeks
Rabbit 2, Right Eye	2GR, No suture fixation	Yes, D = 4 mm, h = 150 μ m	8 weeks

2.2.9.1 Schirmer's Test

Schirmer's test was done to assess regeneration of the tear film. For this a Schirmer's paper is placed on the lower eyelid for 5 min. The amount of wetting due to tear production (the tear travels on the paper strip) is measured in millimeters.

2.2.9.2 Sodium Fluorescein Staining

Sodium fluorescein staining was done to assess integrity of the cornea. Briefly, sodium fluorescein paper was applied to the surface of the eye and the dye disperses throughout the surface with the aid of tears. Any deterioration on the surface is seen green under cobalt blue light instead of yellow.

2.2.9.3 Histological Examination

Corneas of 1GL (on Day 106), 2GR (on Day 57), and 2SL (on Day 57) were removed after the rabbits were sacrificed with an overdose of ketamine. Corneas were embedded in OCT compound, frozen at -80oC and sectioned (6 μ m) by using a freezing microtome (Leica CM1510 S, Germany) (Figure 2.3). Cryostat sections were stained with hematoxylin and eosin by Prof. Dr. Gökhan Gedikoğlu, Hacettepe University. Sections were examined under Zeiss Axio Imager M2 (Germany) fluorescence microscope.

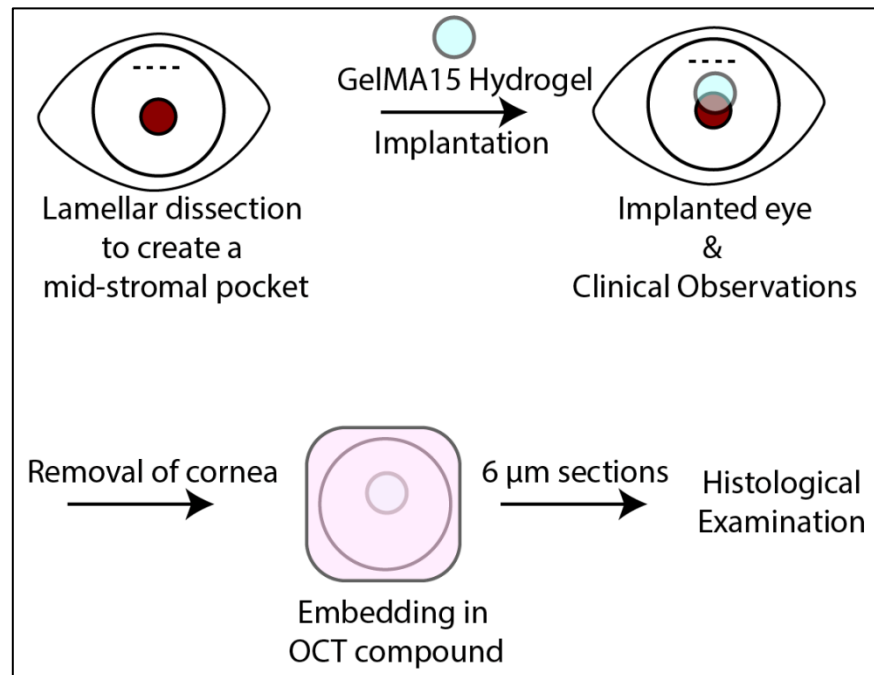


Figure 2.4: Workflow for *in vivo* studies.

2.2.10 Statistical Analysis

Statistical analysis was performed with GraphPad Prism program (Version 6.01) using two-way analysis of variance (ANOVA) with Tukey's post hoc test or Student's t test was used depending on number of comparisons. $p \leq 0.05$ was reported as statistically significant. Data is presented as mean \pm standard deviation (SD) (n=3) and plotted using GraphPad Prism or Microsoft® Excel (Office 2010).

CHAPTER 3

RESULTS AND DISCUSSION

In this study, native microstructure of the corneal stroma is mimicked by 3D bioprinting of cell loaded methacrylated gelatin (GelMA) hydrogels. This study was conducted in four phases: 1) GelMA was produced from the reaction of gelatin and methacrylic anhydride and characterized through NMR. Optimum GelMA concentration and cell loading density were determined, 2) pHEMA was incorporated into the structure to improve the mechanical strength of the GelMA hydrogels, 3) 3D bioprinting was performed at optimized conditions of GelMA to mimic the internal organization of corneal stroma, and 4) In vivo performance of the GelMA hydrogels were tested on rabbits with a short study.

3.1 GelMA Hydrogels

GelMA was synthesized from the reaction of methacrylic anhydride (MA) and porcine skin gelatin (Section 2.2.1). Aqueous solution of GelMA had the ability to be crosslinked in the presence of a photoinitiator and UV exposure that yields a highly stable and transparent hydrogels suitable for corneal tissue engineering applications. In the first phase of this study, GelMA concentration and cell loading density were optimized by *in situ* and *in vitro* tests.

3.1.1 ¹HNMR of GelMA

Degree of methacrylation (DM) is defined as the ratio of number of methacrylated groups attached to gelatin to the number of amine groups (lysine, hydroxylysine) of unreacted gelatin prior to the reaction (Hoch et al., 2012). MestreNova NMR analysis program (version 6.0.2, Mestrelabs Research, SL, Santiago de Compostela, Spain) was used to calculate DM of the GelMA. Firstly, NMR spectra were normalized to the phenylalanine signal (6.9-7.5 ppm) which is proportional with the

concentration of the gelatin and is not reacted during methacrylation. Then, the integrated areas of lysine methylene signals (2.8-2.95 ppm) of gelatin and GelMA were obtained and DM was calculated according to equation 1. NMR results showed the ability to methacrylate gelatin to the extent of about 70% DM in this study (Figure 3.1).

$$DM (\%) = \left(1 - \frac{\text{Peak area (Lysine methylene of GelMA)}}{\text{Peak area (Lysine methylene of non-modified gelatin)}}\right) \times 100 \quad (9)$$

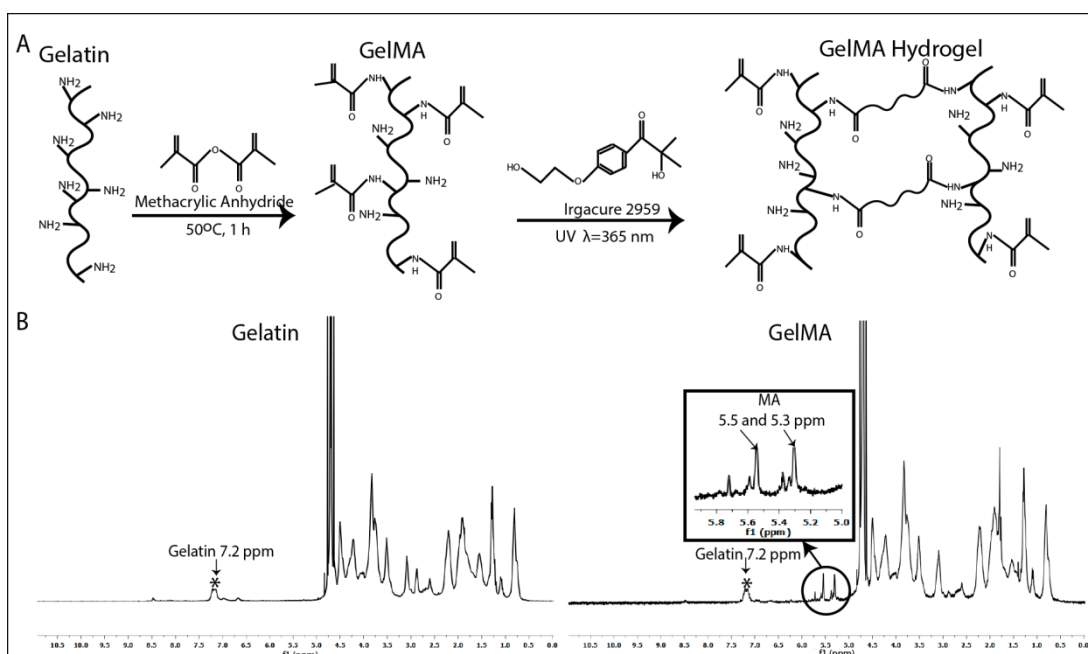


Figure 3.1: ^1H -NMR spectra of gelatin and gelatin methacrylamide prepared in D_2O , RT. A) Methacrylation of gelatin to form GelMA and crosslinking of GelMA to form GelMA hydrogel by UV exposure. B) ^1H -NMR spectra of gelatin and methacrylated gelatin. Inset shows the expanded region between 5 and 6 ppm. Peaks formed in this region indicate the incorporation of double bonds into gelatin methacrylation. Asterisk (*) shows the peaks due to aromatic residues of gelatin that are used in the normalization of the peaks.

3.1.2 Equilibrium Water Content of Hydrogels

Hydrogels are 3D hydrophilic polymeric networks which may absorb water up to a thousand times their dry weight. Mechanical characteristics of the hydrogels and diffusion of the solutes through them are significantly affected by the water content (Peppas et al., 2006). In this study, effects of uncrosslinked methacrylated gelatin concentration and UV exposure duration on equilibrium water content were examined. As GelMA concentration increases water content decreases up to 10% concentration and water content of the hydrogels was similar at 15% GelMA concentration regardless of the UV duration (Figure 3.2). Water content changes with UV duration, as well. Lowest UV duration (1 min) yielded the highest water content for all concentrations. Water content of the 5% and 8% hydrogels were similar when 1.5 and 2 min UV were applied suggesting crosslinking of all the reactive groups. Increase in UV duration decreased water content in 10% and 15% GelMA hydrogels. UV duration of 1 min was chosen for the rest of the study in order to minimize the potential adverse effects of UV exposure might have on the cells and for the minimal restriction for their migration, proliferation and metabolism. Water retention capacity of the hydrogels is highly influenced with the polymer and crosslinking densities; tighter 3D networks due to high crosslinking density are expected to retain lower amount of water.

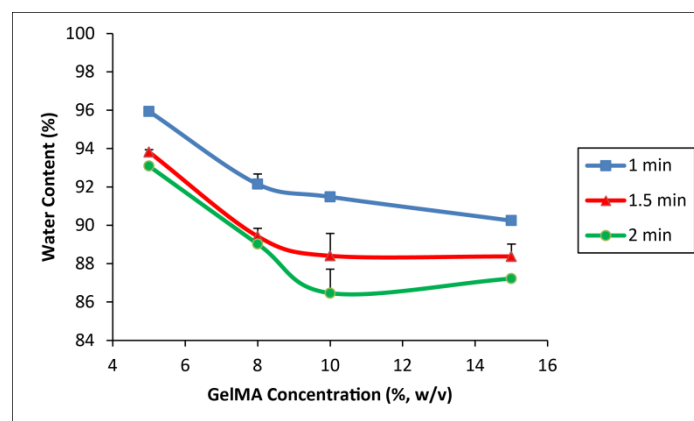


Figure 3.2: Effect of uncrosslinked GelMA concentration and UV exposure duration on the water content of the GelMA hydrogels. n=3.

3.1.3 In Situ Degradation of GelMA Hydrogels

In vitro conditions were mimicked by incubating GelMA hydrogels in PBS (pH 7.4, 10 mM) for three weeks. A high rate of weight loss was observed in the first day of incubation (up to 30%, for GelMA-5 and GelMA-8) and it was lower in the following periods (Figure 3.3). Initial high weight loss can be explained by the leaching out of the uncrosslinked GelMA molecules. Extent of degradation changed with the GelMA concentration in the solution: Degradation rate was high when GelMA concentration is low and vice versa, when GelMA concentration is high. This is because the high uncrosslinked GelMA concentration resulted in more reactive groups which enhanced the crosslinking density and stability of the hydrogels when exposed to same UV duration. This result is in agreement with the previous results obtained with same hydrogels where increased concentration or UV duration resulted in decrease in water content which is related with the crosslinking density of hydrogels created with different parameters (Figure 3.2). Additionally, GelMA-5 and GelMA-8 hydrogels were too fragile to handle and degraded rapidly supporting the above mentioned results. GelMA-10 and GelMA-15 hydrogels, therefore, were used in the rest of the studies due to their better stability compared to other concentrations.

Scaffold stability under biological conditions is an important aspect for tissue engineering studies until regeneration of the tissue. The degradation rate of the scaffold should be in balance since higher degradation rate may result in fail of supporting cells until they synthesize their own extracellular matrix (ECM) and lower rates may cause recognition of the material as foreign leading to inflammation (Williams *et al.*, 1999).

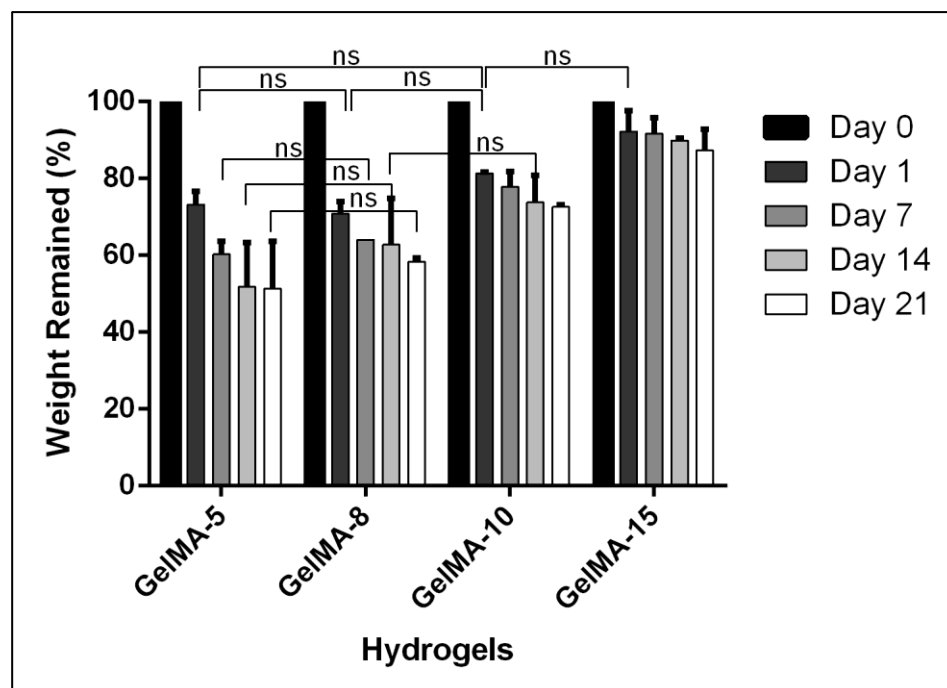


Figure 3.3: Degradation of GelMA hydrogels for up to three weeks in PBS (pH 7.4, 10 mM) at 37°C. Uncrosslinked GelMA concentrations of 5%, 8%, 10%, and 15% were abbreviated as GelMA-5, GelMA-8, GelMA-10 and GelMA-15, respectively. n=3. ns: non significant.

3.1.4 Enzymatic Degradation of GelMA Hydrogels

In vivo conditions in terms of enzymes were mimicked and the stability of the hydrogels was studied in the presence of collagenase type II, a frequently used collagenase type for degradation profiles in the literature. Degradation profile of GelMA-10 and GelMA-15 was studied by incubating them in four different collagenase concentration solutions. Results clearly show that, GelMA-10 hydrogels were affected more than the GelMA-15 ones, supporting the *in situ* degradation results. Even the lowest collagenase concentration caused a significant weight loss (ca. 25% in 4 h) in GelMA-10 hydrogels (Figure 3.4 A). Moreover, they become quite fragile after the first hour of incubation. GelMA-15 hydrogels were more stable and even in the highest collagenase concentration 70% of the weight remained after the 4 h treatment. As a result, GelMA-15 hydrogels are more stable than GelMA-10 hydrogels under *in situ* and enzymatic degradation conditions. Similar results were reported in the literature. Hutson et al. (2011) incubated 10% and 15% GelMA

hydrogels in 2.5 U/mL collagenase Type II and reported that 10% GelMA hydrogels were degraded totally within 12 h while 15% hydrogels survived for up to 36 h. In another study, Benton et al. (2009) incubated 10% GelMA hydrogels in 1 U/mL and 2.5 U/mL collagenase solutions and a higher degradation rate was reported with higher collagenase concentration. These show that the less concentrated hydrogel is weaker, the higher enzyme concentration and longer duration degrades the hydrogel more extensively.

SEM images of the hydrogels degraded with 4h incubation in PBS and 10 U/mL (highest) collagenase clearly show that the pores and whole shape of the GelMA-10 hydrogels compressed compared to open pores of hydrogels incubated in PBS (Figure 3.4 B). Effect of collagenase on GelMA-15 hydrogels was minimal and appearance of hydrogels incubated both in PBS and collagenase were similar. Results were reasonable since GelMA-10 hydrogels lost 90% of their initial weight after 4h incubation in 10 U/mL collagenase while GelMA-15 ones lost only 30% (Figure 3.4 A).

In vivo and clinical degradation conditions are more closely mimicked by the enzymatic degradation tests since the scaffold used for the treatment of corneal defects faces hydrolysis through matrix metalloproteinases (MMPs) and matrix degrading enzymes produced by corneal fibroblasts in addition to hydrolysis. Corneal fibroblasts, called as keratocytes, participate in collagen fibril remodeling which is vital for transparency and other crucial functions of the cornea (Hao et al., 1999). Researchers reported no detectable collagenase (MMP-1) activity on healthy corneas but a significant activity was reported in diseased ones (Riley et al., 1995). Therefore, when gelatin base scaffolds are implanted scaffolds will be degraded by time due to MMP activity of the keratocytes.

Transparency of the hydrogels were studied after PBS and collagenase treatments and results show that regardless of the treatment type, transparency of the hydrogels did not change significantly and were comparable with that of native cornea values (Figure 3.4 C). Transparency is one of the most important properties of the corneal tissue which is around 90% at 700 nm (visible region). Any scaffold intended to be used for the treatment of corneal defects should be optically clear and must retain its transparency in *in vivo* conditions when exposed to enzymatic degradation.

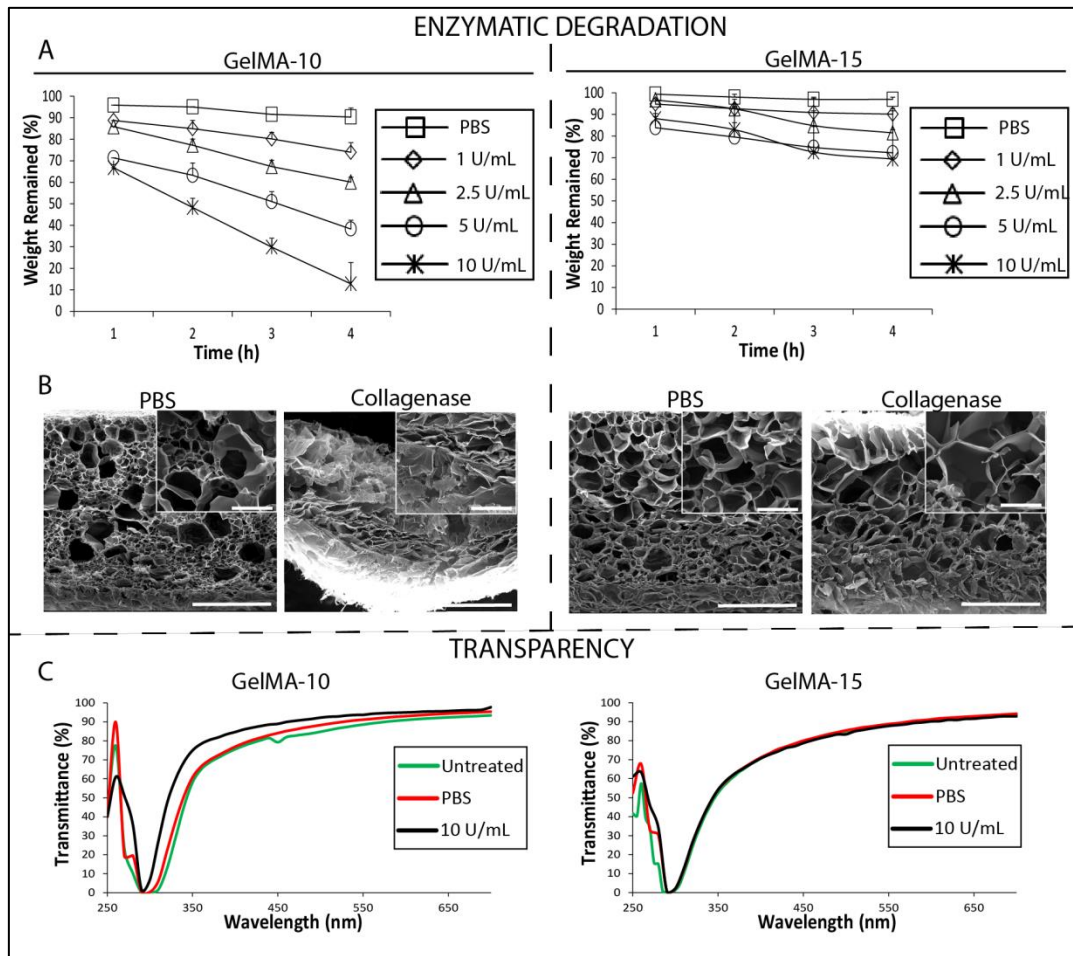


Figure 3.4: Enzymatic degradation and resultant changes in the appearance and transparency of the GelMA hydrogels. A) Enzymatic degradation profiles (weight retention) of hydrogels at 4 different collagenase Type II concentrations. B) SEM micrographs of hydrogels after PBS and 10 U/mL collagenase type II incubation for 4 h. Scale bars are 500 μm and 100 μm for main and inset figures, respectively. C) Transparency of untreated hydrogels, after incubation in PBS and 10 U/mL collagenase for 4 h.

3.1.5 In Vitro Studies

3.1.5.1 Flow Cytometry of Human Keratocytes

In this study flow cytometry was used to determine the phenotype of the isolated human keratocytes to see if they retained their specific surface markers. Human keratocytes between passages 5 and 15 were used throughout the study and p11 cells

were used for flow cytometric analysis to obtain a representative data. Figure 3.5 shows the unstained and isotype control of the samples. The fluorescence intensities were similar at FL1 (Alexa Fluor 488) and FL4 (Alexa Fluor 647) channels. Histograms showed that more than 98% of the cells were positive for mesenchymal stem cell markers CD73 and CD90 (right side of the red line) as reported in the literature (Choong *et al.*, 2007) and the fluorescence intensities were significantly higher (10^5) than the unstained and isotype controls (left side of the red line). On the other hand, CD34 and CD45 (hematopoietic stem/progenitor cell and lymphocyte cell markers, respectively) were negative since these surface markers were not expressed by corneal keratocytes (Choong *et al.*, 2007). Therefore, it was concluded that isolated human keratocytes carry keratocyte markers and could be used in this study to reconstruct the stromal layer of the cornea.

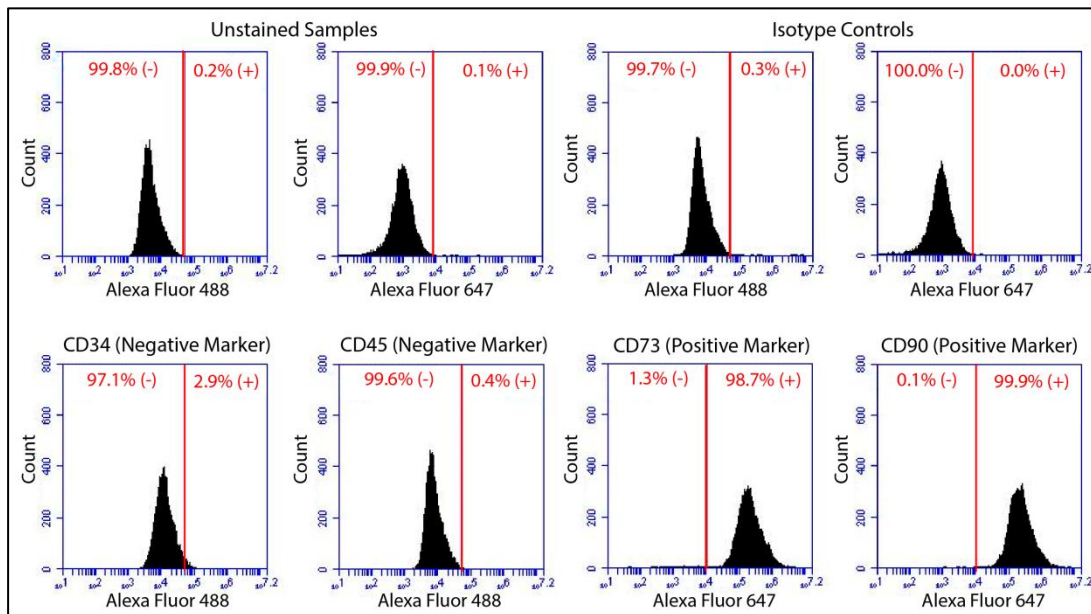


Figure 3.5: Histograms of unstained samples, isotype controls, negative markers (CD34 and CD45, hematopoietic stem/progenitor cell and lymphocyte cell markers, respectively), and positive markers (CD73 and CD90, mesenchymal stem cell markers) after flow cytometry analysis. Red line was drawn according to data obtained from isotype controls to differentiate negative (left) and positive (right) sides of the plot.

3.1.5.2 Optimization of Cell Number in Hydrogels

In order to optimize the number of cells in the hydrogels, achieve better connection between them and preserve their keratocyte functions, cells at different densities (5×10^5 , 1×10^6 , 2.5×10^6 , and 5×10^6 cells/mL) were loaded into the hydrogels. 10% GelMA solution loaded with 2.5×10^6 and 5×10^6 cells/mL did not yield a proper hydrogel, therefore, Figure 3.6 shows only the GelMA-15 hydrogels loaded with 2.5×10^6 and 5×10^6 cells/mL and stained with Live Dead viability assay on days 1 and 7. Cells were observed to interconnect with each other through their dendritic processes starting on day 1 and more connection was observed for hydrogels with 5×10^6 cells/mL. Although interconnectivity increased with seeded cell density and more than 90% of the cells were alive in the hydrogel, too high cell density resulted in unstable and fragile hydrogels. High cell density probably interfered with crosslinking initiated by UV exposure. Then the density was decreased to 5×10^5 and 1×10^6 cells/mL and cells were loaded in both GelMA-10 and GelMA-15 hydrogels. Live-Dead assay showed that more than 90% of the cells were alive and some of them elongated even on Day 1 for both concentrations (Figure 3.7 A and C). They were distributed homogeneously at all depths of the hydrogel and color coded images, for different color cells at different depths, show this (Figure 3.7 B). Z stack projections of the same images given below each color coded image also prove the homogeneous distribution of cells throughout the depth of the hydrogel. Stability of the hydrogels at both cell densities was comparable but more cells could interact and elongate when cell density was 1×10^6 cells/mL (Figure 3.8). This cell density, therefore, was chosen in the following studies.

Cells elongate through their extensions called lamellipodia and filopodia and continuously monitor their environment. Thus, to form stable contacts with the surrounding cells and the extracellular matrix with filopodia, transmembrane proteins like cadherins and integrins are used. However, when the adhesion between the cells and filopodia of another cell fails, they retract (Hoffmann and Schäfer 2010). Corneal keratocytes or fibroblasts are mesenchymal derived cells and are sparsely dispersed in the stroma. Additionally, they are interconnected with each other through dendritic processes and form a cellular network. In case of an injury, keratocytes turn into repair phenotypes by losing their quiescence appearance or

undergo cell death (West-Mays and Dwivedi 2006). Thus, in order for them to preserve their keratocyte functions needed for the transparency of cornea, they should be interconnected with each other.

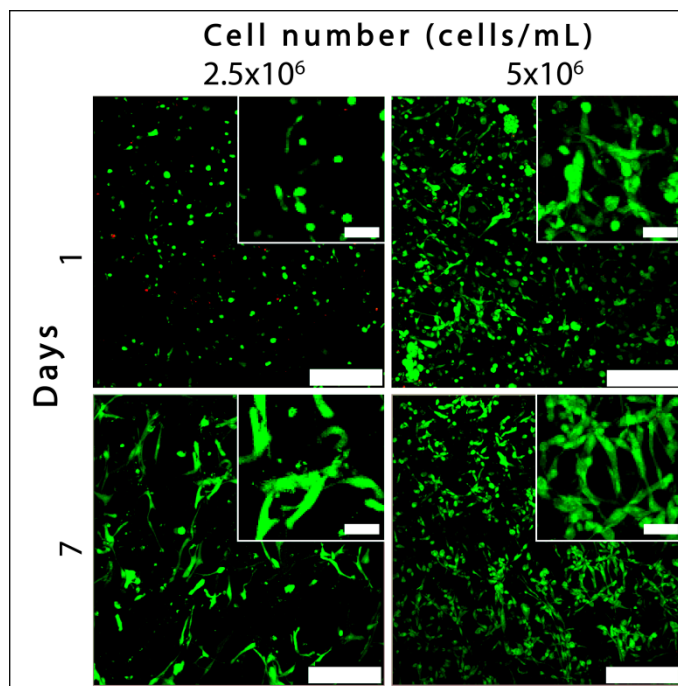


Figure 3.6: CSLM images of Live-Dead assay of keratocytes in GelMA hydrogel on Day 1 and Day 7. Scale bars: 250 μm

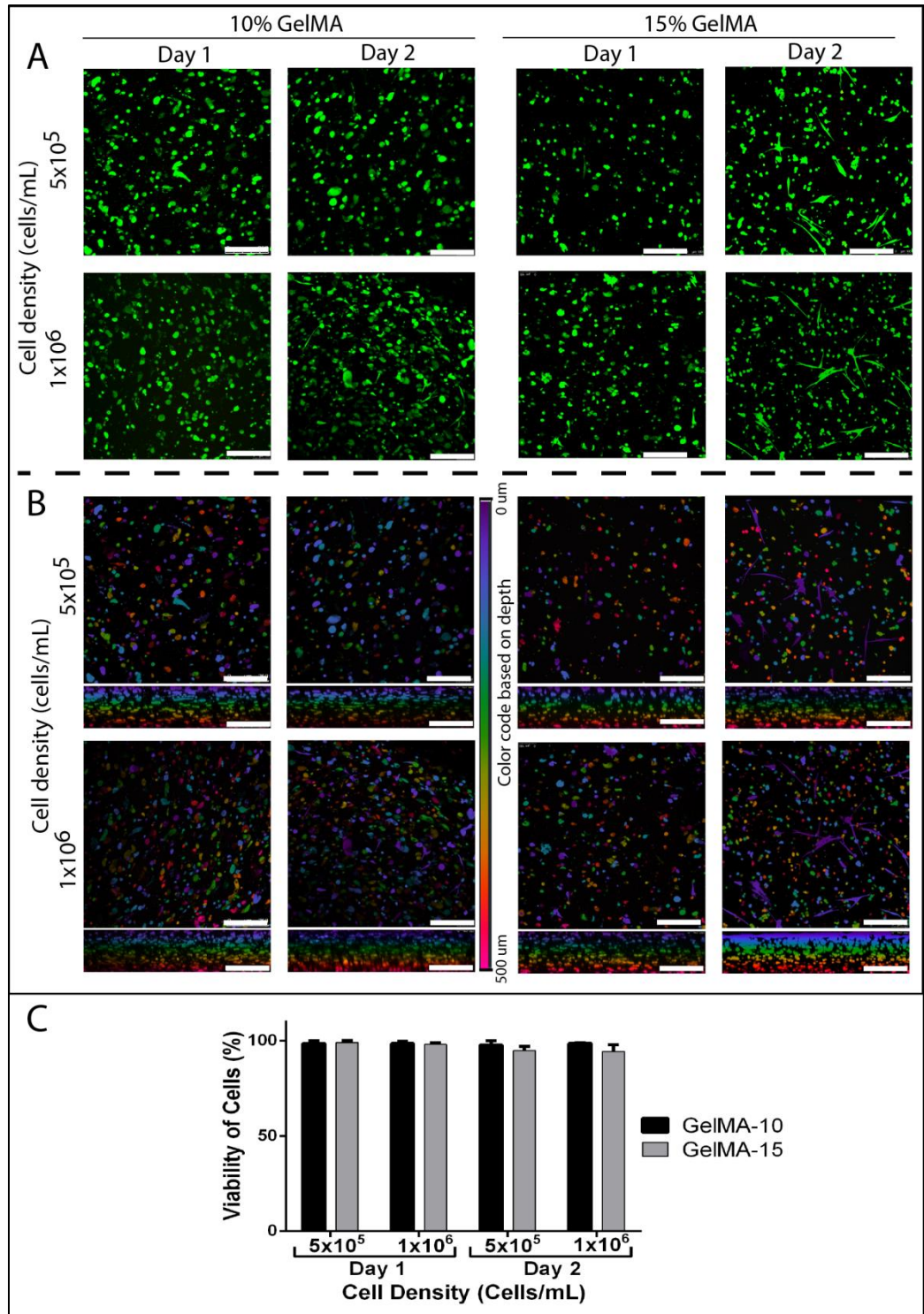


Figure 3.7: CLSM images showing results of Live Dead Cell Viability Assay of GelMA hydrogels on Days 1 and 2. A) Live-Dead assay showing dead (red, ethidium homodimer-1) and live cells (green, calcein). B) Color coded depth profile of the same images showing the distribution of live keratocytes in GelMA hydrogels (purple at the surface and pink at the bottom). Z stack projection is given below each color coded image. Scale bars: 250 μ m. C) Quantitative analysis showing percent viability of cells.

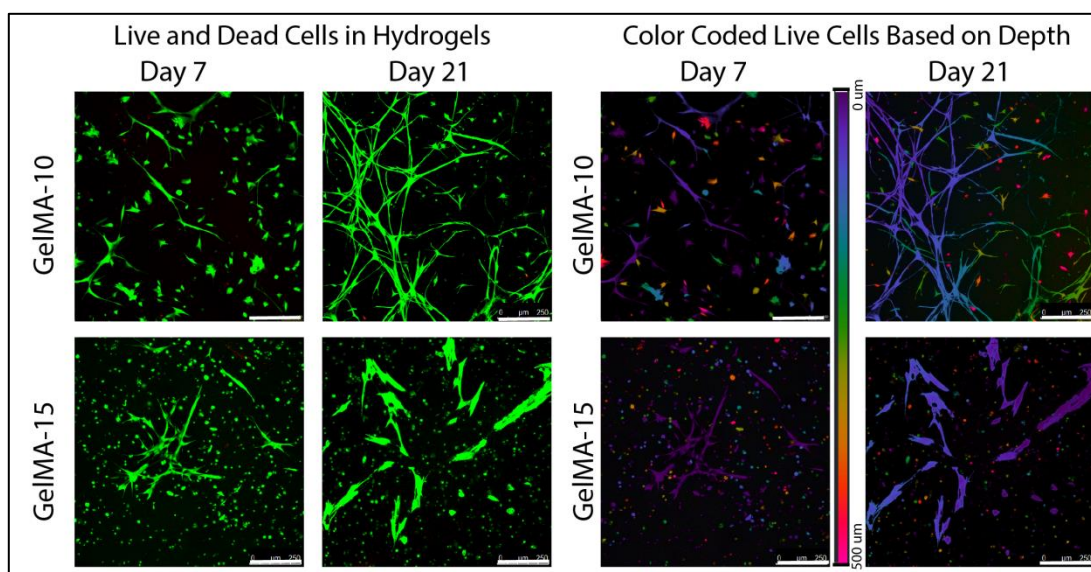


Figure 3.8: CLSM images showing results of Live Dead Cell Viability Assay of GelMA hydrogels on Days 7 and 21. A) Live-Dead assay with red showing dead (ethidium homodimer-1) and green showing live cells (calcein). B) Color coded depth profile of the same images showing the distribution of live keratocytes in GelMA hydrogels (purple at the surface and pink at the bottom). Scale bars: 250 μm .

It was noticed that, elongated cells were mostly located closer to the surface of the hydrogels as can be seen in the color coded images (purple at the surface). Most probably the cells which were homogeneously distributed during hydrogel formation migrated toward the surface of the hydrogels which is richer in growth medium and oxygen. Day 21 data of GelMA-10 hydrogels (Figure 3.8) was examined in more detail in Figure 3.9. Color coded images indicate that there were cells at different planes but only the ones close to the surface were elongated on Day 21 (Figure 3.9 A). Cells in the depth of the hydrogel were also alive but not elongated as much as those on the surface. In order to study the behavior of the cells, hydrogels were cut vertically and cross section images were obtained on Day 1 and 21 (Figure 3.9 B). Cells were homogeneously distributed in the hydrogel on Day 1. However, cells were observed to be accumulated and elongated mostly at the surface of the hydrogels. There were also cells within the cross-section of the hydrogel but they were in round shape. Thus, these results showed that, cells freely migrate inside the hydrogel, moved reach regions rich in nutrients (growth medium and oxygen). Therefore, a

dynamic environment in a bioreactor would help the transport of oxygen and medium within the hydrogels and achieve a more homogenous distribution of the cells within it. Live cell imaging, therefore, was done, in order to observe and study migration, filopodia formation and elongation of the cells.

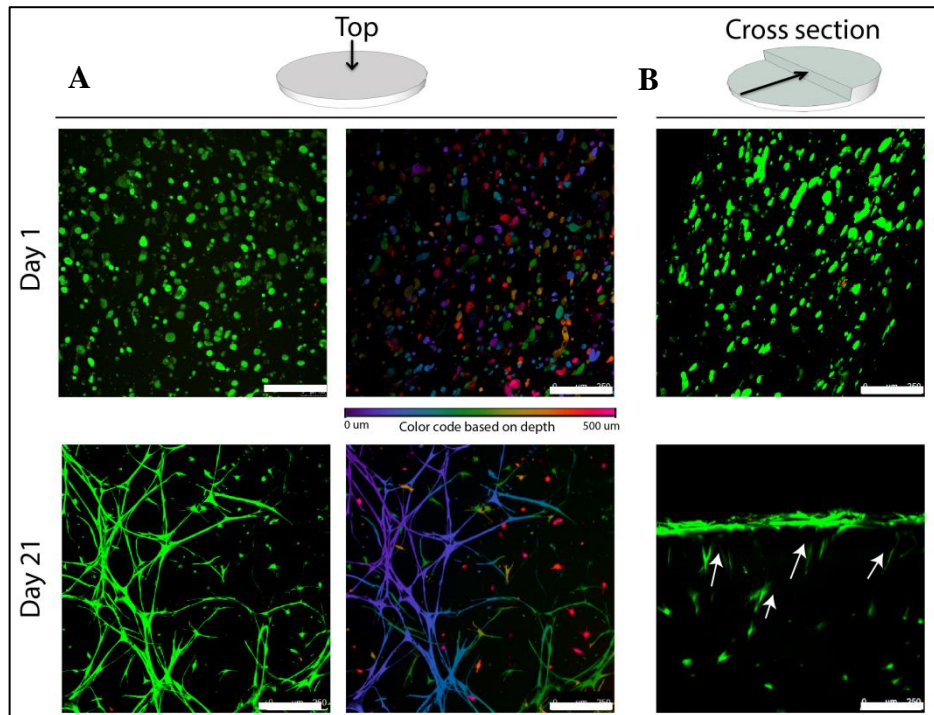


Figure 3.9: CLSM images showing results of Live Dead Cell Viability Assay of GelMA10 hydrogels on Day 1 and 21. A) Live-Dead assay with red showing dead (ethidium homodimer-1) and green showing live cells (calcein). Color coded depth profile of the same images showing the distribution of live keratocytes in GelMA hydrogels (purple at the surface and pink at the bottom). B) Live-Dead assay of the cross-section of the same hydrogel. The sketches represent the imaging direction of the hydrogels. Scale bars: 250 μm .

3.1.5.3 Live Cell Imaging

Imaging live cells by tagging fluorescent proteins (FP), staining with live cell dyes or other labeling methods for the proteins of interest has become an important development in cell biology. For live cell imaging purposes, cells were stained with CellTracker Green, a fluorescent dye that freely passes through cell membranes and are retained in the cells for several generations and fluoresce for up to 72 h. Since the

dye is not toxic it does not affect cell proliferation or viability. In order to be able to study the movement of the cells loaded in 10% GelMA hydrogels 1×10^6 cells/mL incubated in CellTracker Green dye for 1 h. They were then cultured in human keratocyte medium for 30 min and placed into the live cell imaging setup (Figure 2.2). Days 3 and 14 were selected to observe the movement of the cells as the beginning of elongation and the most elongated form of the cells, respectively (Figure 3.10). Since there were cells in different depths of the hydrogel, only one plane (depth) was chosen and observed for 5 h. Results showed that cells were able to elongate and freely move within the hydrogel. During the 5 h observation new extensions were formed by the cells while some of the cells changed shape. It can be deduced from these results that GelMA hydrogel is able to provide a natural environment for the cells where they interact with each other.

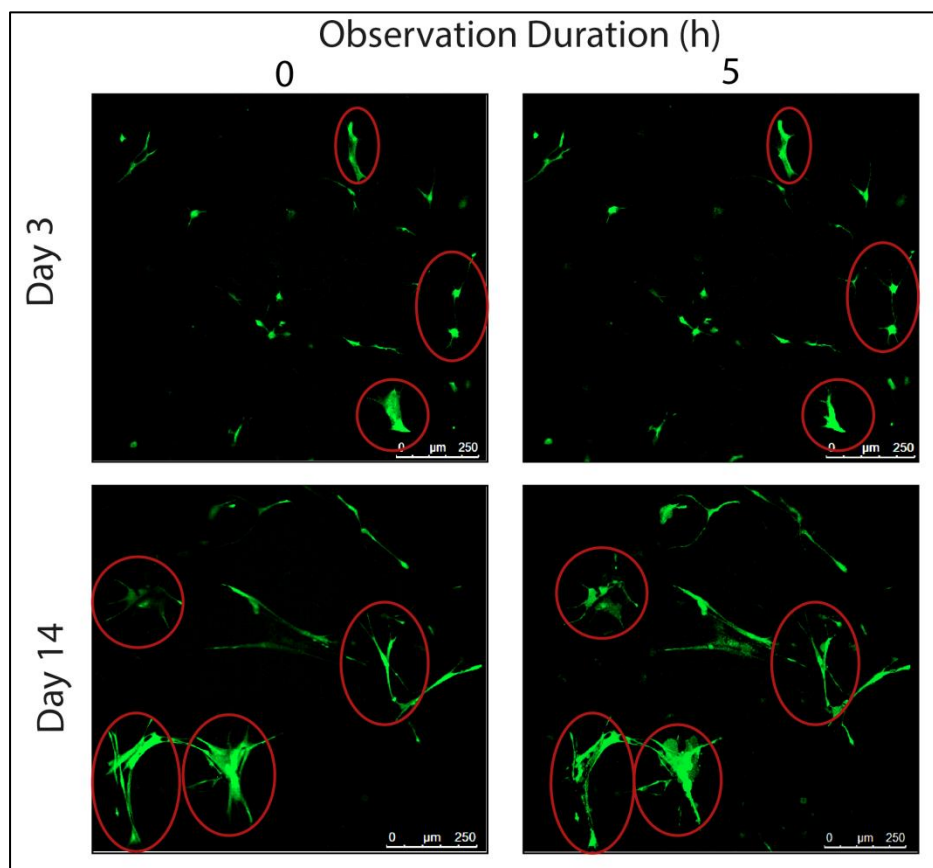


Figure 3.10: Live cell imaging of the HK in GelMA hydrogels on Days 3 and 14. The cells on Day 3 were quite compact while on Day 14 they were branched. Red circles specifically point out the cells which change form during the 5 h observation period. Scale bar is 250 μm .

3.1.5.4 Cell Proliferation in the Hydrogels with Different Stiffness

Cell loaded GelMA-10 and GelMA-15 hydrogels were tested with Alamar Blue cell proliferation assay in order to compare the proliferation rate of the cells in the hydrogels with different stiffness. Figure 3.11 shows that, cell number in both of the hydrogels increased significantly and continuously during 21 days of incubation. The number of cells (or Reduction (%) values) in both hydrogels was comparable; there was no statistically significant difference except for the Day 7 where the cell number was higher in GelMA-10 hydrogels than GelMA-15. The lower cell number in the GelMA-15 hydrogel at the very first week may be due to the higher crosslink density due to 50% higher polymer concentration than GelMA-10 hydrogels. But in both hydrogels cells proliferated and their number increased continuously due to the significant biocompatibility of them.

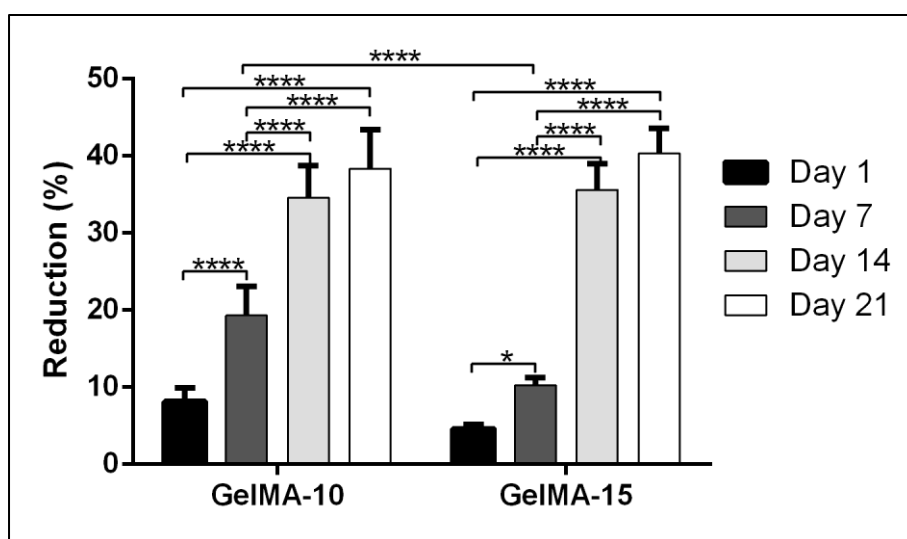


Figure 3.11: Proliferation (as indicated by Reduction % obtained with Alamar Blue test) of human keratocytes in GelMA10 and GelMA15 hydrogels over 3 weeks. * $p < 0.05$, and **** $p < 0.0001$.

3.1.5.5 Cell Morphology Analysis with DAPI/Draq5-Phalloidin Staining and SEM

As was conclusively shown with the Live-Dead viability assay, human keratocytes were alive in the hydrogels and started elongation even on Day 1. In order to study morphology of the cells IN the GelMA-15 hydrogels and to compare them with the cells seeded ON the GelMA-15 hydrogels (after hydrogel formation) both samples were fixed and dyed with DAPI and Phalloidin to stain the cell nuclei and actin filaments, respectively, on Day 21. It was observed that cells elongated and aggregated with neighboring cells. Corneal keratocytes seeded ON and IN GelMA were observed as aligned in one direction locally and formed orthogonal orientation in successive layers on Day 21 (Figure 3.12). These results indicate that whether cells seeded ON or IN the hydrogels, they elongate and interact with each other as in their natural environment. In order to obtain homogeneously distributed cells throughout the hydrogels, cells loaded IN the hydrogels were used in the following studies.

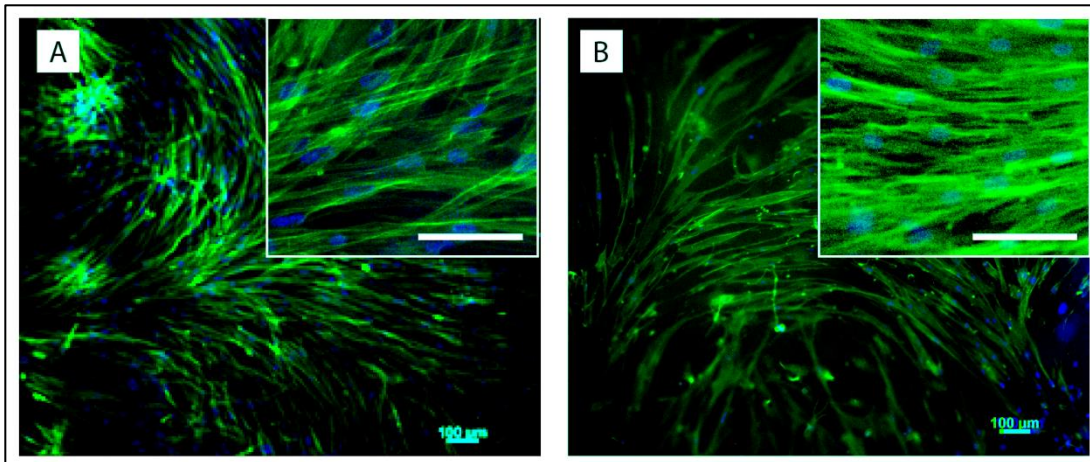


Figure 3.12: Fluorescence micrographs of DAPI (nucleus, blue) –Phalloidin (cytoskeleton, green) stained human keratocytes A) ON and B) IN GelMA. Time of incubation (days): 21. Scale bars: 100 μm.

In order to study distribution of cells in the cell loaded hydrogels, cells were stained with Draq5-Phalloidin and on Day 21 and studied under a CLSM microscope (Figure 3.13 A). Cells from the top to 200 μm depth of the hydrogel were extended and formed networks in both GelMA-10 and GelMA-15 hydrogels. However, the cells in the deeper regions were in circular shape, probably because of the limited access to the oxygen and nutrients. Distribution of cells on the surface and the cross-section of the hydrogels were also studied by scanning electron micrographs (Figure 3.13 B). In both hydrogels cells close to the surface were high in density, and were spread and interacted with each other. However, behavior of the cells in the hydrogels was different; Cells seem to be spread in the GelMA-10 hydrogels but they were in round shape in the GelMA-15 hydrogels. This behavior can be explained by the higher concentration of GelMA-15 hydrogels which results in tighter molecular network surrounding the cells that may limit the mobility of the cells. It should, however, be noted that cells spread all around the hydrogels, proliferate continuously (Figure 3.11), and were alive (Figure 3.7 and 3.8) proving the suitability of the hydrogels for cell growth.

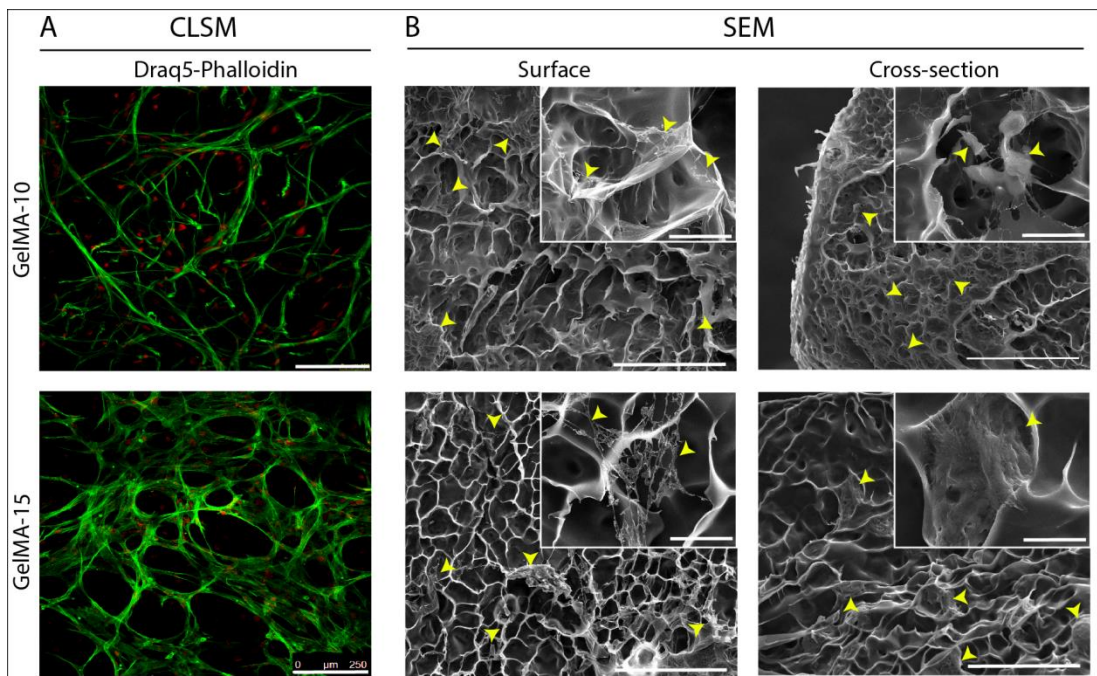


Figure 3.13: CLSM and SEM micrographs of keratocyte seeded GelMA hydrogels after 21 days of culture. A) CLSM. Draq5 stains the nucleus (red), and Phalloidin stains the cytoskeleton (green). Scale bars: 250 μm . B) SEM micrographs showing the surface and the cross-section of the hydrogels. Arrow heads point to the cells on the surface and cross-section. Scale bars: 200 μm . Inset scale bars: 50 μm .

3.1.5.6 Immunofluorescence Staining: Extracellular Matrix Synthesis by the Human Keratocytes in the GelMA Hydrogels

Corneal keratocytes loaded in the GelMA-10 and GelMA-15 hydrogels were studied in terms of their expression of representative collagens (Collagen types I and V), and proteoglycans (decorin and biglycan) (Gil *et al.*, 2010) in 21 days of culture. Results show that the collagens and proteoglycans expressed are dispersed throughout the 500 μm depth of the hydrogels (Figure 3.14). Image J analysis of the images was done to quantitatively analyze the intensity of the expressed products. Intensity of each image was normalized to the intensity coming from the DNA stain (Draq5 in this case). Collagen type I and proteoglycan expression of the keratocytes in GelMA-10 and GelMA-15 hydrogels were similar and there was no statically significant difference. However, collagen type V synthesis of the cells in GelMA-15 hydrogels was shown to be higher compared to ones in GelMA-10 hydrogels. Although a quite high collagen expression was observed in both types of hydrogels, the distribution of the expressed products within the hydrogel was different. Expressed collagens of keratocytes in GelMA-10 hydrogels were in a diffuse form but collagens in GelMA-15 were mostly localized near the cells. This can be explained by the higher rate of degradation of the GelMA-10 hydrogels (28% vs 13% in three weeks). In GelMA-10 mobility of the cells, and the proteins and proteoglycans produced by the cells affect the diffusion of them throughout the molecular chains of the gelatin. On the other hand density of the molecular chains of GelMA-15 hydrogels due to higher initial concentration and the lower degradation rate probably restricted the movement of the products. Expression of representative collagens and proteoglycans specific for corneal keratocytes show that keratocyte phenotype is retained in the hydrogels.

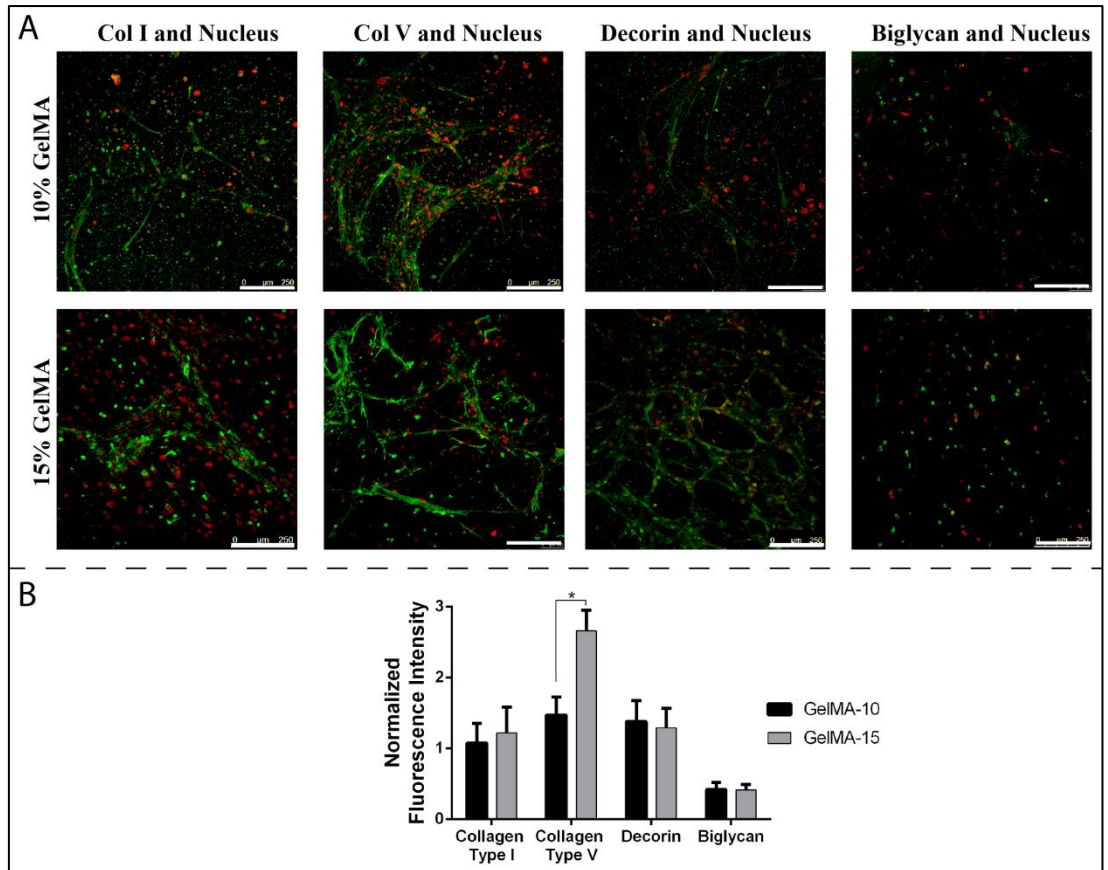


Figure 3.14: Immunocytochemistry of GelMA hydrogels. A) CLSM images on Day 21. Draq5 is for nucleus (red). Representative collagens (Collagen Type I and V) and proteoglycans (Decorin and Biglycan) (green). Scale bar is 250 μm . B) Semi-quantitative fluorescence intensity analysis of CLSM images. $n=3$. * $p < 0.05$, and ** $p < 0.01$.

3.1.5.7 Transparency of the Cell Loaded Hydrogels

Light transmittance and therefore transparency are the most important properties of the cornea because the light is refracted onto the lens as the first step of proper vision. The stereomicrographs of the clear corneal stroma equivalents is shown in Figure 3.15 A. Light transmission of cell loaded (cell seeding density 25,000 cells in 9.8 mm^3) hydrogels was followed for three weeks in the UV-Visible range 250-700 nm. Cell-free GelMA hydrogels served as the control and sample-free wells containing only growth medium served as blank. Light transmittance of cell loaded and control hydrogels were comparable with that of native cornea: Low transmittance in the UVA (320-400 nm) and UVB (290-320 nm) and a high transmittance in the visible range (400-700 nm) (Figure 3.15 B). Similarly, in the native cornea transmittance is ~5% at UVB and 85% at 700 nm for an 8 year old child which decreases by age (Mallet and Rochette, 2013). In the visible region light transmission of the hydrogels was 75% to 93%. Present hydrogel based approach is advantageous over current tissue engineered corneal designs due to its superior transparency even when loaded with cells and at the moment of implantation. Besides, transparency is expected to improve further in time by the ECM production of the cells. Transparency, in fact, is a result of action of keratocytes. ECM secreted by the keratocytes contributes significantly to the transparency through its high water retention capacity due to proteoglycans and proteins. Moreover, organization of the collagen fibrils produced by the keratocytes is essential for the maintenance of the form and other vital functions of the cornea (Maurice 1957; Guo et al., 2007).

In their natural environment, corneal keratocytes change their quiescent phenotype either into a repair phenotype or die upon injury. Regeneration or fibrotic scar formation are the function of repair phenotype. If the cells die however then transparency of the cornea is lost and this may even lead to permanent blindness (Guo et al., 2007). In the current study, transparency of the cell loaded hydrogels could be maintained for the 21 days of incubation indicating the presence of some synthetic activity of cells and thus presence of keratocyte phenotype in the hydrogels.

One of the important observations with these hydrogels of these results is the lower light transmission in the UV region. The lowest light transmission was around 280 nm and this was due to the aromatic amino acids of the proteins (Diffey, 1991). This result is in agreement with that of native cornea where almost all light is absorbed up to 280 nm and light transmission gradually increases at wavelengths higher than this. Epithelial layer of the cornea is mainly responsible for the high level of absorbance at UVA and UVB regions because of high protein and nucleic acid contents of the epithelial cells (Ringvold, 1998). Incorporation of epithelial cells, therefore, to this design would significantly contribute to the light absorption at UV regions.

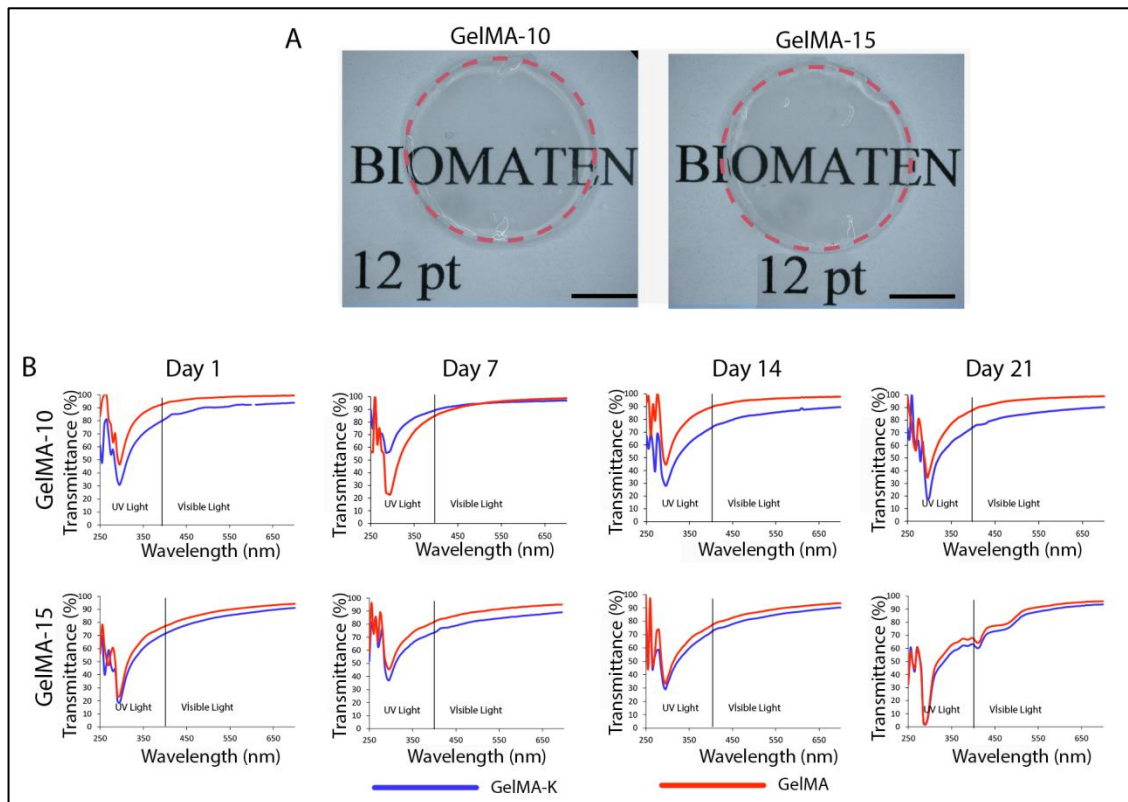


Figure 3.15: Transparency of hydrogels. A) Stereomicrographs showing transparency of the two cell free hydrogels on Day 0 (Outlined in red). Scale bar is 5 mm. B) Variation of transparency of the cell free GelMA hydrogels (GelMA) and keratocytes carrying GelMA hydrogels (GelMA-K) with time and wavelength.

3.1.5.8 Compressive Mechanical Properties of Hydrogels

For the maintenance of the normal functions of the cornea, satisfactory mechanical properties are needed. It was shown that GelMA10 and GelMA15 hydrogels were highly biocompatible and had excellent transparency in the visible light region (>90%). Hydrogels loaded with human keratocytes and their cell free controls were incubated in the growth medium for 3 weeks and tested under compression on Days 1, 7, 14 and 21. Results showed that mechanical properties of both cell loaded and cell free GelMA-10 and GelMA-15 hydrogels increased significantly during the three weeks period and had about 10 times more compressive moduli compared their starting value (Figure 3.16). Compressive moduli of cell loaded GelMA-10 hydrogels were significantly higher on Days 14 and 21 than cell loaded GelMA-15 hydrogels. The reason for this observation may be the higher compressive moduli of the cell-free GelMA-10 hydrogels compared to cell-free GelMA-15 hydrogels rather than the effects of the cells since the number of cells in these hydrogels were comparable on these days (Figure 3.11). It seems that, the contribution of cells to the compressive moduli of the hydrogels is minimal since there is no significant difference in the compressive moduli of cell free and cell loaded hydrogels. Similar results were reported in the literature due to nonenzymatic glycation (crosslinking of proteins by reducing sugar) where high amounts of glucose and ribose in culture medium stiffen and strengthen the tissue engineered constructs and enhance their resistance to degradation by collagenases (Girton et al., 1999; Girton et al., 2000).

Cornea is subjected to traumatic impacts and the tensile stress imposed by the intraocular pressure (IOP). Cornea is also subjected to shear forces created by the eyelids and tear films. This load bearing capability is a result of the complex organization of the stromal tissue (Ethier, Johnson and Ruberti, 2004; Ruberti, Zieske and Trinkaus-Randall, 2007). Any artificial cornea construct should, therefore, be strong enough to handle during implantation and be able to withstand the external forces afterwards.

In the measurement of the Young's Modulus, under tensile load, of the cornea various methods were used and very different results (0.1-57 MPa) were reported probably due to the differences in the testing conditions (Schwartz, Mackay and

Sackman, 1966; Andreassen, Hjorth Simonsen and Oxlund, 1980; Jue and Maurice, 1986; Hoeltzel *et al.*, 1992). In a recent study the mechanical strength of the native corneas of people aged 50-64 was measured to be in the range 403 to 624 kPa under tensile load (Elsheikh *et al.*, 2007). Although starting compressive moduli of the cell free and cell loaded hydrogels were significantly lower, they continuously increased during the incubation period. It should also be noted that, when these hydrogels are used in *in vivo* studies, the observation period will be longer than 21 days and the compressive moduli of the hydrogels might reach the values reported above.

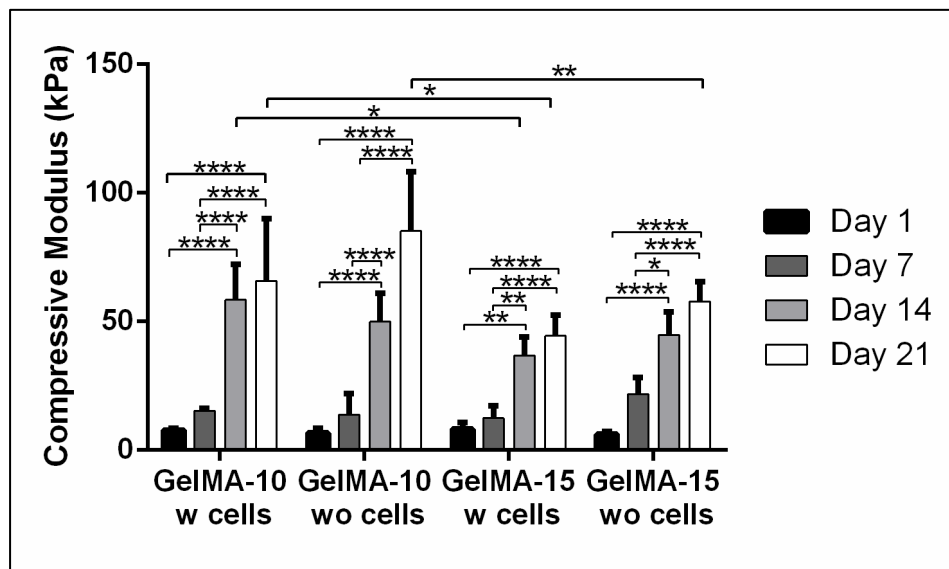


Figure 3.16: Change of compressive moduli change of cell loaded GelMA10 and GelMA15 hydrogels over 3 weeks. $*p < 0.05$, $**p < 0.01$, and $****p < 0.0001$. w: with, w/o: without.

3.1.5.9 Mechanical Strength Testing of GelMA Hydrogel with Artificial Anterior Chamber

Mechanical stability of GelMA-15 hydrogels was tested with a device called artificial anterior chamber and the hydrogel was failed upon application of pressure (Figure 3.17). For this reason various proteins and synthetic polymers including collagen, methacrylated collagen, silk fibroin and HEMA was added in the structure of GelMA in order to enhance its mechanical properties and only GelMA-HEMA combination gave viable results (Others even did not yield any hydrogel). In the following section results of GelMA-HEMA combination is given. In the light of above mentioned results, GelMA-15 hydrogels were chosen for the following studies due to their higher stability against in situ and enzymatic degradation conditions.

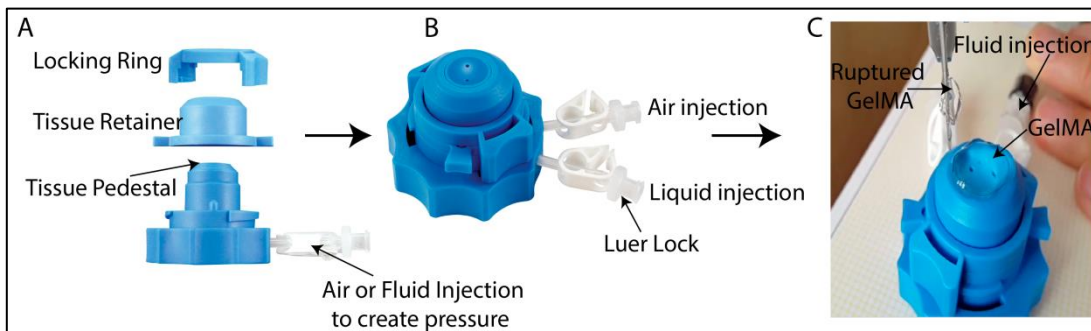


Figure 3.17: Scheme of artificial anterior chamber. A) Components of the system, B) Closed form of the chamber, and C) Rupture of the GelMA-15 due to intraocular pressure simulated with artificial anterior chamber.

3.2 GelMA-HEMA Hydrogels

3.2.1 Characterization of the GelMA-HEMA Hydrogels

In the above mentioned studies reported until this point, GelMA hydrogels prepared with various concentrations were tested *in situ* and *in vitro*. However, because of mechanical weakness of the hydrogels 2-(hydroxyethylmethacrylate) (2-HEMA), another monomer, was introduced to the hydrogel composition to enhance mechanical properties. pHEMA is one of the most studied synthetic polymers because of its well tolerated *in vivo* (Homsy, 1970; Lee and Mooney, 2001). It is widely used in ophthalmic, drug delivery and tissue engineering applications due to its tunable hydrophilicity and mechanical properties (Ratner and Miller, 1973; Peppas, Moynihan and Lucht, 1985; Bakshi *et al.*, 2004). In the literature only a few hydrogels containing GelMA and pHEMA were reported for tissue engineering applications (Dragusin *et al.*, 2012; Wang *et al.*, 2016). Long processing time for hydrogel formation and seeding cells after the process were some of the disadvantages of the reported products. In this study, however, cells were loaded prior to polymerization and GelMA-HEMA hydrogels with cells were prepared for the first time in the literature.

3.2.2 FTIR-ATR Spectra of GelMA-HEMA Hydrogels

Presence of pHEMA in the hydrogel structure was confirmed by IR spectroscopy of GelMA, GelMA-HEMA (8:2) and HEMA hydrogels (Figure 3.18). GelMA has characteristic bands around 3310 cm^{-1} due to N-H stretching (amide A), 3063 cm^{-1} related with C-H stretching (amide B), 1657 cm^{-1} is for C=O stretching (amide I), 1557 cm^{-1} is for N-H deformation (amide II), and 1239 cm^{-1} related with N-H deformation (amide III) (Zhou *et al.*, 2014). pHEMA has characteristic vibrational bands in the stretching O-C-O group ($\sim 1079\text{ cm}^{-1}$), carbonyl ($\sim 1720\text{ cm}^{-1}$) and hydroxyl ($\sim 3400\text{ cm}^{-1}$) stretching regions both of which are absent in GelMA. There are also additional bands due to symmetric and asymmetric C-H vibrations of $-\text{CH}_2$ and $-\text{CH}_3$ groups between $2600 - 3050\text{ cm}^{-1}$ (Perova, Vij and Xu, 1997). Figure 1 shows the FTIR-ATR spectra of GelMA, GelMA-HEMA, and HEMA hydrogels. Peaks due to Amide I and Amide II bonds are only observed in protein-derived

materials and seen only in GelMA hydrogel spectrum. Same peaks are also observed in GelMA-HEMA spectrum, indicating successful addition of HEMA into the structure of the GelMA.

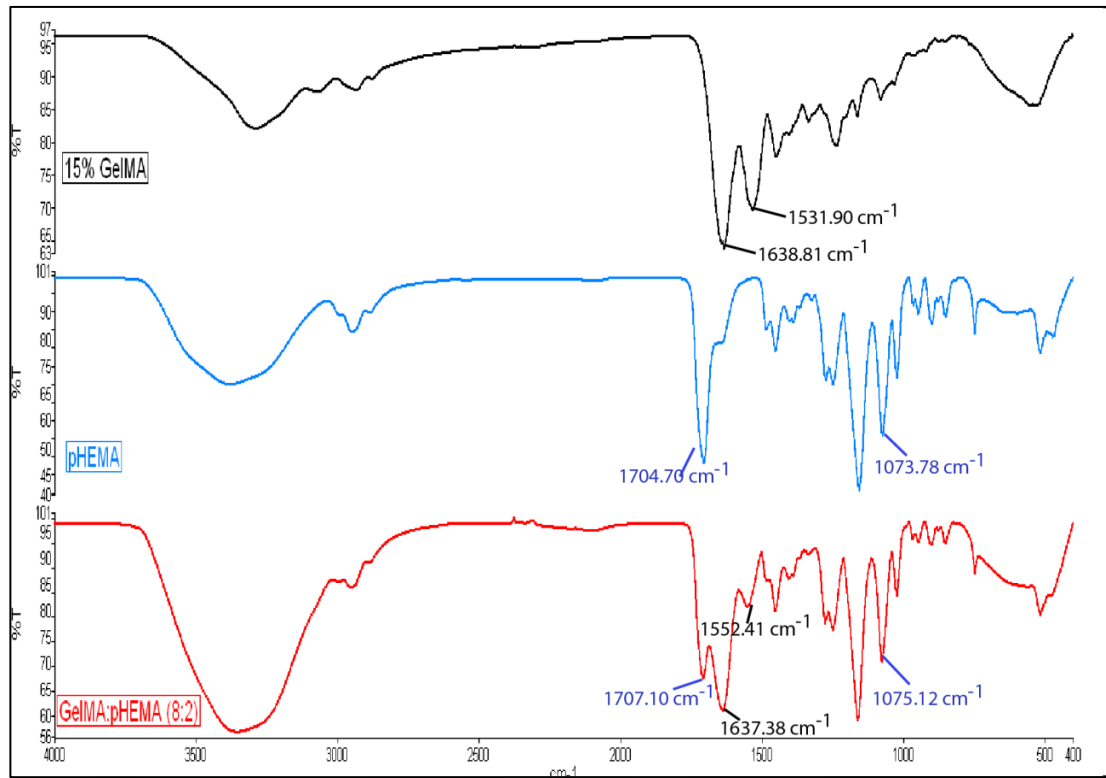


Figure 3.18: FTIR-ATR spectra of GelMA, HEMA and GelMA-HEMA hydrogels. Peaks on GelMA-HEMA coming from GelMA and HEMA were written on the figure.

3.2.3 Compressive Mechanical Tests

Compressive modulus of the GelMA, GelMA-HEMA and HEMA hydrogels were determined and GelMA hydrogels were significantly strengthened with the addition of HEMA in their structure ($p < 0.05$) (Table 3.1). In a recent study the mechanical strength of the native corneas of people aged 50-64 was measured to be in the range 403 to 624 kPa under tensile load (Elsheikh et al, 2007). Compressive modulus of the 15% GelMA was the lowest (Table 3.1) and that of the HEMA hydrogels was the highest, and GelMA-HEMA hydrogels being in between.

Matching of the hydrogel mechanical properties with that of native tissue is important in having suitable implants for *in vivo* and clinical applications. Any tissue engineered construct should be able to withstand external forces upon implantation and should not be too rigid so that it does not damage the surrounding tissue. Although compressive modulus of the GelMA-HEMA hydrogels is lower than the native cornea, the hydrogels produced were stronger and more flexible compared to pure GelMA hydrogels. It should also be noted that, the compressive modulus of the GelMA hydrogels increased significantly in culture conditions as mentioned in Section 3.1.5.8. Moreover, previous studies in our group had demonstrated that the mechanical properties of the keratocyte seeded scaffolds increased significantly in time (Vrana *et al.*, 2007; Zorlutuna *et al.*, 2007). GelMA-HEMA hydrogels, therefore, might be suitable for use as corneal stroma equivalents.

In the literature values around 0.29 MPa were reported for the compressive modulus of HEMA hydrogels and varied with the crosslinking procedures and water contents of the hydrogels (Johnson *et al.*, 2002; Flynn, Dalton and Shoichet, 2003). The relatively higher compressive moduli obtained in this study is about the lower water content of the only HEMA containing hydrogels (Section 3.2.4) (17.62% vs 39.6% reported in Flynn *et al.* 2003). High water content of GelMA-HEMA blend decreased the compressive modulus of the HEMA hydrogels.

3.2.4 Equilibrium Water Contents (EWC) of the GelMA-HEMA Hydrogels

Mechanical characteristics, diffusion of solutes and mobility of the surface molecules are significantly affected by the water content of the scaffolds (Peppas *et al.*, 2006). As observed in table 3.1 EWC of the HEMA hydrogels were significantly lower than other hydrogels with 17.62%. GelMA hydrogels retained a significant amount of water in their structures and since GelMA content of the GelMA-HEMA hydrogels was higher (8:2). One of a few studies containing GelMA and pHEMA by Wang *et al.* (2016) reported the equilibrium water content of the pure GelMA, pHEMA and GelMA-HEMA double network hydrogels as 91%, 30.36% and 74.4%, respectively. Different processing methods and compositions for crosslinking resulted in difference in the water content of the pure pHEMA but the water contents of the GelMA and GelMA-HEMA blend were comparable with this study. Water

content of the GelMA-HEMA hydrogels are comparable with the water content of the native stroma (78%, w/w) (Chirila *et al.*, 1998) and high water content is desirable since it leads to enhanced nutrient permeability which is important for the cells to be alive proliferate.

Table 3.1: Compressive modulus and EWC of the hydrogels.

Samples	Compressive Modulus (kPa)	Water Content (% , w/w)
GelMA-15	6.53 ± 0.84	88.10 ± 0.11
GelMA-HEMA (8:2)	155.49 ± 19.94	73.05 ± 2.55
HEMA	1119.32 ± 406.52	17.62 ± 1.58

3.2.5 In Situ Degradation of GelMA-HEMA Hydrogels

In vitro culture conditions were mimicked by incubating GelMA-HEMA hydrogels in PBS (pH 7.4, 10 mM) for 21 days (Figure 3.19 A). As in the case of in situ degradation test of pure GelMA hydrogels (Section 3.1.3) a high rate of weight loss was observed in the first day (about 7-8%) followed by a much lower. It is most probably because of leaching out of the uncrosslinked GelMA and HEMA molecules. Weight loss was slower with more than 87% of the hydrogels remaining on Day 21. Extent of degradation was similar for both GelMA and GelMA-HEMA hydrogels.

3.2.6 Enzymatic Degradation with Collagenase

Stability of the scaffolds against enzymatic degradation was studied with collagenase type II. Four enzyme concentrations were used. Since gelatin is the only molecule attacked by the enzymes, presence of HEMA in the structure did not change the degradation profile of the hydrogels where a continuous decrease in weight loss is observed (Figure 3.19 B). However, when treated with the highest collagenase concentration solutions (5 U/mL and 10 U/mL) presence of HEMA enhanced stability of the hydrogels against enzymatic attack (72% vs 77% and 69% vs 70%, for 5 U/mL and 10 U/mL and for GelMA and GelMA-HEMA, respectively). Pure

pHEMA hydrogels were not included in the results since they are not attacked by the collagenase. In the literature, researchers reported similar results where an enhanced stability against collagenase attack is reported as pHEMA proportion increases in the structure (Dragusin *et al.*, 2012). It is worth to note that, hydrogels were stable enough to handle even after 4 hour incubation with the highest collagenase concentration.

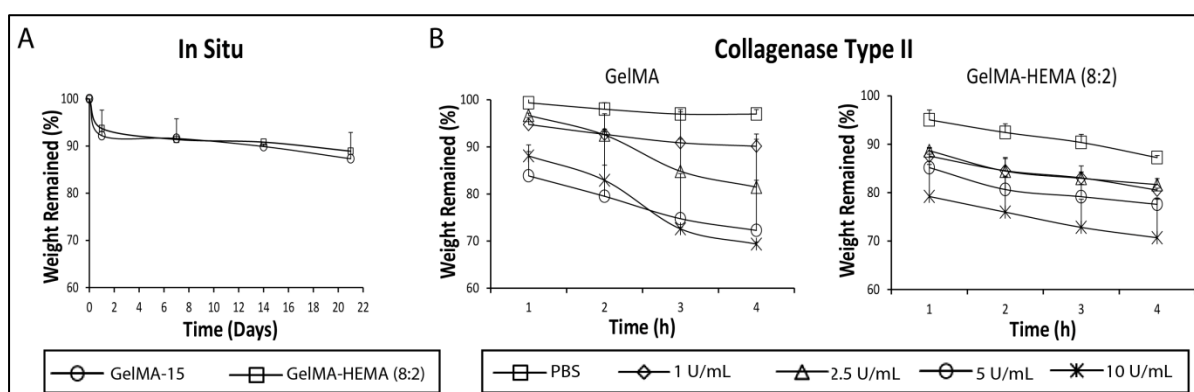


Figure 3.19: Stability of GelMA and GelMA-HEMA hydrogels A) In situ B) Enzymatic degradation (4 h).

3.2.6.1 Transparency of Hydrogels during Collagenase Assay

Transparency of the hydrogels was also studied in the range 250-700 nm after being exposed to collagenase. Transparency of GelMA-15 was above 90% (at 700 nm) before and after all treatments (Figure 3.20 A). Addition of HEMA into the composition decreased the transparency significantly in the whole range and it was about 70-75% at 700 nm (Table 3.2). Although same amount of GelMA degraded during collagenase degradation as mentioned above for GelMA and GelMA-HEMA hydrogels, due to lower GelMA content of the GelMA-HEMA hydrogels, observed degraded amount most probably affected the bulk structure which resulted in decreased transparency after collagenase incubations when compared control ones (incubated in PBS). Transmittance (%) at 300 nm was not affected with the collagenase incubation but a decrease was observed at 700 nm for GelMA-HEMA hydrogels (Table 3.2). However, such a difference was not observed for GelMA hydrogels where they preserved their transparency during all the treatments for 4

hour (Figure 3.20 A and Table 3.2). Most probably bulk structure of the hydrogel was not affected extensively with the collagenase incubation. Transparency of the GelMA-HEMA hydrogels was lower than the native cornea (Figure 3.20 B) but it is thought that extracellular matrix synthesis of the cells in the hydrogels will compensate for the loss of transparency by time in *in vivo* applications. Stereomicrographs (Figure 4C) show the highly transparent corneal constructs at time 0.

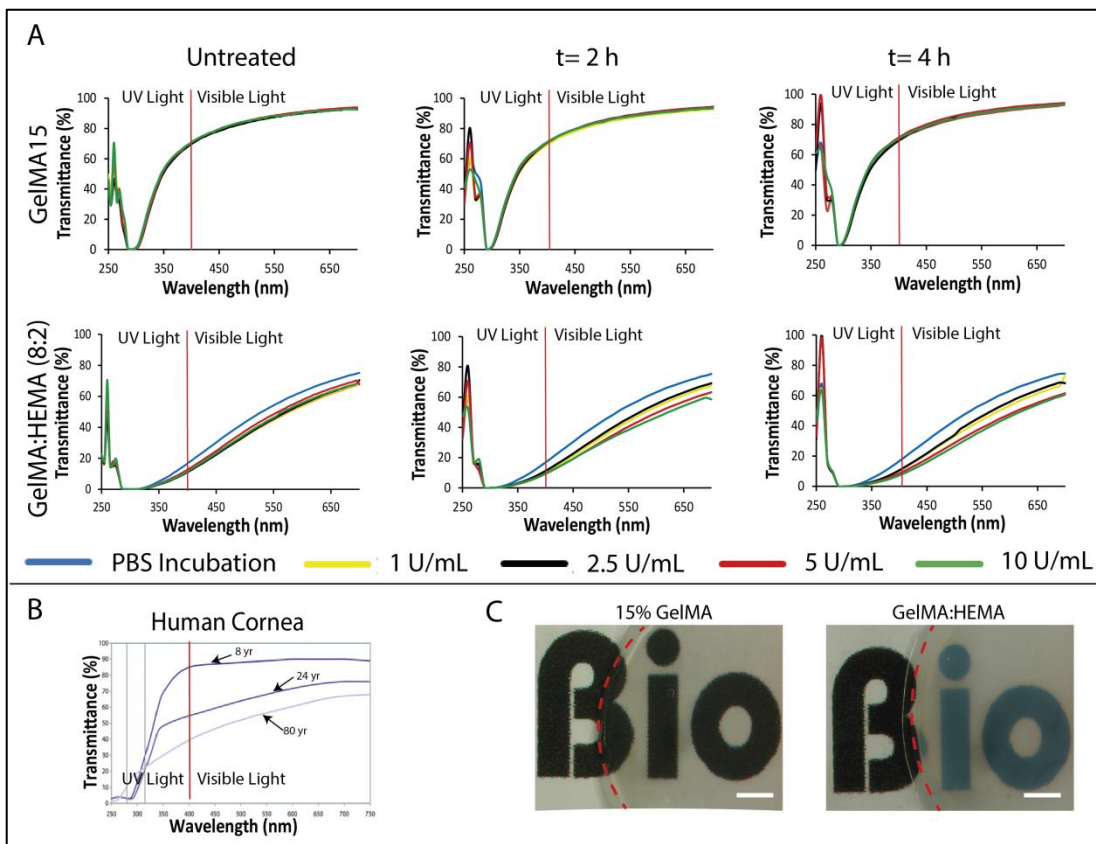


Figure 3.20 Transparency of GelMA and GelMA-HEMA hydrogels. A) After incubation in PBS and 4 different collagenase concentrations. B) Transparency of the films was compared with transparency of native cornea from subjects of different ages (Mallet and Rochette, 2013). C) Stereomicrographs of hydrogels over a printed text showing their transparency. Dotted red line shows the border of the hydrogels. Scale bar is 2.5 mm.

Table 3.2: Transmittance (%) of GelMA and GelMA-HEMA (8:2) at 300 and 700 nm, after incubation in PBS and 4 different collagenase concentrations.

		GelMA				
WL (nm)	Time (h)	PBS	1 U/mL	2.5 U/mL	5 U/mL	10 U/mL
300	Untreated	1.36494	0.85358	0.55682	0.66089	1.18001
	2	2.15029	1.45612	1.42779	1.74102	2.16791
	4	2.14265	1.53735	1.4451	1.9441	2.24478
700	Untreated	93.8256	93.5128	93.0089	93.771	92.3422
	2	94.4614	92.7667	94.2038	94.1185	93.2894
	4	94.1576	93.0413	92.8955	94.1632	92.8389
		GelMA-HEMA (8:2)				
		PBS	1 U/mL	2.5 U/mL	5 U/mL	10 U/mL
300	Untreated	0.02727	0.02643	0.02598	0.0276	0.02914
	2	0.06361	0.02672	0.04077	0.02787	0.04441
	4	0.02823	0.02687	0.03721	0.02771	0.02991
700	Untreated	75.1735	68.618	70.4811	67.6031	68.2375
	2	75.3521	67.5219	69.1655	63.2312	58.5205
	4	74.4	73.629	68.1498	61.5053	60.6097

3.2.7 In vitro Studies

3.2.7.1 Live-Dead Assay and Draq5-Phalloidin Staining of Hydrogels

Cell loaded hydrogels were incubated in the human keratocyte growth medium and their behavior in the hydrogels were studied under CSLM on Day 3 (Figure 3.21). Live-Dead Assay showed that, more than 90% of the cells in the GelMA and GelMA-HEMA hydrogels were alive as judged by NIH Image J program. However, only about 50% of the cells were alive in the HEMA hydrogels. Presence of GelMA, therefore, contributed viability of the cells significantly. It should be noted that,

however, although cells were found throughout the bulk of GelMA hydrogels (down to 500 μm depth), cells were detected only at the top 250 μm depth of the GelMA-HEMA hydrogels as judged by Z-stack mode of CLSM. With the HEMA hydrogels, cells were observed only on the surface. Lower water content of the GelMA-HEMA and HEMA hydrogels compared to GelMA hydrogels may be the reason for this growth behavior (Table 3.1). Same cell distribution difference was observed when the cells stained with Draq5-phalloidin. A smaller number of cells were observed in HEMA hydrogels, than in GelMA and GelMA-HEMA. Another important point here is the morphology of the cells; cells were extended in the GelMA hydrogels but they were all round in the GelMA-HEMA and HEMA hydrogels. It is again most probably because of less space for the cells to move around freely. Small pores of GelMA-HEMA hydrogels and no pores of HEMA hydrogels were seen clearly from the cross section SEM images (Figure 3.22). Other researchers reported the similar results as in this study where cells spread throughout the surfaces of GelMA and GelMA-HEMA hydrogels, there were either no cells or very low amount of accumulated cells on the pure HEMA hydrogels (Dragusin *et al.*, 2012; Wang *et al.*, 2016). Also, their studies showed that increased concentration of GelMA in the network structure enhances the viability of the cells.

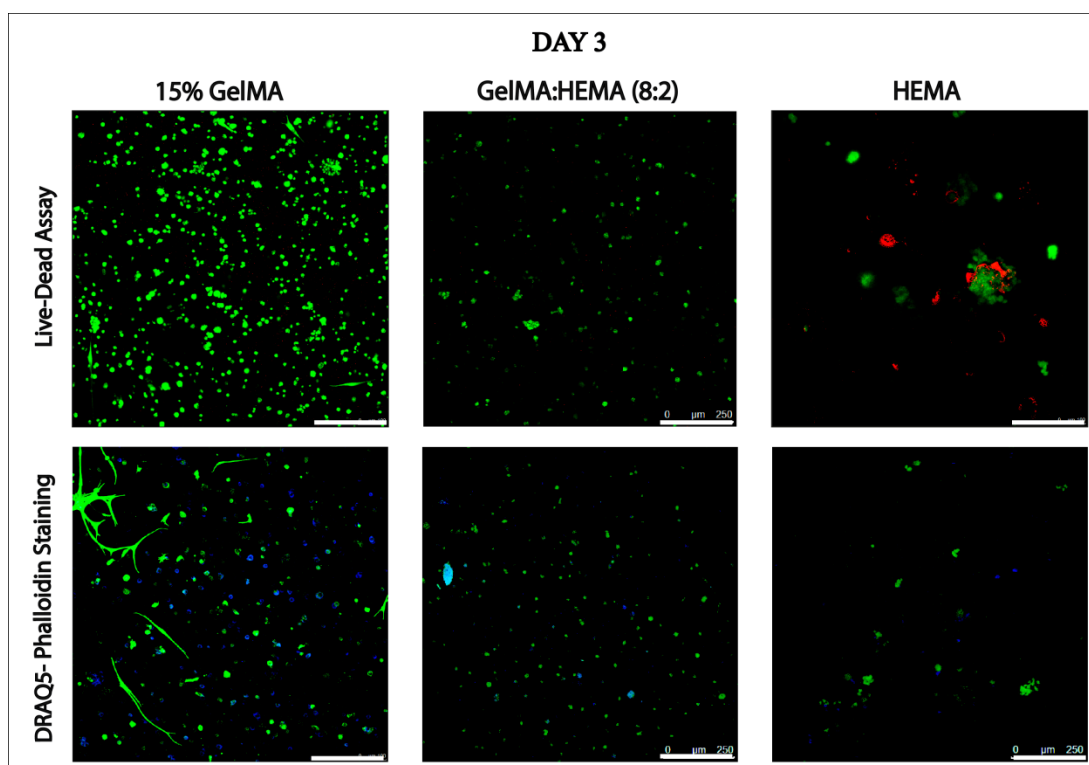


Figure 3.22: Live-Dead Assay and Draq5-Phalloidin staining of hydrogels on Day 3, studied by CSLM. Calcein AM: Live Cells, green; Ethidium Homodimer: Dead Cells, red. Draq5: Nucleus, Blue; Phalloidin: Cytoskeleton, green. Scale bar: 250 μm .

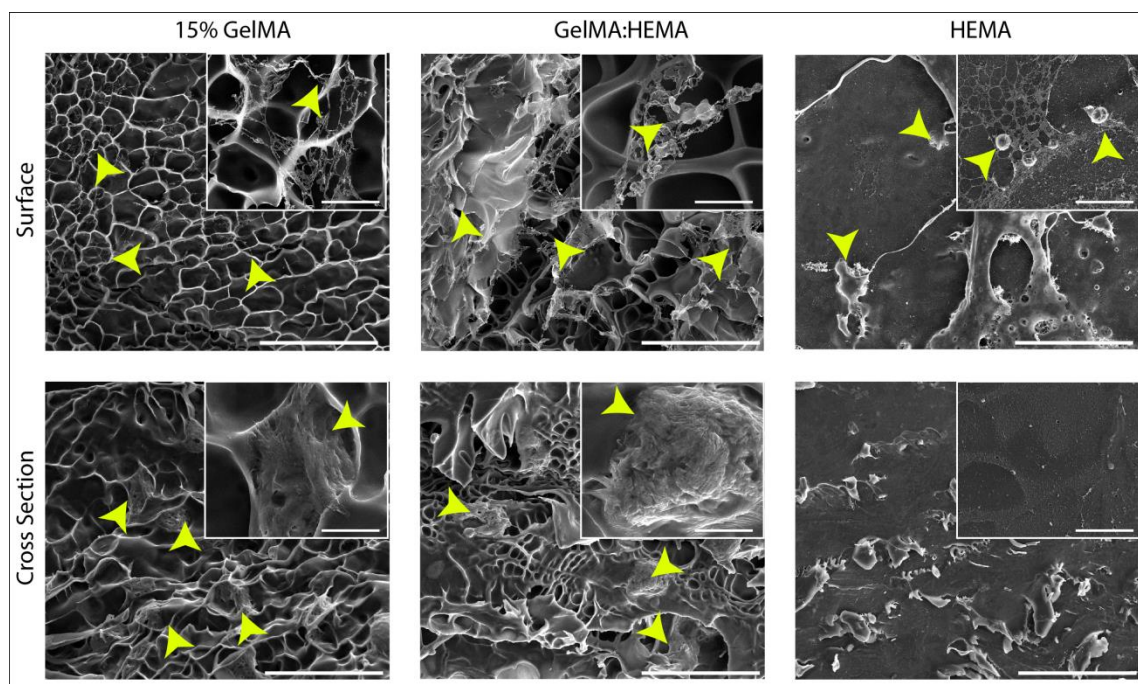


Figure 3.21: SEM images of cell loaded hydrogels. Arrow heads point to cells on day 21. Scale bars: 200 μm , and inset scale bars: 25 μm .

3.2.7.2 Cell Proliferation in the Hydrogels

Proliferation of the cells in the hydrogels was studied with Alamar Blue cell proliferation assay. Proliferation of the cells in GelMA hydrogels was significantly higher than cells in other hydrogels at all time points (except for Day 1 of GelMA-HEMA hydrogels) (Figure 3.23). Although number of detected cells (Reduction %) in the GelMA-HEMA and pHEMA hydrogels was low, it was increased significantly in three weeks of incubation. Number of cells on Day 21 was significantly higher in GelMA-HEMA hydrogels compared to cells on pure HEMA hydrogels. Incorporation of GelMA in the structure, therefore, enhanced the growth of cells. As mentioned above cells were found accumulated on the pure HEMA hydrogels but spread around on GelMA and GelMA-HEMA hydrogels. Thus, cells in GelMA-HEMA hydrogels have more space to proliferate but because of the non-porous nature of the pHEMA hydrogels cells could not proliferate in the hydrogels but only grow on it. Also because of cell repellent nature of the pHEMA cells were found in accumulated form (See Figure 3.21) which prevent the cells to spread and proliferate throughout the hydrogel. Moreover, any remnants of toxic crosslinkers like TEMED and EGDMA and APS (initiator) may also have negative effect on cell attachment, viability, and proliferation. HEMA hydrogels were reported to have poor cell

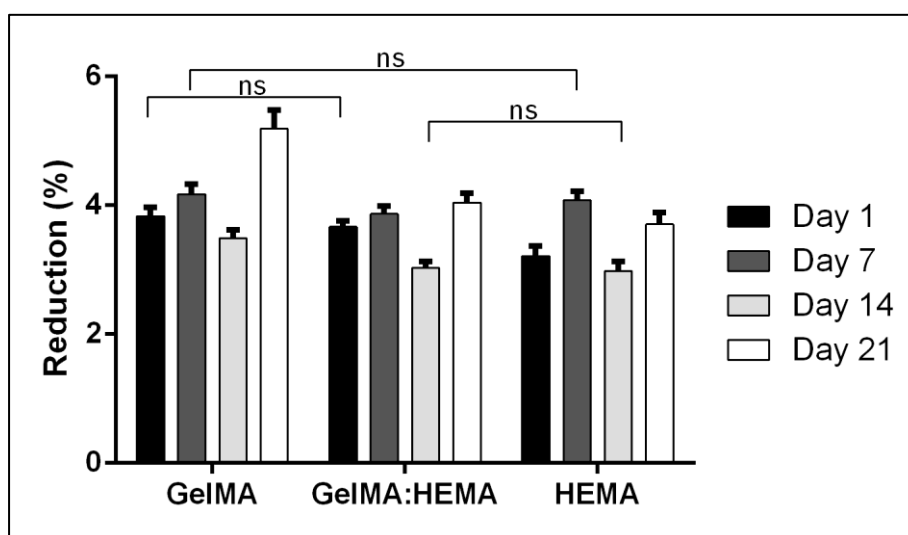


Figure 3.23: Proliferation (as indicated by Reduction %) of human keratocytes in GelMA, GelMA-HEMA and HEMA hydrogels over 3 weeks. Only non-significant (ns) data is shown on the figure.

adhesion and low protein adsorption properties by other studies as well (Merrett *et al.*, 2001; Kubinová, Horák and Syková, 2009). Because of these disadvantages researchers modified or mixed HEMA with other biological molecules including gelatin (Çetin, Kahraman and Gümüşderelioğlu, 2011), collagen (Li *et al.*, 2013), GelMA (Dragusin *et al.*, 2012; Wang *et al.*, 2016), and cholesterol (Kubinová, Horák and Syková, 2009) and enhanced proliferation of cells were reported.

3.2.7.3 Immunofluorescence Staining: Extracellular Matrix Synthesis by the Human Keratocytes in the GelMA, GelMA-HEMA and HEMA Hydrogels

Immunocytochemistry of 21 day cultured keratocytes seeded in the hydrogels were performed to study the expression of collagen type I and V (collagens specific for human cornea), decorin and biglycan proteoglycans (proteoglycans specific for human cornea) to study the accumulation of the main components of the corneal stroma. As in the previous tests in this study (Section 3.1.5.6), collagens and proteoglycans were observed throughout the GelMA hydrogels (Figure 3.24 A). However, these molecules would be detected down to 250 μm depth of the GelMA-HEMA and only at the surface for HEMA as judged by the Z-stack mode of CLSM. In GelMA-HEMA and HEMA hydrogels collagens and proteoglycans were detected near the cells, and the intensity of the collagens was significantly lower compared to GelMA. Normalized fluorescence intensities of the Decorin and Biglycan were similar in all samples (Figure 3.24 B). However, it should be noted that, when the images are examined synthesis of proteoglycans seems higher in GelMA compared to others, but when the signal intensity coming from the proteoglycans are divided to intensity coming from Draq5 (nucleus) results in similar normalized fluorescence intensities. On the other hand, synthesis of representative collagens and proteoglycans in all samples indicate that cells did not lose their keratocyte functions.

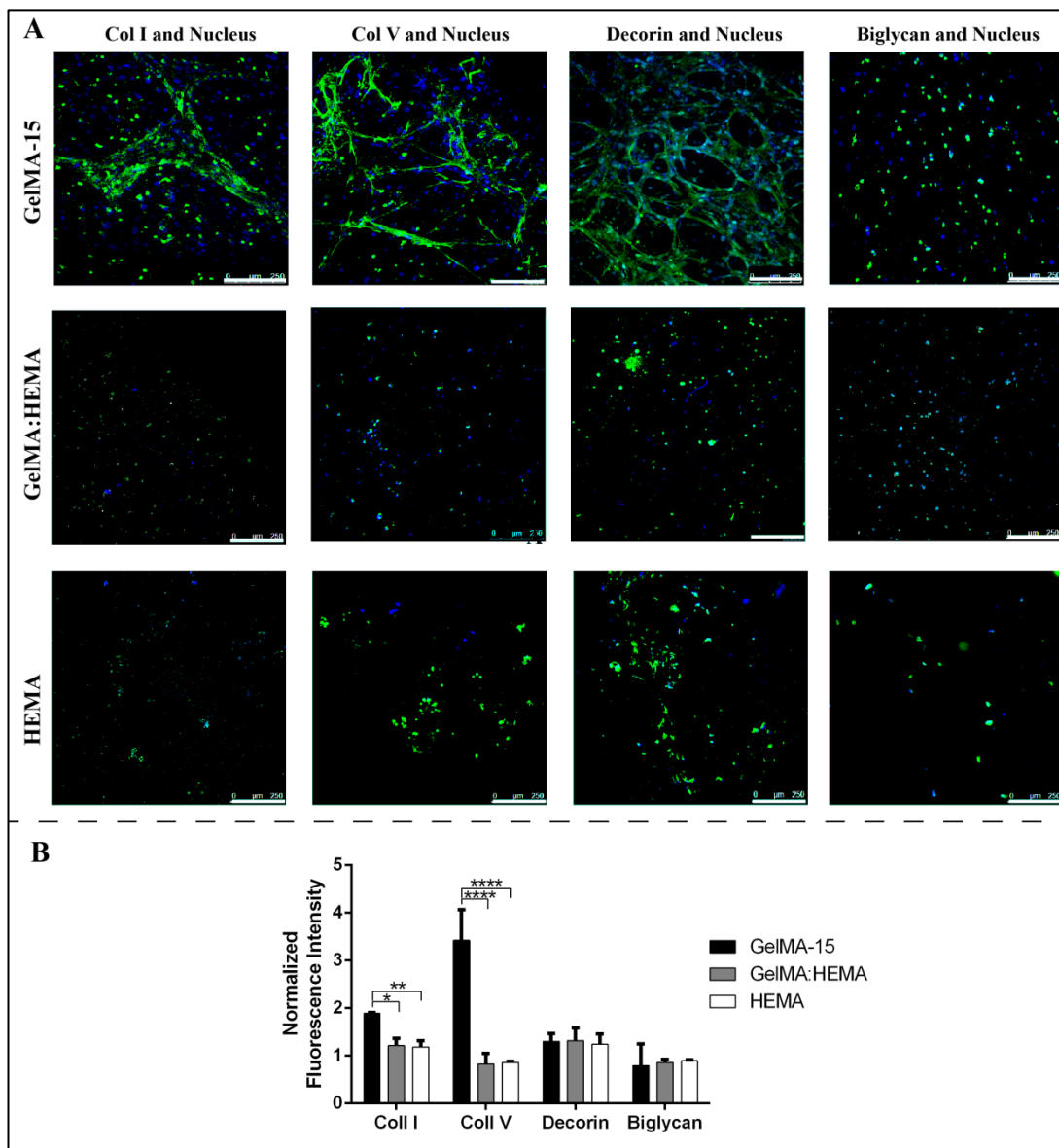


Figure 3.24: Immunocytochemistry of GelMA-15, GelMA-HEMA and HEMA hydrogels. A) CLSM images on Day 21. DraG5 is for nucleus (blue). Representative collagens (Collagen Type I and V) and proteoglycans (Decorin and Biglycan) (green). Scale bar is 250 μ m. B) Semi-quantitative fluorescence intensity analysis of CLSM images. n=3. * $p < 0.05$, ** $p < 0.01$, and **** $p < 0.0001$.

3.2.7.4 Light Transmission of the GelMA-HEMA Hydrogels

Transparency of GelMA, GelMA-HEMA, and HEMA hydrogels was measured for up to 21 days by scanning the spectrum in the range 250-700 nm. Hydrogels without cells were used as the blank. Transmittance of the GelMA hydrogels were low in UVA (320-400 nm) and UVB (290-320 nm) regions as in the natural cornea and the transparency was between 75% - 93% in the visible range (400-700 nm) (Figure 3.25). Transparency of cell loaded GelMA-HEMA was higher at all time points than unseeded which is desired. Transparency of cell loaded GelMA-HEMA hydrogels was about 78% at 700 nm on Day 1 but with the activity of cells it increased significantly to 90% at 700 nm and became comparable with GelMA hydrogels. On the other hand, transparency of the unseeded hydrogels decreased from 62% to 48% during 21 days of incubation. This transparency loss can be explained by the in situ degradation of the samples where during incubation periods only GelMA part of the GelMA-HEMA hydrogels degrade and remaining hydrogel have more HEMA as proportion whose transparency is significantly lower than GelMA-HEMA hydrogels. Activity of the cells, therefore, seems to enhance transparency of the GelMA-HEMA hydrogels. Transparency of HEMA hydrogels, on the other hand, was lower in seeded hydrogels but higher in unseeded ones. This result can be explained by the behavior of cells on HEMA hydrogels where they were found accumulated on the surface compared to individual cells in others (see Figures 3.21 and 3.22). Although an increase in transparency of both seeded and unseeded HEMA hydrogels are observed, it was significantly lower than GelMA and GelMA-HEMA hydrogels. Overall lower transparency of the HEMA hydrogels can be because of the rough surface of them due to removal of unreacted monomers from the surface during washing. Similar results was reported by other researchers where transparency of GelMA hydrogels was about 95%, it was about 75% and 30% for GelMA-HEMA and HEMA hydrogels (Wang *et al.*, 2016). Use of different crosslinkers, modification of the pHEMA surface and addition of water in the initial polymerization mixture yields a wide range of pHEMA hydrogels with different transmittance (%) values ranging from 2% to 90% (Gulsen and Chauhan, 2006; Seo *et al.*, 2017).

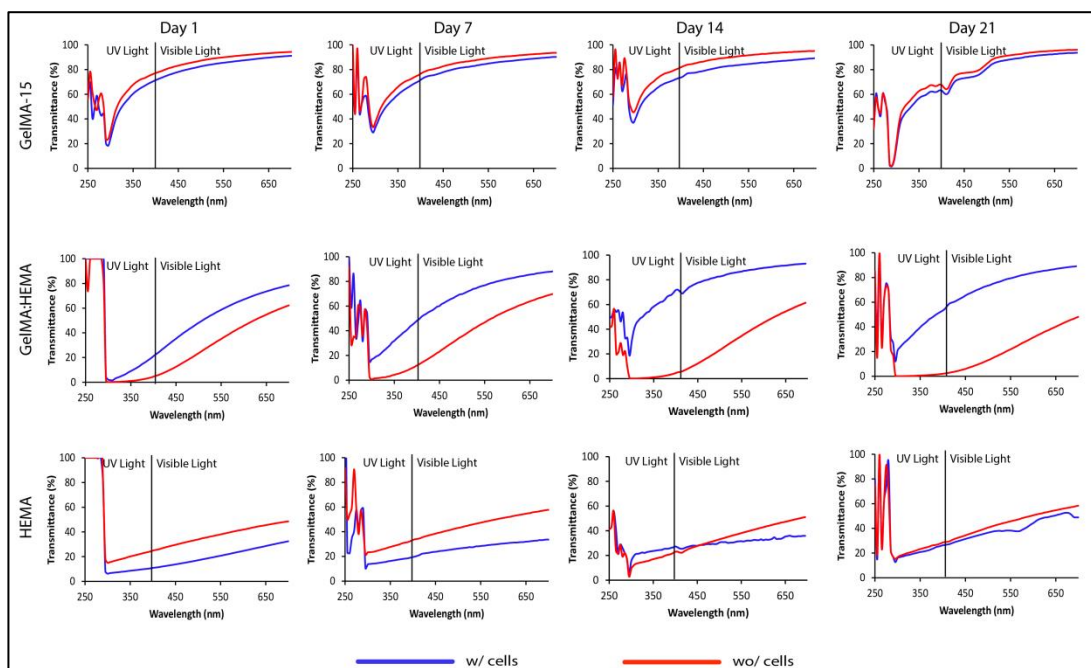


Figure 3.25: Change of transparency of the hydrogels with and without keratocytes in the hydrogel bulk in 21 days. Blue: Cell loaded hydrogels, Red: Unseeded control hydrogels.

3.3 3D Printed GelMA15 Hydrogels

As mentioned earlier, corneal stroma consists of 200-400 lamellae parallel to the cornea surface and orthogonal to adjacent lamellae as plywood. This organization is very crucial for optical and biomechanical properties of the cornea. Above mentioned studies with GelMA10 and GelMA15 hydrogels showed that the hydrogel use in the preparation of a substitute for corneal stroma presents a significant potential and use of GelMA hydrogels in this context were reported by Kilic Bektas and Hasirci (2018). This hydrogel design did not have any internal organization to guide the cells to orient and synthesize collagens and proteoglycans. 3D printed hydrogels with pre-determined shapes, dimensions, and organization should be a viable candidate as corneal stroma substitutes in mimicking the corneal microstructure.

3D printed corneal stroma constructs have been reported by two researchers up to now and both in 2018 (Isaacson, Swioklo and Connon, 2018; Sorkio *et al.*, 2018). In their study Isaacson *et al.* (2018) entrapped corneal keratocytes in a bioink composed of methacrylated collagen type I and alginate, and printed concentric fibers beginning from the center and spiraling upwards and outwards. Although the circular nature of the native cornea was well mimicked and high cell viability was achieved, microarchitecture of the corneal stroma especially orthogonal alignment of the collagen fibers was not mimicked. Moreover, the need for a gelatin slurry increases the complexity of the system. Sorkio *et al.* (2018), on the other hand, reported use of a more complex 3D printing setup based on laser-assisted printing with human adipose tissue derived stem cells (hASC) entrapped in a bioink composed of collagen type I, EDTA, human blood plasma, and thrombin from blood plasma. They reported high cell viability, proper organization of cells after printing, and collagen Type I expression in the constructs. However, complexity of the system due to preparation of each individual ribbon to setup and low flow rate for high print fidelity makes printing time-consuming. Moreover, high cost of this system was a concern for widespread use of the technique (Murphy and Atala, 2014).

In this study natural micro-organization of the corneal stroma is mimicked with GelMA bioink containing corneal keratocytes and printing orthogonal layers by employing a simple pneumatic extruder.

3.3.1 Optimization of Printing Conditions

In this study, models created by Sketchup program were transferred as .stl files to the 3D printer, Bioscaffolder®. Low temperature dispense head of the Bioscaffolder® was used and hydrogels with different fiber thicknesses were obtained by controlling parameters such as movement speed of the nozzle in x-y direction (Fxy, mm/min) and spindle speed (R/S, Dots/min). Hydrogels were crosslinked after all the layers were printed. As a starting movement speed of the nozzle, Fxy 200 mm/min was chosen and R/S was varied between 0.01 and 0.04 dots/min (Figure 3.26). Stereomicrographs showed that as the R/S value increases the fiber thickness also increases since more solution is extruded in a given time. At 0.04 dots/min, fiber thickness was so high that it damaged the underlying layer. Therefore 0.01, 0.02, and 0.03 dots/min were later tested. Fxy speed was changed while R/S was kept constant. In contrast to R/S values, as Fxy increases, fiber thickness decreases since the same amount of polymer is extruded in a shorter time since the movement of the nozzle in x-y direction increases (Figure 3.27). When Fxy was 100, the duration for fiber deposition was long which resulted in thick fibers and the fidelity of the

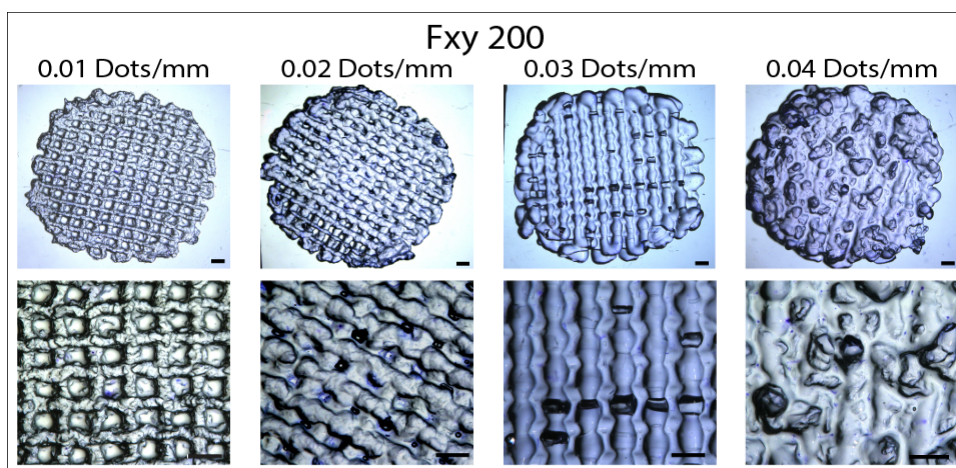


Figure 3.26: Stereomicrographs of 3D printed GelMA hydrogels. Spindle speed was changed in the range 0.01-0.04 dots/mm while Fxy speed was constant at Fxy 200. Scale bar is 1 mm.

subsequently deposited layers was lost. Fxy 200 speed was better than Fxy 100 where regular layers were obtained and were not distorted in the following layers and it was possible to print properly shaped constructs very similar to the model. For Fxy 300 setting, R/S 0.02 and 0.03 produced properly printed hydrogel. This speed was very high for R/S 0.01 since the amount of extruded solution was very low. R/S 0.02 and Fxy 200 yielded a viable construct as well.

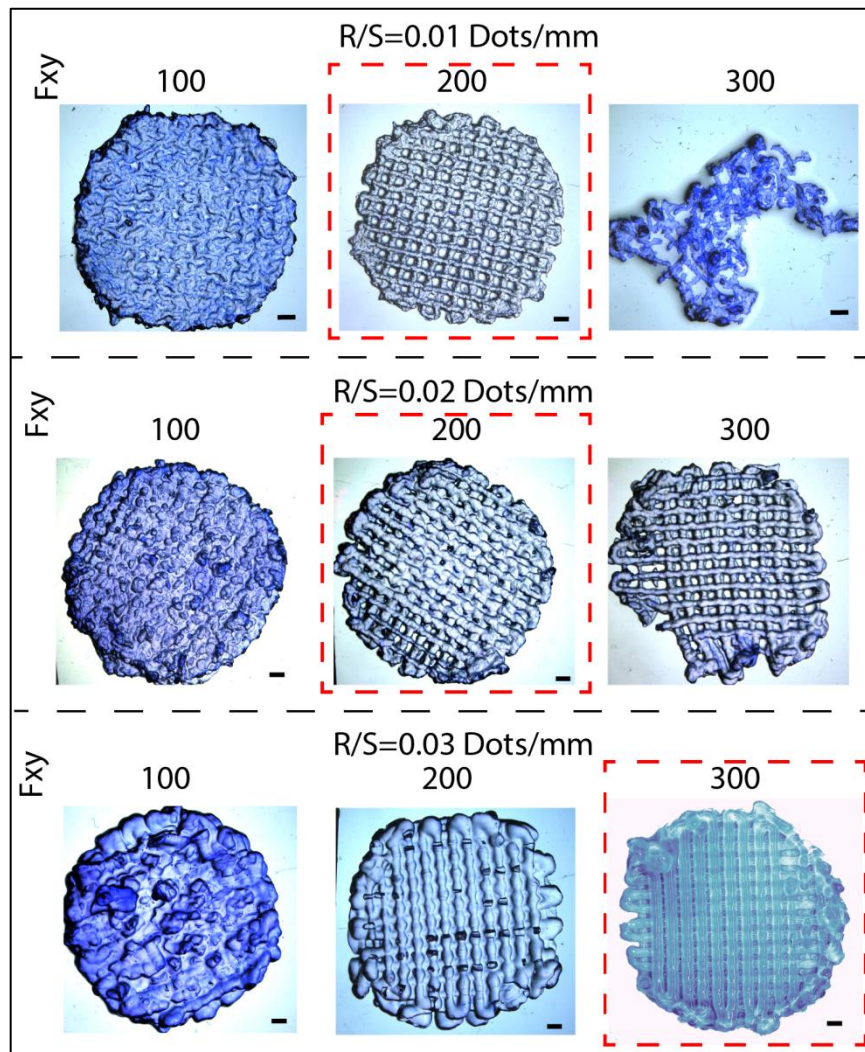


Figure 3.27: Stereomicrographs of 3D printed GelMA hydrogels. Fxy speed was changed from 100 to 300 mm/min while spindle speed was constant at 0.01, 0.02 or 0.03 dots/min. Scale bar is 1 mm. Dotted red lines indicate chosen parameters for the following studeis.

Obtaining an orderly formed hydrogel with proper organization in a short time is critical when printing in the presence of cells. To obtain a 3D printed hydrogel, Fxy 100 needs almost 5 min where it is 3 and 2 mins for Fxy 200 and Fxy 300, respectively. In the later characterization studies, R/S 0.01 and Fxy 200 (GelMA15-0.01), R/S 0.02 (GelMA15-0.02) and Fxy 200, and R/S 0.03 and Fxy 300 (GelMA15-0.03) (Selected parameters marked with dotted red lines, Figure 3.27 and Table 3.3) were chosen which yielded best pattern fidelity. Hydrogels which were not printed but obtained as slabs (Section 2.2.6) were labeled as GelMA15-Slab.

Table 3.3: Printability of the GelMA hydrogels as a function of movement speed of the nozzle in x-y direction (Fxy, mm/min) and spindle speed (R/S, Dots/min). Dotted red lines indicate chosen parameters for the following studeis.

Fxy (mm/min)	300	X	✓	✓	X
	200	✓	✓	✓	X
	100	X	X	X	X
		0.01	0.02	0.03	0.04
		R/S (Dots/min)			
		✓ Printable		✗ Unprintable	

3.3.2 Equilibrium Water Content (EWC) of Printed Hydrogels

Equilibrium water contents of the 3D printed and slab hydrogels are shown in Table 3.4. All of the hydrogels absorbed a significant amount of water in their structures, about 90% EWC, which is important to give cells space to proliferate.

Table 3.4: Equilibrium Water Content (EWC) of the hydrogels.

Samples	EWC (% , w/w)
GelMA15-Slab	92.0 ± 0.4
GelMA15-0.01	90.6 ± 0.8
GelMA15-0.02	88.0 ± 0.4
GelMA15-0.03	90.8 ± 0.8

3.3.3 *In Situ* Degradation of Hydrogels

In order to determine the stability of the 3D printed hydrogels samples were incubated in PBS (pH 7.4, 10 mM, 0.5 mg/mL sodium azide) for three weeks. 3D printed and slab hydrogels lost up to 8% in Day 21 (Figure 3.28) which is basically minimal degradation. There was no statistically significant difference between the degradation rates of the various 3D printed and slab hydrogels. Stability of the 3D printed hydrogels seems to be slightly better than the earlier hydrogels prepared in other sections (13% weight loss vs 8%). This difference in the stability of the hydrogels arises most probably from the processing conditions: 1) Different UV sources were used in crosslinking, 2) 3D printed hydrogels were incubated at 4°C prior to crosslinking. Incubation of hydrogel solution at 4°C to initiate a physical gel formation prior to UV exposure to enhance the stability of the hydrogels since dual crosslinking mechanism worked which are physical (at lower temperature) and covalent (due to UV exposure). Enhanced hydrogel properties in terms of stability and mechanics are also reported by other researchers due to physical gelation prior to covalent crosslinking (Hellio-Serughetti and Djabourov, 2006; Rizwan *et al.*, 2017; Yin *et al.*, 2018). This physical gelation (by cooling to +4°C) is known as sol-gel transition and is induced thermally and a physical crosslinking takes place through noncovalent interactions (Zhang *et al.*, 2017). Most of the natural polymers like gelatin (Bohidar and Jena, 1993), agarose (Chen *et al.*, 2013), and cellulose (Jeong, Kim and Bae, 2012) exhibit sol-gel behavior upon reduced temperature (Jeong, Kim and Bae, 2012). Researchers suggest that crosslinking after these physical association caused by temperature drop results in more efficient covalent bond formation due to increased proximity of the polymer chains (Hellio-Serughetti and

Djabourov, 2006). Another advantage of reversible physical network formation before irreversible photocrosslinking through UV exposure is the enhanced shape fidelity before and after 3D printing; otherwise it is impossible to obtain printed architecture in a liquid phase.

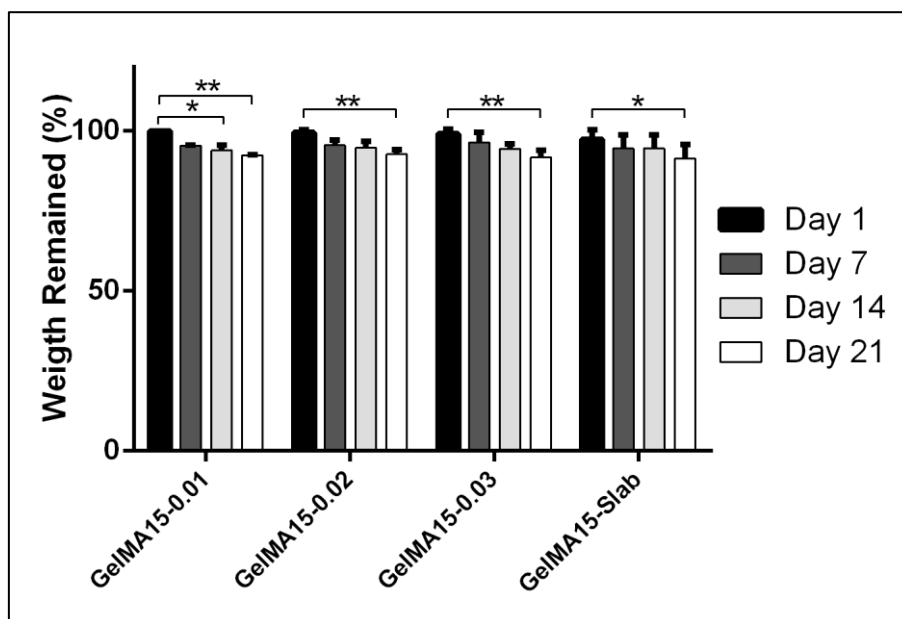


Figure 3.28: *In situ* stability test of 3D printed hydrogels (in PBS, pH 7.4, 10 mM) for 1 week). * $p < 0.05$, ** $p < 0.01$, and *** $p < 0.001$.

3.3.4 In vitro Studies

3.3.4.1 Viability of Keratocytes in 3D Printed Hydrogels

Human keratocyte loaded 3D printed hydrogels were double stained with Calcein AM (Stains live cells green), and Ethidium homodimer (Stains dead cells red) in order to determine the viability in the hydrogels. Figure 3.29 shows three 3D printed hydrogels and GelMA-15 slab on Days 1, 7, and 14. Figure 3.30 A shows viability of cells on Day 21 and the figure includes depth profile of the Day 21 data to show homogenous distribution of cells within the hydrogels. NIH Image J program was used to quantitatively analyze the fraction of the live cells in the hydrogels (Figure 3.30 B). Results showed that over 95% of the cells were alive in all types of the hydrogels at all time points and color coded depth profile indicated that cells were distributed homogeneously throughout the whole 500 μm thickness. High viability of cells proves that the printing conditions are suitable for cell viability. In the literature a wide range of viability results (changing from 35% to 92%) of the cells in GelMA hydrogels were reported depending on the printing conditions, GelMA concentrations, and crosslinking parameters (Bertassoni *et al.*, 2014; Colosi *et al.*, 2015; Joung *et al.*, 2018; Yin *et al.*, 2018).

It should however be noted that the cells in printed hydrogels were mostly in round shape while elongated in GelMA-10 and GelMA-15 hydrogels. As mentioned in Section 3.3.3 both more intense UV exposure and physical crosslinking prior to UV exposure most probably resulted in much more dense network formation. This dense crosslinking limited the mobility of the cells and they could not interact with each other and elongate. Studies suggest that cells try to form stable contacts with the surrounding cells through their extensions and if this contact does not occur they retract them (Hoffmann and Schäfer, 2010). Cells in the hydrogels, therefore, could not interact with each other due to dense crosslinking and as a result could not elongate. In their study Yin *et al.* (2018) reported similar results where high GelMA concentration (30%, w/v) resulted in increase in covalent bond abundance which leads enhanced rigidity, low porosity and thus more round shaped cells compared to hydrogels prepared from 5% and 8% GelMA concentrations. Several researchers, therefore, attempted to find new methodologies like pre-crosslinking of the hydrogel

solution (GelMA + gelatin or alginate) physically by thermal or ionic interactions to enhance printability of GelMA at low concentrations (as low as 5%) (Colosi *et al.*, 2015; Yin *et al.*, 2018). Increasing the number of loaded cells prior to printing can be another viable option to obtain more interacting cells. In Section 3.1.5.2, the number of cells was optimized as 1×10^6 cells/mL since higher cell densities resulted in fragile hydrogels. However, higher crosslinking density of the 3D printed constructs may allow entrapment of more cells. A moderate entrapment density of cells reported as 2×10^6 cells/mL by many researchers (Duan *et al.*, 2012; Kolesky *et al.*, 2014; Isaacson, Swioklo and Connon, 2018) can be used to enhance the interactions of the cells with each other.

Mimicking the curved nature of the native cornea may also help to obtain elongated cells in the constructs where this concept was shown recently by Gouveia *et al.* (2017). Researchers used a smart peptide amphiphile (PA) coated curved agarose template to grow corneal keratocytes. Their studies showed that substrate curvature alone is an enough cue for the cells to orient, produce aligned extracellular matrix and express corneal stromal cell markers without the need of any additional topographical cues. Our study, therefore, can be further improved by mimicking the curvature of the cornea either by printing on a curved template or crosslinking the printed structure on a curved template for the construct to take shape of it.

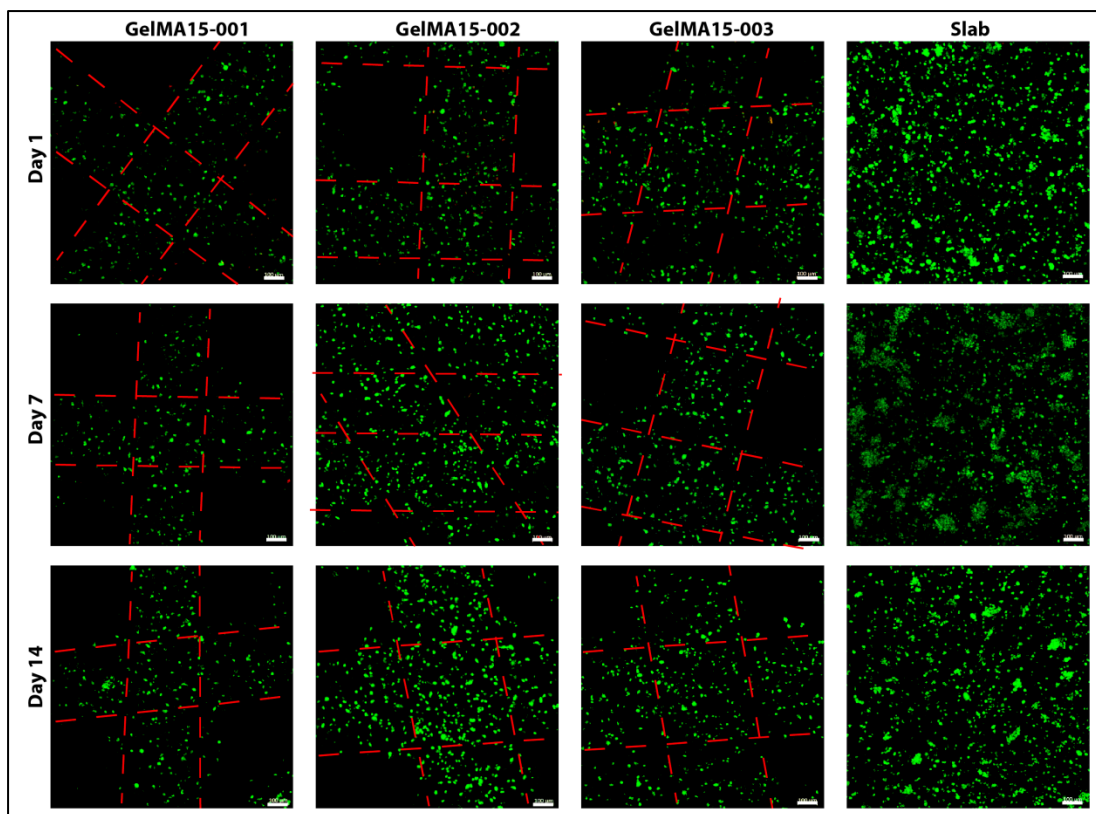


Figure 3.29: CLSM images showing results of Live Dead Cell Viability Assay of 3D printed GelMA hydrogels on Day 21. A) Live-Dead assay with red showing dead (ethidium homodimer-1) and green showing live cells (calcein). Scale bars: 100 μm . Dotted red lines indicate the pattern borders. Percent viability of the cells is shown in Figure 3.30 B.

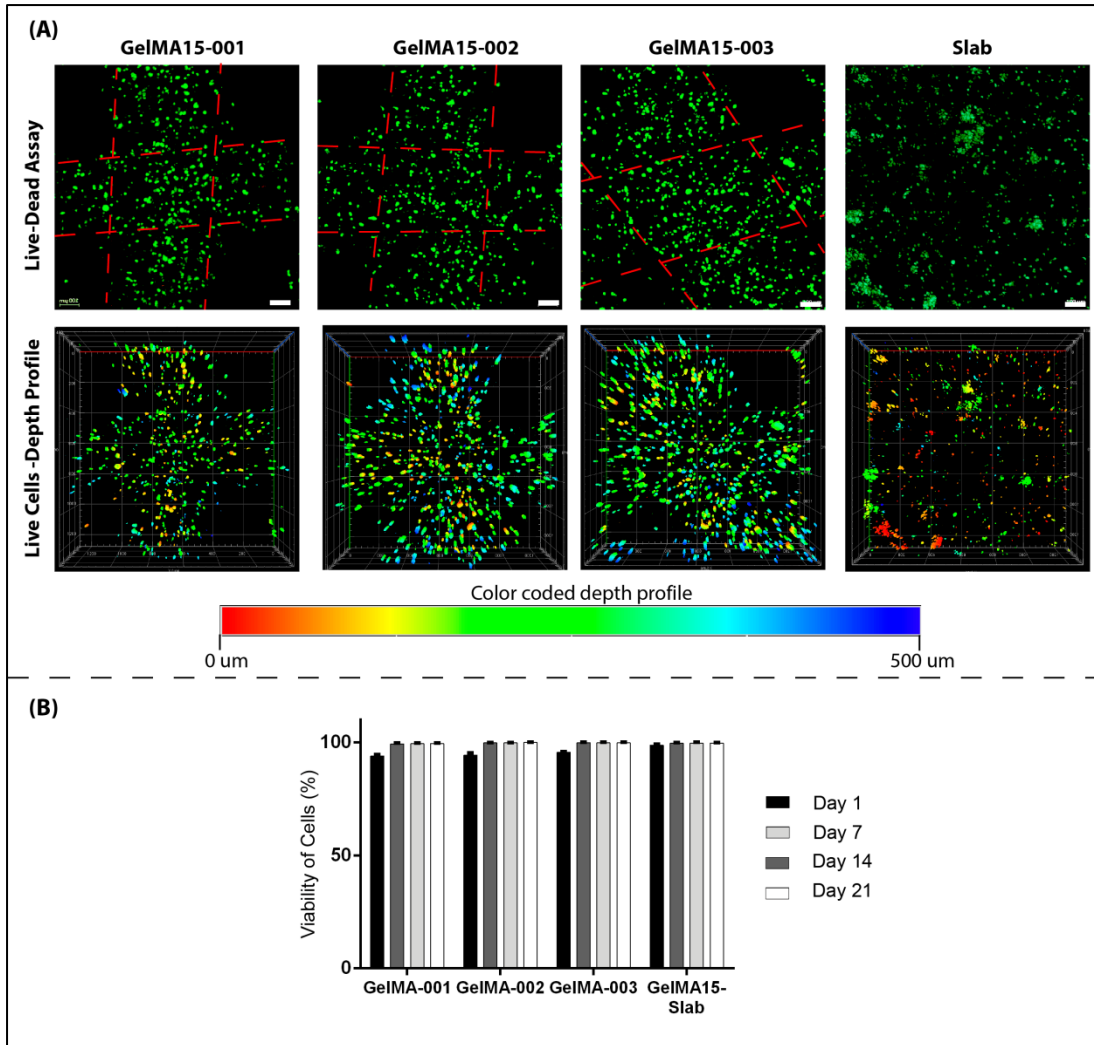


Figure 3.30: CLSM images showing results of Live Dead Cell Viability Assay of 3D printed GelMA hydrogels on Day 21. A) Live-Dead assay with red showing dead (ethidium homodimer-1) and green showing live cells (calcein). Color coded depth profile of the same images showing the distribution of live keratocytes in 3D printed GelMA hydrogels (red at the surface and blue at the bottom). Scale bars: 100 μm . Dotted red lines indicate the pattern borders. B) Quantitative analysis showing viability of cells (%).

3.3.4.2 Cell Proliferation in 3D Printed Hydrogels

Proliferation of cells in 3D printed hydrogels was studied by Alamar Blue assay which reflects the metabolic activity of the cells and results were compared with the number of cells counted by NIH Image J program from the Live-Dead Viability assay images (n=3). The cell numbers were much lower than on TCPS (data not shown) because they were entrapped in the hydrogels. The cell number (or activity) in slab gels is apparently higher on Day 1 and 7 than those 3D printed hydrogels (Figure 3.31). Same proliferation trend was observed in Figures 3.31 A and B where the metabolic activity of the cells in all 3D printed was similar and did not change during incubation period. However, metabolic activity and number of cells in the GelMA15-Slab hydrogels decreased significantly from Day 7 to Day 14 (Figure 3.31). This decrease on Day 14 at all samples probably because of the tendency of the cells to produce extracellular matrix rather than proliferation. Another reason can be the degradation of the scaffolds which leads to material and cell loss. Previous results (Section 3.1.5.4) showed a continuous increase in metabolic activity of the cells in GelMA-10 and GelMA-15 hydrogels during 21 days of incubation. The difference can be because of the variation in the crosslinking density of the hydrogels due to different UV sources and physical crosslinking of 3D printed hydrogels prior to UV exposure (Sections 3.3.3 and 3.3.4.1) which may limited the

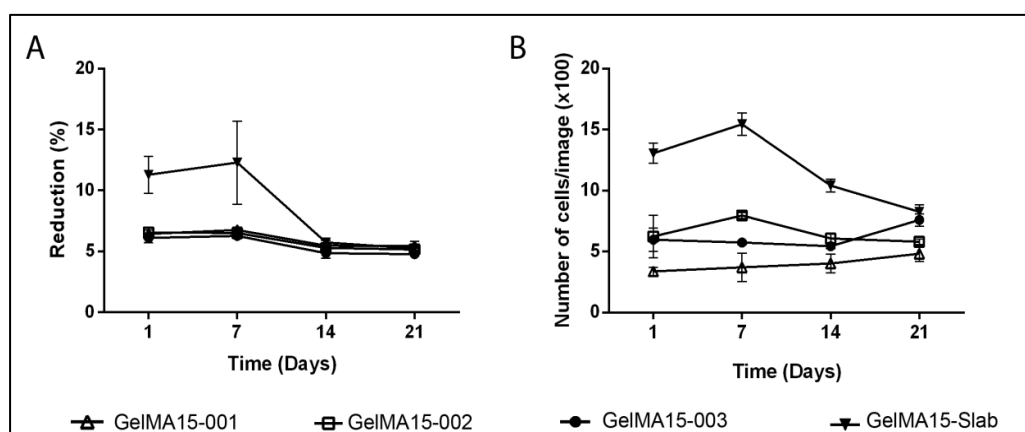


Figure 3.31: Proliferation of human keratocytes in 3D Printed and GelMA15-Slab hydrogels over 3 weeks. A) Alamar Blue Assay shows proliferation of cells in the hydrogels as indicated by Reduction %, and B) Number of cells per image is counted from Live-Dead viability assay images (n=3) by NIH Image J program.

mobility of the cells, nutrient and oxygen transport throughout the hydrogels. These limitations also explain the quite high metabolic activity of the previous hydrogels compared to 3D printed ones (40% vs 7%, for GelMA-15 vs 3D printed hydrogels, Day 21).

3.3.4.3 Mechanical Properties of Cell Loaded Hydrogels under Compression

3D printed, cell loaded and unseeded (control) hydrogels were tested under compression to determine their mechanical properties. Results showed that compressive modulus of only the cell loaded 3D printed hydrogels increased significantly from Day 1 to Day 21 and there was no statistically significant difference between other groups (Figure 3.32). In the literature, the mechanical strength of the native corneas of people aged 50-64 was measured to be in the range 403 to 624 kPa under tensile load (Elsheikh et al, 2007). Compressive moduli of the 3D printed hydrogels were around 20 kPa on Day 21 which is lower than the native cornea values. However, we expect that the strength of the hydrogels will increase in time, because previous studies by our group had shown that culturing the scaffolds with corneal keratocytes for a month enhances their mechanical properties significantly (Zorlutuna et al., 2007; Vrana et al., 2007).

It should be noted that starting compressive moduli of the samples were higher than the compressive moduli of the hydrogels mentioned in Section 3.1.5.8 most probably due to differences in crosslinking conditions as explained in previous sections. Positive effect of increased crosslinking density to the modulus due to increase in UV exposure duration is also reported by other researchers (Schuurman *et al.*, 2013; Colosi *et al.*, 2015). However, the increase in the moduli during three weeks of incubation is higher in GelMA-10 and GelMA-15 hydrogels (around 50 kPa for GelMA-15 vs 20 kPa for 3D printed hydrogels, Day 21). This increase is explained in the literature by the nonenzymatic glycation through crosslinking of proteins by reducing sugars during incubation in growth medium (Girton, Oegema and Tranquillo, 1999; Girton *et al.*, 2000). As explained above, crosslinking density of the 3D printed hydrogels is predicted to be higher than GelMA-10 and GelMA-15 hydrogels due to dual crosslinking mechanism (physical and covalent) and therefore it probably less affected from nonenzymatic glycation mechanism than others.

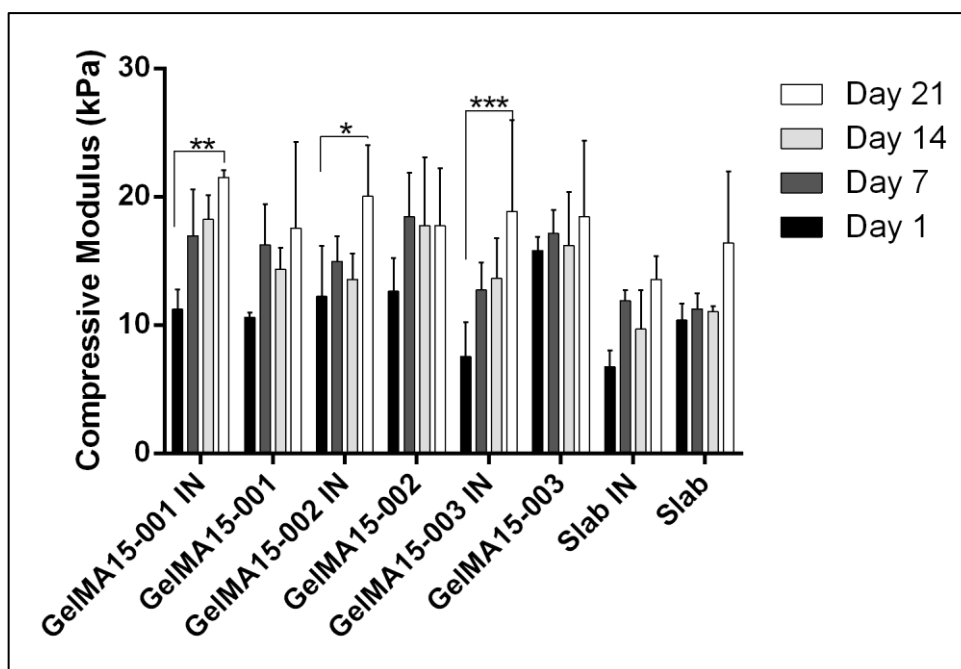


Figure 3.32: Compressive moduli change of cell loaded 3D Printed, unloaded 3D printed, cell loaded GelMA15-Slab and unloaded GelMA15-Slab hydrogels over 3 weeks. * $p < 0.05$, ** $p < 0.01$, and *** $p < 0.001$. IN: with cells.

3.3.4.4 Immunofluorescence Staining: Extracellular Matrix Synthesis of the Human Keratocytes in the 3D Printed Hydrogels and Hydrogel Slabs

Extracellular matrix synthesis of the keratocytes loaded in the 3D printed hydrogels and hydrogel slabs were studied on Day 21. Samples were stained for collagen types I and V, decorin, and α -SMA. Results showed that collagens and decorin synthesized by only the cells at the edge of the fibers synthesized in the 3D printed samples (Figure 3.33) because very low or no signal was detected in the core of the fibers. Similarly, only the keratocytes close to the surface of the hydrogel slabs synthesized ECM molecules as can be seen with Z-stack mode of CLSM. These results suggest that cells have more access to the growth medium and oxygen could express ECM molecules but others could not even though cells inside the hydrogels were alive (Figure 3.29); apparently they were not metabolically active. In the previous sections, ECM expression from the whole thickness of the GelMA hydrogels could be detected (Sections 3.1.5.6 and 3.2.7.3). High crosslinking density of 3D printed hydrogels due to different UV source and dual crosslinking most probably restricted the mobility of the cells, limited their access to oxygen and growth medium, and

there was no ECM expression. Keratocytes in GelMA15-001 and GelMA15-002 hydrogels, however, expressed more collagen and decorin compared to GelMA15-003 hydrogels. This may be because of lower surface area of GelMA15-003 hydrogels due to its thicker fibers than other 3D printed hydrogels. Alpha smooth muscle actin (α -SMA) expression could not be detected or was significantly lower than other corneal keratocyte specific markers. In intact cornea, the corneal are relatively quiescent, function to maintain collagen and other ECM components and do not normally express α -SMA. However, corneal injuries result in transformation of the keratocytes to myofibroblasts-like cells. This transformation is characterized by pharmacologic, morphologic and biochemical features similar to that of myofibroblasts. Alpha-SMA, vimentin and desmin expressions are the indicators of this transformation as a part of corneal wound healing (Jester *et al.*, 1995, 1996). Corneal crystallin production of the myofibroblasts is very limited which leads to corneal stromal opacity and fibrosis (Fini, 1999; Torricelli *et al.*, 2016). Significantly lower expression of α -SMA suggests that the keratocytes did not transform into myofibroblasts-like cells and protected their keratocyte features.

Cell density into the hydrogels can be increased to help cells interconnect with each other which may increase the expression of corneal specific proteins and proteoglycans. Optimizing the crosslinking conditions to obtain hydrogels with less crosslinking density may also enhance the growth medium and oxygen transport into the hydrogels.

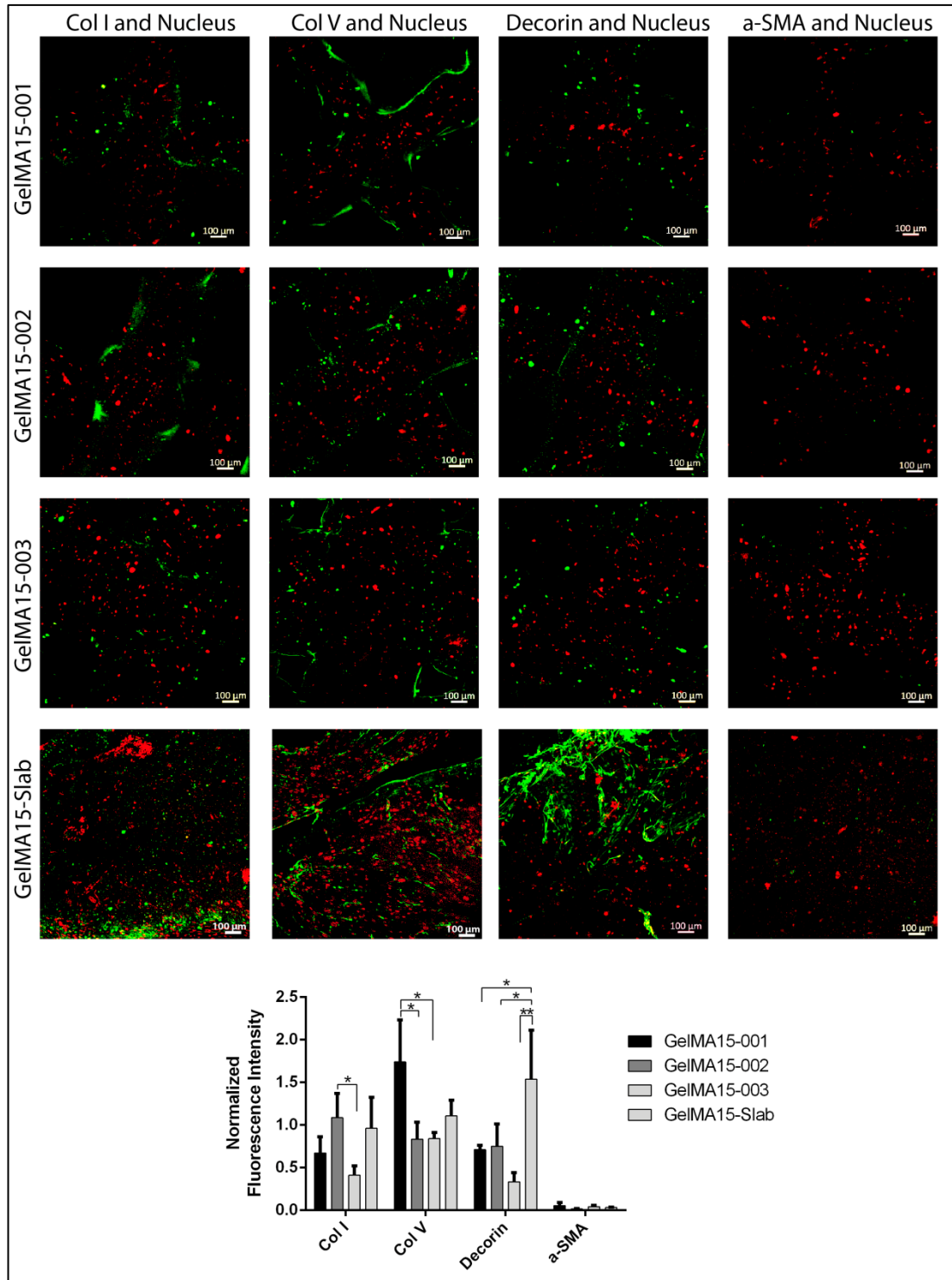


Figure 3. 33: Immunocytochemistry of 3D printed hydrogels and hydrogel slabs. A) CLSM images on Day 21. Draq5 is for nucleus (red). Representative collagens (Collagen Type I and V), proteoglycan (Decorin), and myofibroblast marker α -SMA are shown in green. Scale bar is 100 μ m. B) Semi-quantitative fluorescence intensity analysis of CLSM images. $n=3$. * $p < 0.05$ and ** $p < 0.01$.

3.3.4.5 MMP Activity of the Keratocytes Loaded into 3D Printed Hydrogels and Hydrogel Slabs

MMP activity of the keratocyte loaded 3D printed hydrogels and hydrogel slabs was studied for 21 days. Culture medium was collected at every medium change, MMPs secreted and diffused into the culture medium was detected by MMP assay kit as mentioned in Section 2.2.8.9. MMP activity of the keratocytes in 3D printed hydrogels was similar and significantly lower than ones in the slabs (Figure 3.34). MMP levels did not change during the culture period but a continuous increase was observed in GelMA15-Slab. This difference can be explained by the cell proliferation profile of the samples. As discussed in Section 3.3.4.2, proliferation of the cells in the 3D printed hydrogels was very low compared to cells in GelMA15-Slab. Since MMPs activity of the samples are given as cumulative (Day 21 medium also contains Days 1, 7, and 14 media), effect of cell number decrease is not seen on the graph. Moreover, decrease in cell number can be explained by continuous increase in MMP activity. MMPs (especially collagenase and gelatinase) are activated in injured corneas for wound healing mechanism (Riley *et al.*, 1995; Sivak and Fini, 2002) which also degrade GelMA constructs (Section 3.1.4). Material loss due to collagenase activity, therefore, may also have led to cell loss. As discussed in the previous section (Section 3.3.4.4), cells in the strands of the 3D printed hydrogels were most probably not metabolically active due to limited nutrients and oxygen, which explains the low MMP activity. *In vivo* degradation of the constructs by MMPs is essential for the regeneration of tissue and removal of the constructs by the mechanisms of the host. MMPs of the surrounding tissue may also help degradation of the constructs *in vivo*.

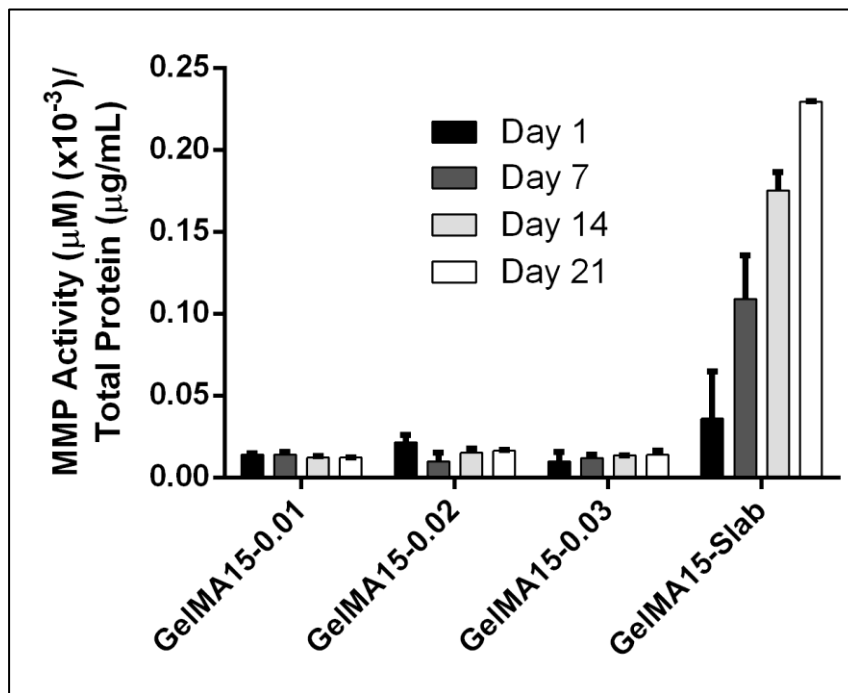


Figure 3. 34: MMPs activity of the keratocytes in the 3D printed hydrogels and hydrogel slabs during 21 days of culture. MMP concentrations were normalized by the total protein content of the test media.

3.3.4.6 Transparency of Cell Loaded, 3D Printed Hydrogels

The most important property of cornea is to refract light onto the lens where it is refracted further for vision. In order to achieve this, corneal construct has to be transparent and refract and transmit the light. Transparency of the hydrogels was studied by scanning with a UV-Vis spectrophotometer in the range 250-700 nm. Transparency of all hydrogels was 80% or higher except for the cell loaded slab hydrogels on Day 1, which was about 75% at 700 nm (Figure 3.33 A and Table 3.5). The reason for this lower transparency is most probably because of the light scatter due to higher number of cells in it compared to others (Section 3.3.4.2). Light transmittance of the cell loaded slab hydrogels, however, increased during incubation period up to 83%. Transmittance of the samples was lower in the 290-400 nm which is UVA and UVB regions than in the visible range (400-700 nm) and is comparable with the natural cornea (~5% at UVB and 85% at 700 nm for a cornea of an 8 year old) (Mallet and Rochette, 2013). However, GelMA15-Slab hydrogels were better than 3D printed hydrogels in terms of UV transmittance (at 300 nm, Table 3.5). This result may be because of the compact nature of the hydrogel slabs compared to 3D printed samples since 3D printed hydrogels have holes between the strands where light directly pass without any absorption. This may also explain the higher light transmittance of the 3D printed samples than hydrogel slabs at 700 nm (Table 3.5). In conclusion, although light was refracted because of the patterns of 3D printed hydrogels, their transparency was still comparable with each other and the with native cornea. Overall transparency of all samples were slightly lower than the transparencies recorded for GelMA-10 and GelMA-15 hydrogels (Section 3.1.5.7) (85-90% for 3D printed hydrogels vs 90-93% for GelMA-10 and 15 hydrogels). Estimated higher crosslinking density of the 3D printed hydrogels most probably affected the light transmission of the samples. Clarity of the 3D printed and slab hydrogels is seen in the stereomicrographs (Figure 3.33 B).

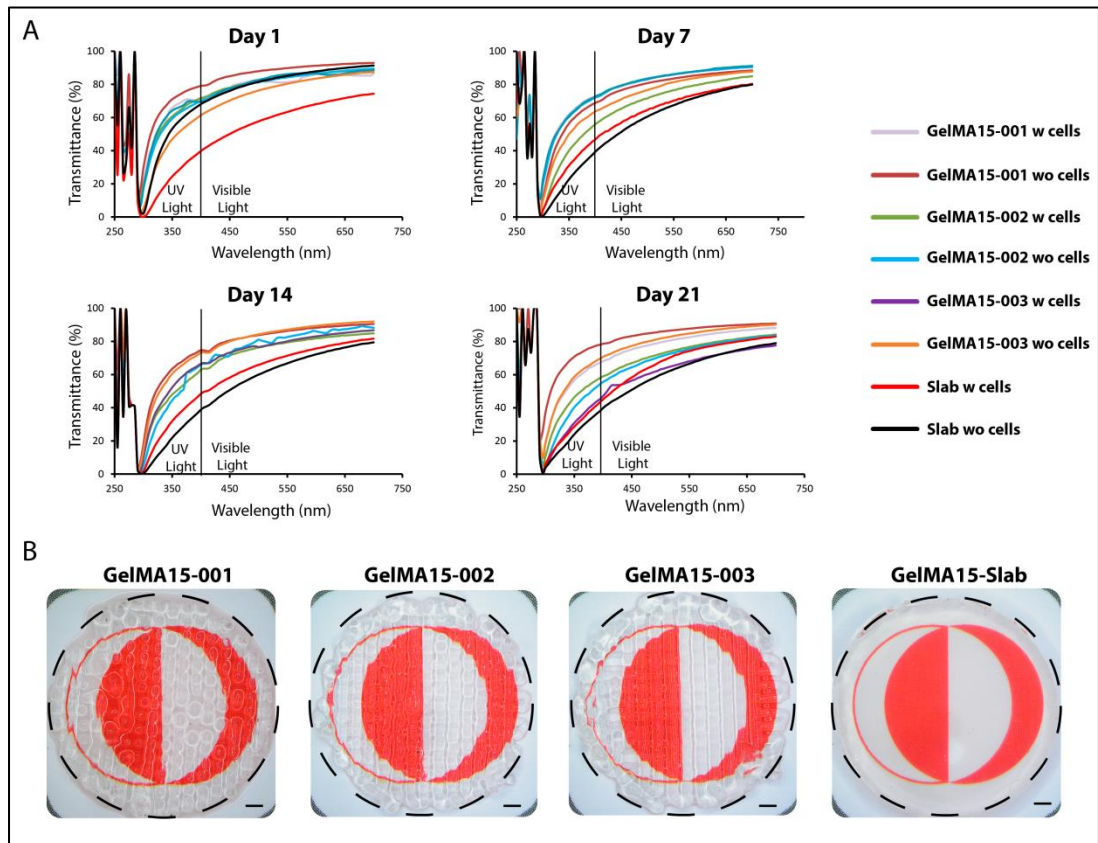


Figure 3.35: Transparency of the 3D printed hydrogels. A) Change of transparency of the cell free and keratocytes carrying hydrogels with time. B) Stereomicrographs showing transparency of cell free hydrogels on Day 0 (Outlined in black). Scale bar is 1 mm. w: with, wo: without.

Table 3.5: Transmittance (%) of cell loaded (w cells) and cell free (w/o cells) 3D printed and hydrogels slabs at 300 and 700 nm during 21 days of incubation.

WL (nm)	Time (Days)	GelMA15-001 w cells	GelMA15-001 w/o cells	GelMA15-002 w cells	GelMA15-002 w/o cells
300	1	20.1765184	29.3379768	19.2509828	17.13652416
	7	18.8324615	11.2718937	4.08090055	19.69267504
	14	17.8591085	17.8591085	10.1057138	5.036739612
	21	19.2247324	36.9693232	10.6567176	5.38985665
700	1	86.6741956	92.9434362	89.2370422	89.43966458
	7	90.4534913	88.4066323	84.8939531	90.38800043
	14	90.4905884	90.4905884	84.8365522	88.27172026
	21	88.1715365	90.8663405	84.2661479	83.65687875

Table 3.5: Continue

WL (nm)	Time (Days)	GelMA15-003 w cells	GelMA15-003 w/o cells	GelMA15-Slab w cells	GelMA15-Slab w/o cells
300	1	17.1975113	5.08958932	0.0795624	2.013928873
	7	22.4052977	9.73952051	4.01279564	0.634114331
	14	9.93904114	14.3953374	1.50944869	0.471419869
	21	12.0264185	16.6860766	6.0450489	3.843676175
700	1	88.5701093	87.4990581	75.2825221	91.35097336
	7	91.1990041	87.7767928	80.3229594	79.875691
	14	86.7422906	92.0079293	81.6721495	79.43520204
	21	83.8577219	88.5475813	83.0231162	79.04014989

3.4 *In Vivo* Studies

3.4.1 Implantation and Examination in Rabbits

Above mentioned *in situ* and *in vitro* studies showed that GelMA hydrogels are quite stable, have excellent transparency, sufficient mechanical strength and highly biocompatible by allowing over 90% cell viability.

In order to test the *in vivo* performance of the GelMA15-Slab hydrogels, firstly left eye of one New Zealand rabbit was operated as mentioned in Section 2.2.9. Briefly, cell-free hydrogel (300 μm in thickness and 5 mm in diameter) was inserted into a mid-stromal pocket in the cornea of the left eye and fixed with a suture. Operated eye was labeled as 1GL (See Table 2.2). Right eye of the same rabbit was left untouched to serve as control (was labeled 1BR). Netildex™, a common eye drop prescribed after eye operations (Pianini *et al.*, 2010), was started after 2 days of implantation in order to prevent any inflammation. Figure 3.36 shows the implantation and 15 weeks follow-up under slit lamp. Rabbit's first examination was on Day 2 under slit lamp and no edema, ulcer or infection was observed in either eye. Sutures were intact and hydrogel was at the implantation site. First week observation (Figures 3.36 C and D) showed a fibrous reaction and loss of clarity in the left eye (Figures 3.36 A and B) most probably not applying Netlidex™ soon after surgery. Besides, hydrogel was prepared under sterile conditions but during surgery it was exposed to an unsterile environment. Maxidex® eye drop containing dexamethasone was started on Day 7 to prevent fibrous reaction according to Loftsson and Stefánsson (2003). Beside this fibrin reaction, no other reaction such as edema, ulcer or infection was observed. Schirmer's test was done to both eyes of the rabbit and no difference in tear production was observed (Figure 3.37). Sodium fluorescein staining was done to assess corneal integrity and edema formation, and there was no difference between the control and test eye (Figure 3.37). On the 3rd week a deep vascularization was observed in the left eye (1GL) and 1BR was normal (Figure 3.38). Neovascularization of cornea is seen in cases of chemical burns, trauma, infection, inflammation and ischemia (Chang *et al.*, 2012). To avoid

vascularization one dose of sub-conjunctival Eyelea (anti-VEGF) was applied to 1GL. Anti-VEGF application is a common treatment for diseases like macular edema, neovascular glaucoma, neovascular age-related macular degeneration and other diseases causing neovascularization (Brown and Regillo, 2007; Chang *et al.*, 2012; Amadio, Govoni and Pascale, 2016). In the following weeks (Figure 3.36 I-P) neovascularization was reduced significantly and cornea regained significant clarity.

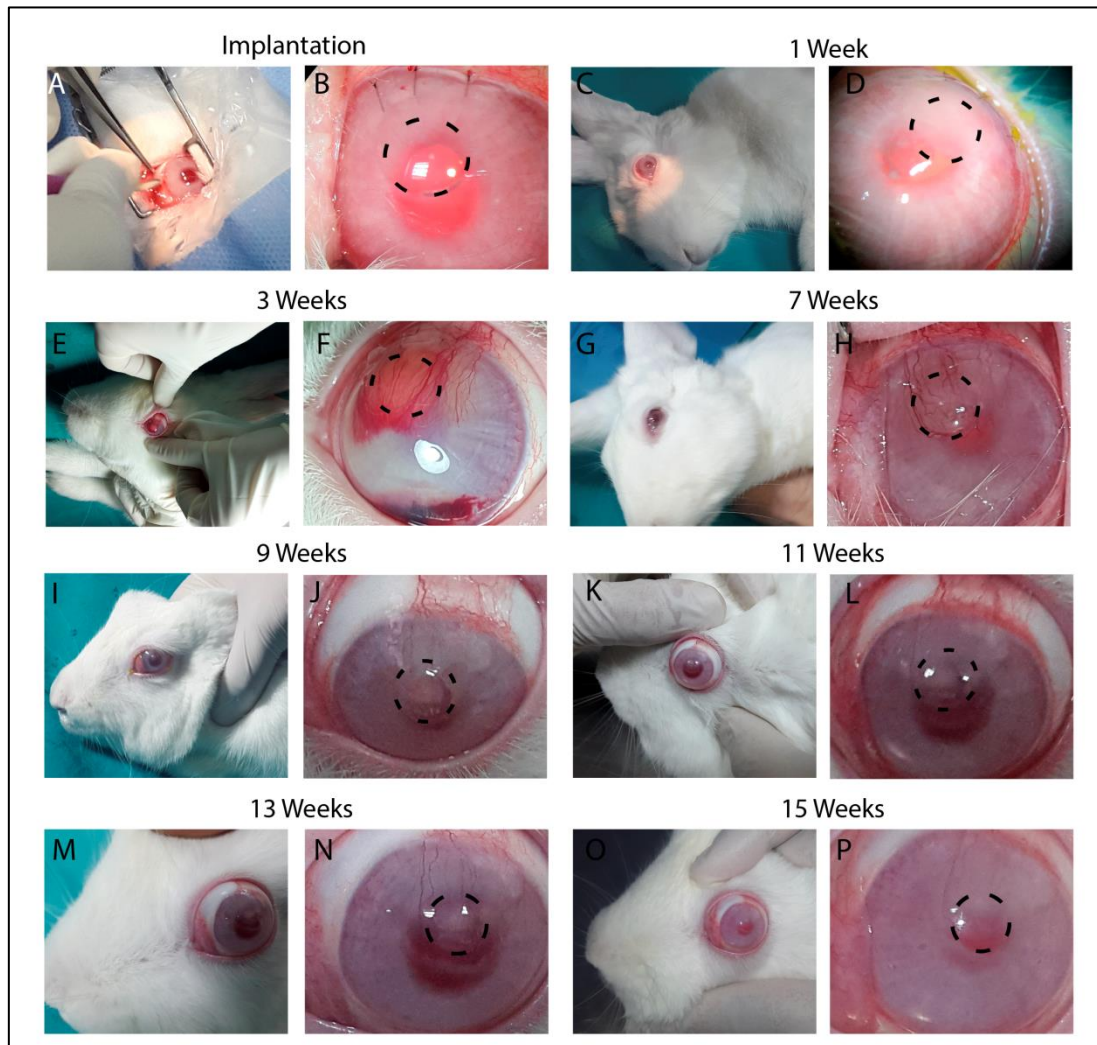


Figure 3.36: Implantation of GelMA15-Slab hydrogel in one eye of a New Zealand white rabbit. A) Lamellar dissection in cornea, B) implanted hydrogel into mid-corneal pocket, C-P) Examination of test eye during 15 weeks. Black circles show the implantation site.

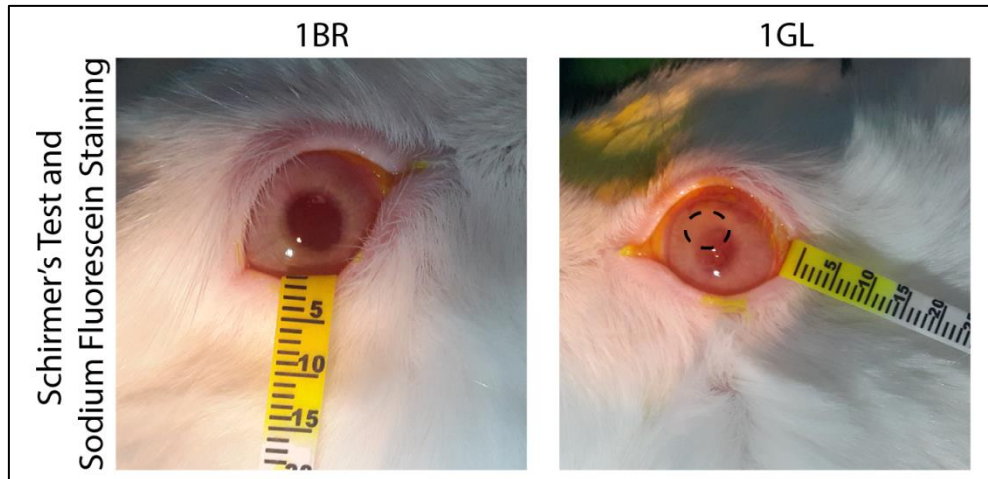


Figure 3.37: Examination of control and test eye on Day 7 with Schirmer's test and sodium fluorescein staining. Black circle indicates implantation site.

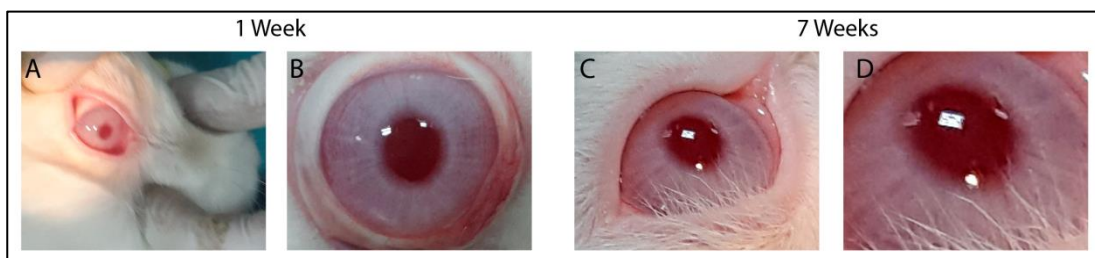


Figure 3.38: Examination of control eye. A-B) First Week, C-D) 7th Week.

Cornea of the rabbits is different than human cornea. They are about 410 μm in thickness where stroma constitutes 90% (Kaye and Pappas, 1962; Chan, Payor and Holden, 1983). Thickness of the implant was about 300 μm and was quite a thick insert for a 410 μm thick cornea. Moreover, it was difficult to track the effect of suture on the implanted eye since other eye was left intact.

In the light of these results, one more rabbit was tested with a much thinner GelMA hydrogel (150 μm thick, 4 mm in dia) (labeled 2GR, right eye) without any suture fixation (Figure 3.39) and Netildex® eye drop was started immediately following implantation. A mid-stromal corneal pocket was also prepared in the left eye as test eye but it served as sham; no implantation was done, it was done to study the effect of the surgical procedure (labeled 2SL, S:Sham).

GelMA15-Slab hydrogel was successfully implanted in the mid-stromal pocket of the cornea (Figures 3.39 A, B). Hydrogel did not cause any infection, inflammation, edema or ulcer as 2SL. However, on the 3rd week a slight vascularization and loss of clarity was detected probably due to foreign body reaction of the eye (Figure 3.39 E, F) but the vascularization was not as deep as the 1GL. One dose of Eyelea removed

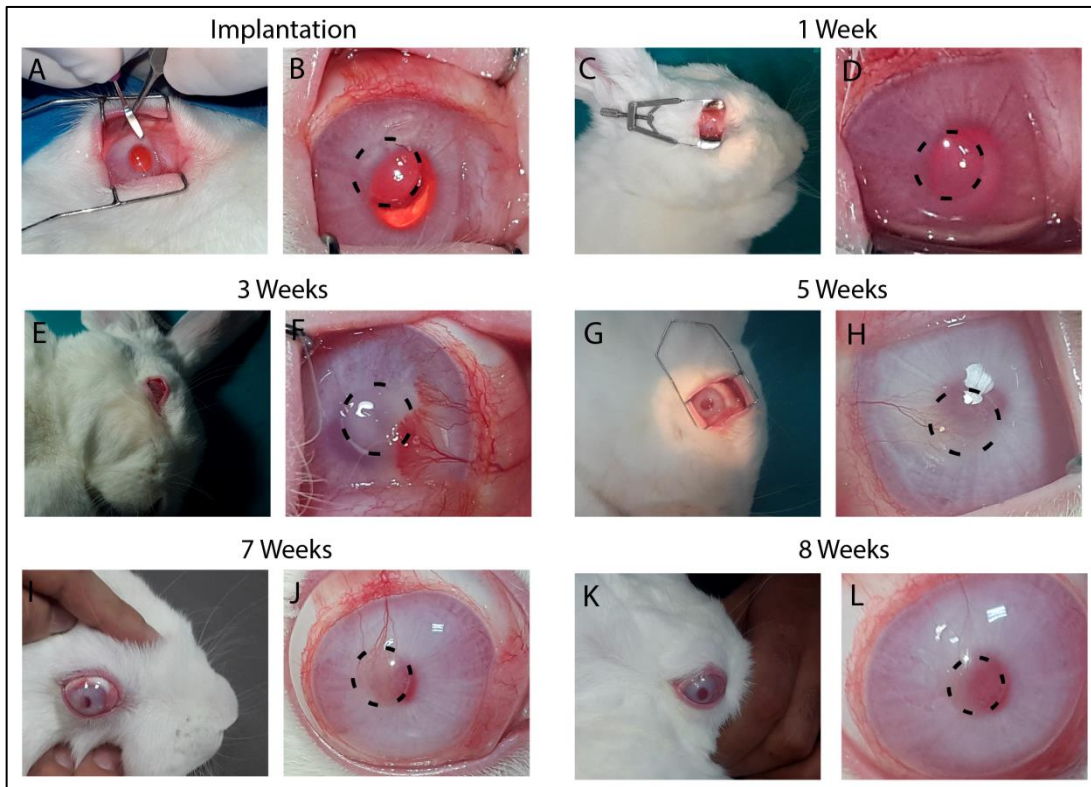


Figure 3.39: Implantation of GelMA15-Slab hydrogel on one eye of one rabbit. A) Lamellar dissection in cornea, B) implanted hydrogel into mid-stromal pocket, C-P) Examination of test eye during 8 weeks. Black circles show the implantation site.

the vascularization and cornea regained most of its clarity in the rest of the 8 weeks of observation (Figure 3.39 G-L). Control eye (Sham, 2SL) was healthy and no reaction was observed indicating that operation was successful and did not harm the cornea (Figure 3.40 A-L). Schirmer's test showed that tear production of both eyes were similar and no edema was observed by sodium fluorescein staining (Figure 3.41).

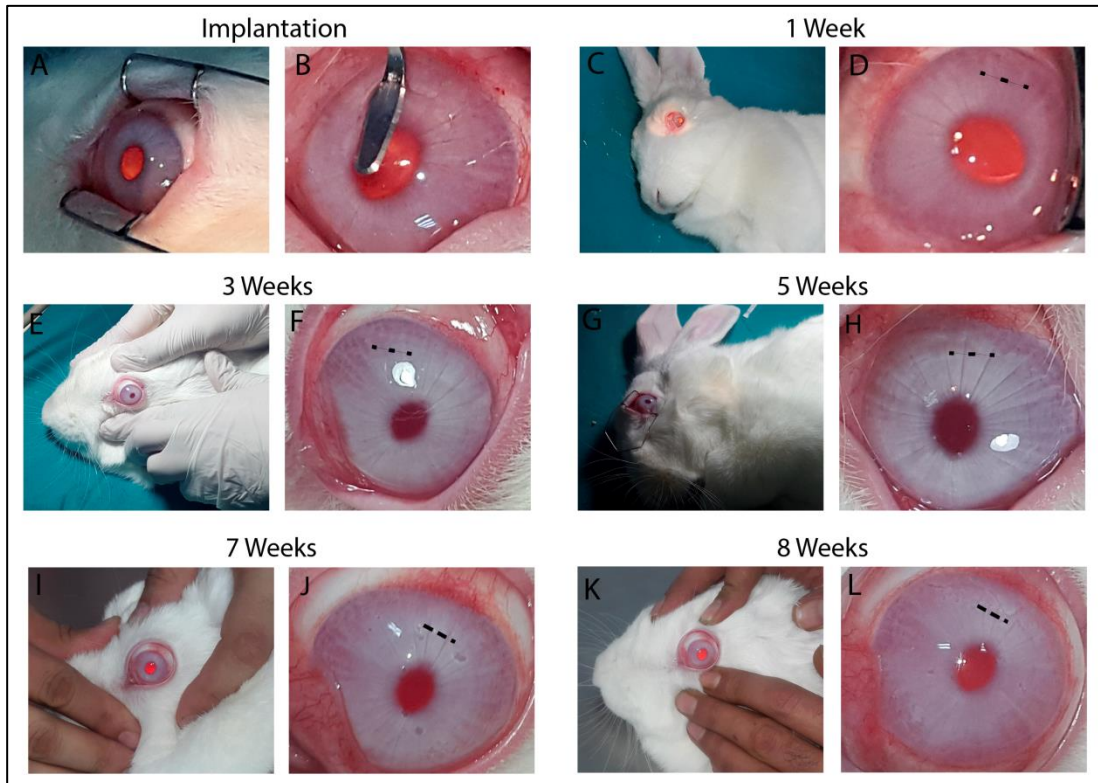


Figure 3.40: Operation of left cornea of the rabbit to serve as Sham control (A-B) Lamellar dissection in cornea, (C-L) Examination of implanted eye during 8 weeks. Black dotted lines show the implantation site.

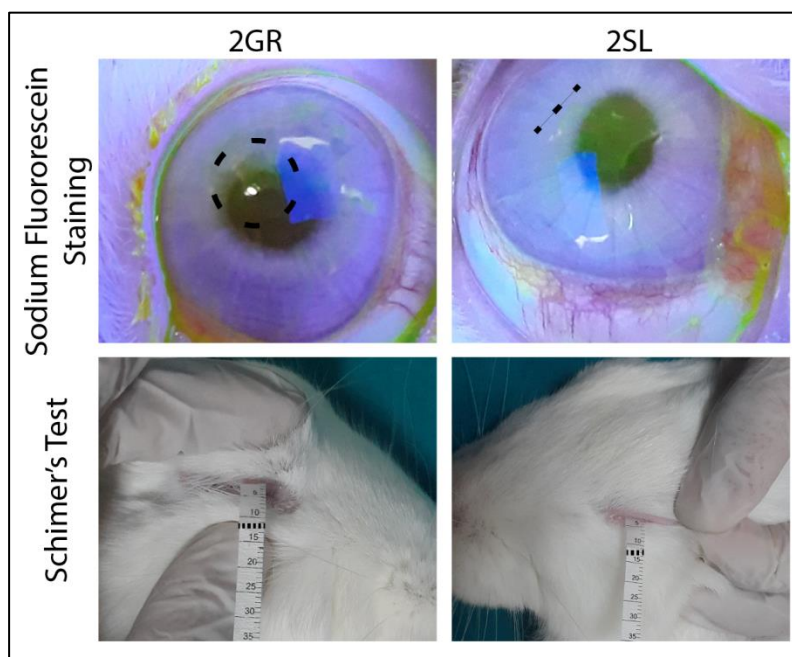


Figure 3. 41: Examination of control and test eye on Day 7 with Schirmer's test and sodium fluorescein staining. Black circle indicates implantation site.

Implantation of corneal constructs to an opened mid-stromal pocket was reported several times in the literature (Mimura *et al.*, 2008; Hashimoto *et al.*, 2010; Du and Wu, 2011; Xiao *et al.*, 2011; Cui *et al.*, 2018; Long *et al.*, 2018). Long *et al.* (2018) implanted cell free collagen–hydroxypropyl methylcellulose membranes with suture fixation to study corneal regeneration and they also reported a mild reaction followed by neovascularization which disappeared after 1 week. Cui *et al.* (2018) prepared cell laden and orthogonally aligned collagen membrane constructs to study *in vitro* and *in vivo* performance. Researchers implanted the constructs into mid-stromal pocket with suture fixation and reported no reaction or loss of clarity during 6 weeks of observation. Mimura *et al.* (2008) implanted gelatin hydrogels to the stromal pocket. They reported no side effects and adverse reactions in the eyes of the rabbits during 4 weeks of implantation. Importantly, researchers did not generally use sutures during implantation. The limitation of studies published by Cui *et al.* (2018) and

Mimura et al. (2008) is the quite short observation period which is not enough to make a conclusion about the overall effects of the constructs in terms of their safety which may cause rejection, infection and corneal opacity in long term. When these studies are considered, implantation of the constructs in the mid-stromal pocket seems quite safe and does not cause any problems that can threaten the integrity of the cornea.

Cornea of the first test rabbit 1GL was removed after 15 weeks, and those of the second rabbit, 2SL and 2GR, were removed after 8 weeks (Figure 3.42 A-C) by terminating the rabbits with an overdose ketamine for histological examinations.

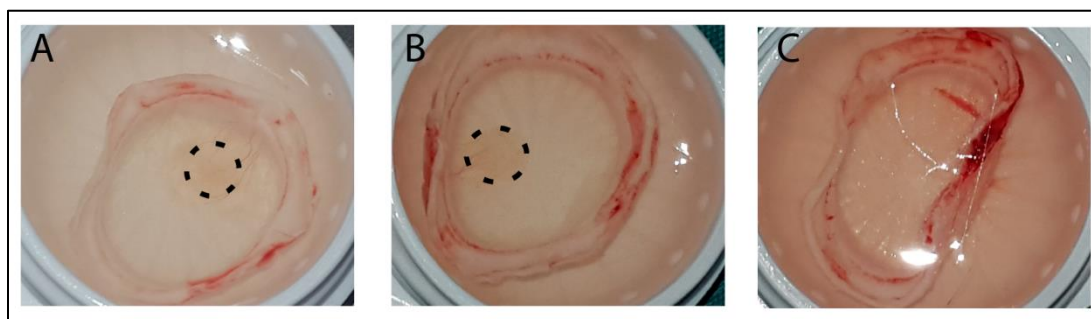


Figure 3. 42: Corneas removed at the end of the test period. A) 1GL on 15th week, B) 2GR after 8th week, and C) 2SL. Black circles indicate the implanted constructs.

3.4.2 Histological Examination of the Constructs

Corneas removed from the rabbits were embedded in OCT medium, frozen and 6 μm sections were made using a freezing microtome. Figure 3.41 shows the Hematoxylin and Eosin stained samples. Histological results showed that the implanted constructs integrated well into the host cornea. Giant cells surrounded the 1GR implant (Figure 3.43 A) due to foreign body reaction of the eye. The hydrogel was 5 mm in diameter and 300 μm in thickness during implantation and the histological examination shows that after 15 weeks construct was 2.6 mm in diameter and about 180 μm in thickness (measured by NIH Image J program) indicating that the construct was partially degraded and replaced by the own tissue of the rabbit.

2GR, on the other hand, initiated a minimal foreign body reaction and well integrated with the host tissue (Figure 3.43 B). The hydrogel was 4 mm in diameter and 150 μm in thickness during implantation and it was 1.7 mm in diameter and about 120 μm in thickness after 8 weeks. Sham (2SL) cornea was intact and completely recovered after operation (Figure 3.43 C).

Foreign body reaction is a normal response of the tissues to any biomaterials regardless of their nonimmunogenic, nontoxic, and physically and chemically stable nature. The response of the body varies including thrombosis, infection, inflammation, and fibrosis leading to accumulation of phagocytic cells. Although it is not clear how the body detects these inert and nontoxic materials, it is thought that the phagocytes interact with the proteins adsorbed on the surface of the biomaterial upon implantation which leads to a cascade of reactions for tissue repair (Hu *et al.*, 2001; Franz *et al.*, 2011; Trindade *et al.*, 2014; Chung *et al.*, 2017).

The reaction following implantation, therefore, is a normal reaction of the body to repair the tissue. However, a higher number of giant cells observed in 1GL implant are most probably due to bigger dimensions of the implanted construct compared 2GR. Moreover, sutures used in the first implant may be caused initiation of a more intense reaction. However, effect of sutures could not be tracked because of the lack of control cornea with sutures.

In conclusion, the integration of the constructs with the host body, degradation of them during observation period and minimal foreign body reaction of the 2GR shows the potential of the constructs to be used as corneal stroma equivalents. It is worth to mention that, pre-*in vivo* studies was carried out with only 2 rabbits only to have an idea about the *in vivo* performance of the constructs. In order to derive a conclusion about the clinical potential of the constructs, *in vivo* studies should be carried out with more rabbits (at least 6 rabbits/construct) for a longer period. Moreover, corneal stroma specific matrix molecules like collagen type I, laminin, keratocan, and keratan sulfate should studied to further assess the *in vivo* performance of the GelMA hydrogels.

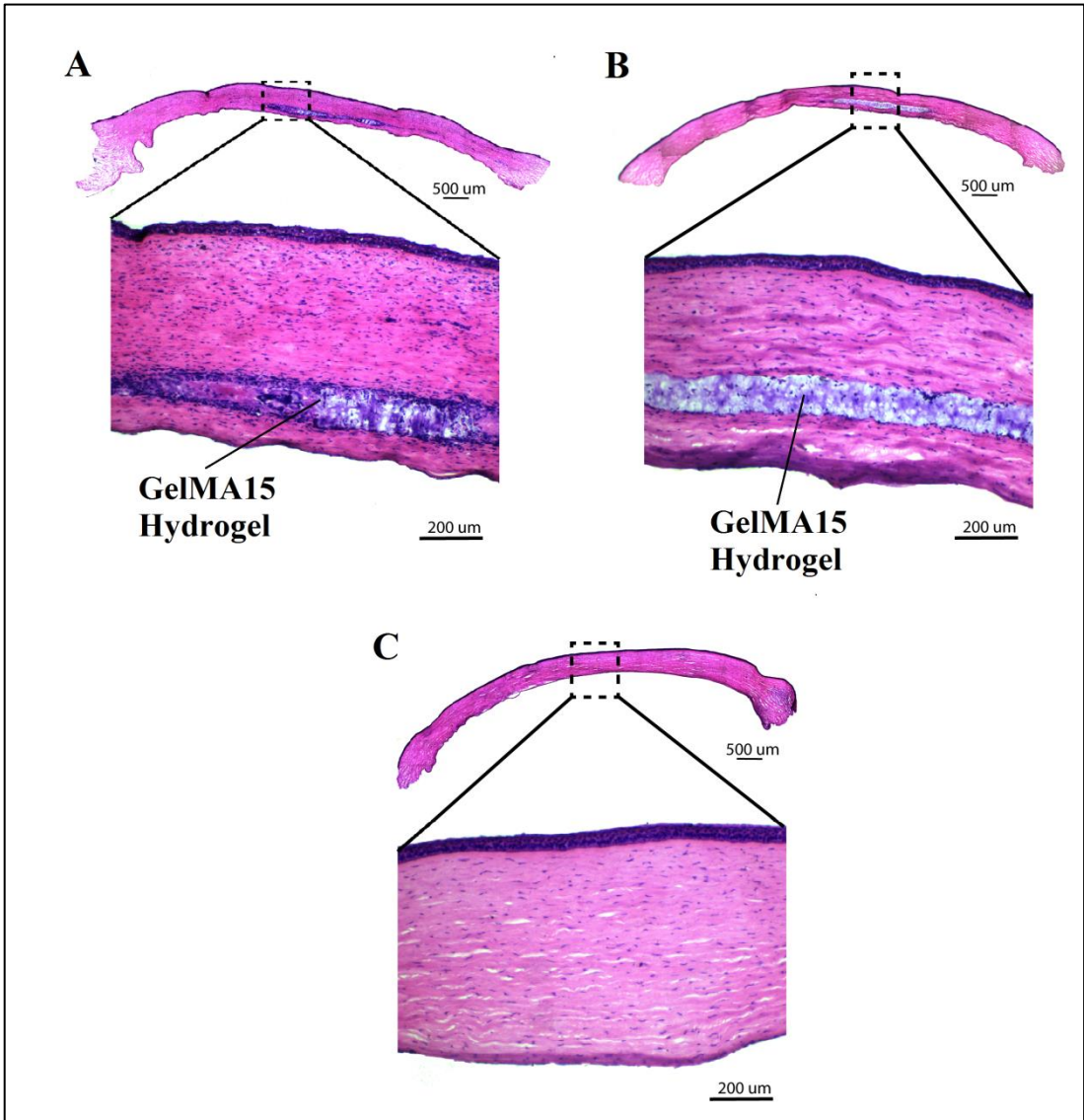


Figure 3. 43: Hematoxylin and Eosin (H&E) staining of sections of the rabbit cornea after implantation. A) 1GL on week 15, B) 2GR on week 8, and C) 2SL on week 8. GelMA15 hydrogels are seen in mid-stroma of figures A and B.

CHAPTER 4

CONCLUSION

Corneal diseases and injuries are the second most common causes of blindness after cataract. Currently transplantation and keratoprotheses are the only options for the treatment of blindness resulting from corneal damages and due to their limitations in donor numbers. Tissue engineering has emerged as a modern solution in the last few decades.

In this study tissue engineering methods were used to closely mimic the native ultrastructure of the corneal stroma by 3D bioprinting of cell loaded GelMA hydrogels.

This study was conducted in four phases: 1) Optimization of GelMA concentration and cell loading density, 2) Improving mechanical strength of the GelMA hydrogels by incorporating HEMA in the structure, 3) 3D bioprinting of GelMA hydrogel at optimized conditions, 4) A short *in vivo* test of the GelMA15-Slab hydrogels.

In the first section optimum GelMA concentration was determined as 10% and 15% (w/v) as a result of *in situ* and enzymatic stability tests. Optimum number of cells loaded into the hydrogels was 1×10^6 cells/mL which yielded stable hydrogels and elongated cells inside. Although mechanical strength of the hydrogels enhanced in the presence of HEMA polymer, number of cells and protein synthesis of the cells in the hydrogels were substantially decreased. Optimized conditions, therefore, were used for the 3D bioprinting of the pure GelMA hydrogels and high cell viability (98%) was obtained after three weeks of incubation. Mechanical strength of the cell loaded hydrogels increased significantly in 21 days. *In vivo* studies were conducted with GelMA15-Slab hydrogels and no adverse side effects were observed during the

8 week observation. H&E staining revealed the integration of the scaffold with the host with minimal foreign body reaction and degradation of it.

In the future studies, in vivo studies of the slab and 3D printed hydrogels with and without cells should be carried out with at least 6 rabbits/sample for at least 6 months to prove their safety and potential as corneal equivalents before moving on to clinical trials. Immunohistochemical studies of the implanted sections should also be conducted to show the protein and glycosaminoglycan synthesis of the cells.

In conclusion, the proposed 3D printed construct in the current study highly mimics the ultrastructural organization of the native cornea and have a potential to be used as a corneal stroma equivalent.

REFERENCES

- Acun, A. and Hasirci, V. (2014). Construction of a collagen-based, split-thickness cornea substitute. *Journal of Biomaterials Science, Polymer Edition*. 25(11):1110–1132.
- Amadio, M., Govoni, S. and Pascale, A. (2016). Targeting VEGF in eye neovascularization: What's new?: A comprehensive review on current therapies and oligonucleotide-based interventions under development. *Pharmacological Research*. 103:253–269.
- Ambati, B. K., Nozaki, M., Singh, N., et al. (2006). Corneal avascularity is due to soluble VEGF receptor-1. *Nature*. 443:993–997.
- Andreassen, T. T., Hjorth Simonsen, A., Oxlund, H. (1980). Biomechanical properties of keratoconus and normal corneas. *Experimental Eye Research*. 31(4):435–441.
- Bakshi, A., Fisher, O., Dagci, T., et al. (2004). Mechanically engineered hydrogel scaffolds for axonal growth and angiogenesis after transplantation in spinal cord injury. *Journal of neurosurgery. Spine*. 1(3):322–329.
- Barron, J. A., Wu, P., Ladouceur, H. D. et al. (2004). Biological Laser Printing: A Novel Technique for Creating Heterogeneous 3-dimensional Cell Patterns. *Biomedical Microdevices*. 6(2):139–147.
- Benton, J. A., DeForest, C. A., Vivekanandan, V. et al. (2009). Photocrosslinking of Gelatin Macromers to Synthesize Porous Hydrogels That Promote Valvular Interstitial Cell Function. *Tissue Engineering. Part A*. 15(11):3221–3230.
- Bertassoni, L. E., Cardoso, J. C., Manoharan, V. et al. (2014). Direct-write bioprinting of cell-laden methacrylated gelatin hydrogels. *Biofabrication*, 6(2):024105.
- Billiet, T., Vandenhaute, M., Schelfhout, J. et al. (2012). A review of trends and

limitations in hydrogel-rapid prototyping for tissue engineering. *Biomaterials*. 33(26):6020–41.

Bohidar, H. B., Jena, S. S. (1993). Kinetics of sol–gel transition in thermoreversible gelation of gelatin. *The Journal of Chemical Physics*. 98(11):8970–8977.

Bourne, W. M., McLaren, J. W. (2004). Clinical responses of the corneal endothelium. *Experimental Eye Research*. 78(3):561–572.

Brinkman, W. T., Nagapudi, K., Thomas, B. S., et al. (2003). Photo-Cross-Linking of Type I Collagen Gels in the Presence of Smooth Muscle Cells: Mechanical Properties, Cell Viability, and Function. *Biomacromolecules*. 4(4):890–895.

Brown, D. M., Regillo, C. D. (2007). Anti-VEGF Agents in the Treatment of Neovascular Age-related Macular Degeneration: Applying Clinical Trial Results to the Treatment of Everyday Patients. *American Journal of Ophthalmology*. 144(4):627–637.e2.

Bulcke V. D., A. I., Bogdanov, B., De Rooze, N., et al. (2000). Structural and Rheological Properties of Methacrylamide Modified Gelatin Hydrogels. *Biomacromolecules*. American Chemical Society, 1(1):31–38.

Burton, M. J. (2009). Corneal blindness. Prevention, treatment and rehabilitation. *Community Eye Health Journal*. 22(71):33–35.

Byambaa, B., Annabi, N., Yue, K., et al. (2017). Bioprinted Osteogenic and Vasculogenic Patterns for Engineering 3D Bone Tissue. *Advanced Healthcare Materials*.

Çetin, D., Kahraman, A. S., Gümüşderelioğlu, M. (2011). Novel Scaffolds Based on Poly(2-hydroxyethyl methacrylate) Superporous Hydrogels for Bone Tissue Engineering. *Journal of Biomaterials Science, Polymer Edition*. 22(9):1157–1178.

Chan, A. A., Hertsensberg, A. J., Funderburgh, M. L., et al. (2013). Differentiation of Human Embryonic Stem Cells into Cells with Corneal Keratocyte Phenotype. *PLoS ONE*, 8(2):e56831.

- Chan, T., Payor, S., Holden, B. A. (1983). Corneal thickness profiles in rabbits using an ultrasonic pachometer. *Investigative Ophthalmology & Visual Science*. 24(10):1408–1410.
- Chang, J.-H., Garg, N. K., Lunde, E., et al. (2012). Corneal Neovascularization: An Anti-VEGF Therapy Review. *Survey of Ophthalmology*. 57(5):415–429.
- Chen, G.-Q. and Wu, Q. (2005). The application of polyhydroxyalkanoates as tissue engineering materials. *Biomaterials*. 26(33):6565–6578.
- Chen, Q., Zhu, L., Zhao, C., et al. (2013). A Robust, One-Pot Synthesis of Highly Mechanical and Recoverable Double Network Hydrogels Using Thermoreversible Sol-Gel Polysaccharide. *Advanced Materials*. 25(30):4171–4176.
- Chirila, T. V., Hicks, C. R., Dalton, P. D., et al. (1998). Artificial cornea. *Progress in Polymer Science (Oxford)*. 23(3):447–473.
- Choong, P.-F., Mok, P.-L., Cheong, S.-K. et al. (2007). Mesenchymal stromal cell-like characteristics of corneal keratocytes. *Cytherapy*. 9(3):252–258.
- Chung, L., Maestas, D. R., Housseau, F. et al. (2017). Key players in the immune response to biomaterial scaffolds for regenerative medicine. *Advanced Drug Delivery Reviews*. 114:184–192.
- Colosi, C., Shin, S. R., Manoharan, V., et al. (2015). Microfluidic Bioprinting of Heterogeneous 3D Tissue Constructs Using Low-Viscosity Bioink. *Advanced Materials*. 28(4):677–684.
- Connon, C. J. (2015). Approaches to Corneal Tissue Engineering: Top-down or Bottom-up?. *Procedia Engineering*. 110:15–20.
- Correlo, V. M., Oliveira, J. M., Mano, J. F., et al. (2011). "Chapter 32 - Natural Origin Materials for Bone Tissue Engineering: Properties, Processing, and Performance". in *Principles of Regenerative Medicine (Second edition)*. (ed. Atala, Anthony; Lanza, Robert; Mikos, Antonios G.; Nerem, Robert), 557–586. Academic Press

- Cui, Z., Zeng, Q., Liu, S., et al. (2018). Cell-laden and orthogonal-multilayer tissue-engineered corneal stroma induced by a mechanical collagen microenvironment and transplantation in a rabbit model. *Acta Biomaterialia*. 75:183–199.
- Dababneh, A. B., Ozbolat, I. T. (2014). Bioprinting Technology: A Current State-of-the-Art Review. *Journal of Manufacturing Science and Engineering*. 136:061016-1–11.
- Diffey, B. L. (1991). Solar ultraviolet radiation effects on biological systems. *Physics in medicine and biology*. 36(3):299–328.
- Doshi, J. and Reneker, D. H. (1995). Electrospinning process and applications of electrospun fibers. *Journal of Electrostatics*. 35(2):151–160.
- Dragusin, D.-M., Van Vlierberghe, S., Dubruel, P., et al. (2012). Novel gelatin–PHEMA porous scaffolds for tissue engineering applications. *Soft Matter*. 8:9589–9602.
- Du, L., Wu, X. (2011). Development and Characterization of a Full-Thickness Acellular Porcine Cornea Matrix for Tissue Engineering. *Artificial Organs*. 35(7):691–705.
- Du, Y., Roh, D. S., Funderburgh, M. L., et al. (2010). Adipose-derived stem cells differentiate to keratocytes in vitro. *Molecular Vision*. 16:2680–2689.
- Duan, B. (2016). State-of-the-Art Review of 3D Bioprinting for Cardiovascular Tissue Engineering. *Annals of Biomedical Engineering*. 45(1):195–209. Duan, B., Hockaday, L. A., Kang, K. H., Butcher, J. T. (2012). 3D Bioprinting of heterogeneous aortic valve conduits with alginate/gelatin hydrogels. *Journal of Biomedical Materials Research Part A*. 101A(5):1255–1264.
- Duan, B., Hockaday, L. A., Kang, K. H. et al. (2012). 3D Bioprinting of heterogeneous aortic valve conduits with alginate/gelatin hydrogels. *Journal of Biomedical Materials Research Part A*. 101A(5):1255–1264.
- Eghrari, A. O., Riazuddin, S. A., Gottsch, J. D. (2015). Overview of the Cornea:

Structure, Function, and Development. *Progress in Molecular Biology and Translational Science*. 134:7-23.

Ethier, C. R., Johnson, M., Ruberti, J. (2004). Ocular Biomechanics and Biotransport. *Annual Review of Biomedical Engineering*. 6(1):249–273.

Fagerholm, P., Lagali, N. S., Merrett, K., et al. (2010). A biosynthetic alternative to human donor tissue for inducing corneal regeneration: 24-month follow-up of a phase 1 clinical study. *Science translational medicine*. 2(46):46ra61.

Falcinelli, G., Falsini, B., Taloni, M., et al. (2005). Modified Osteo-odonto-keratoprosthesis for Treatment of Corneal Blindness. *Archives of Ophthalmology*. 123:1319–1329.

Fini, M. (1999). Keratocyte and fibroblast phenotypes in the repairing cornea. *Progress in Retinal and Eye Research*. 18(4):529–551.

Flynn, L., Dalton, P. D., Shoichet, M. S. (2003). Fiber templating of poly(2-hydroxyethyl methacrylate) for neural tissue engineering. *Biomaterials*. 24(23):4265–4272.

Franz, S., Rammelt, S., Scharnweber, D. et al. (2011). Immune responses to implants- A review of the implications for the design of immunomodulatory biomaterials. *Biomaterials*. 32(28):6692–6709.

Friess, W. (1998). Collagen – biomaterial for drug delivery. *European Journal of Pharmaceutics and Biopharmaceutics*. 45(2):113–136.

Fullwood, N. J. (2004). Collagen fibril orientation and corneal curvature. *Structure*. 12(2):169–70.

Funderburgh, J. L., Hevelone, N. D., Roth, M. R., et al. (1998). Decorin and biglycan of normal and pathologic human corneas. *Investigative Ophthalmology & Visual Science*. 39(10):1957–1964.

Funderburgh, J. L., Mann, M. M., Funderburgh, M. L. (2003). Keratocyte Phenotype Mediates Proteoglycan Structure: A Role for Fibroblasts in Corneal Fibrosis. *Journal*

of Biological Chemistry. 278(46):45629–45637.

Gain, P., Jullienne, R., He, Z., et al. (2016). Global survey of corneal transplantation and eye banking. *JAMA Ophthalmology*. 134(2):167-73

Garg, P., Rao, G. N. (1999). Corneal Ulcer: Diagnosis and Management. *Community Eye Health*. 12(30):21–23.

Germain, L., Carrier, P., Auger, F. A., et al. (2000). Can we produce a human corneal equivalent by tissue engineering?. *Progress in Retinal and Eye Research*. 19(5):497–527.

Ghezzi, C. E., Rnjak-Kovacina, J., Kaplan, D. L. (2015). Corneal tissue engineering: recent advances and future perspectives. *Tissue engineering. Part B, Reviews*. 21(3):278–87.

Gil, E. S., Mandal, B. B., Park, S.-H., et al. (2010). Helicoidal multi-lamellar features of RGD-functionalized silk biomaterials for corneal tissue engineering. *Biomaterials*. 31(34):8953–63.

Gilbert, C., Foster, A. (2001). Childhood blindness in the context of VISION 2020 - The right to sight. *Bulletin of the World Health Organization*. 79(3):227–232.

Girton, T. S., Oegema, T. R., Grassl, E. D., et al. (2000). Mechanisms of Stiffening and Strengthening in Media-Equivalents Fabricated Using Glycation. *Journal of Biomechanical Engineering*. 122(3):216–223.

Girton, T. S., Oegema, T. R., Tranquillo, R. T. (1999). Exploiting glycation to stiffen and strengthen tissue equivalents for tissue engineering. *Journal of Biomedical Materials Research*. 46(1):87–92.

Gouveia, R. M., Koudouna, E., Jester, J., et al. (2017). Template Curvature Influences Cell Alignment to Create Improved Human Corneal Tissue Equivalents. *Advanced Biosystems*. 1(12):1700135.

Guillemot, F., Souquet, A., Catros, S. et al. (2010). Laser-assisted cell printing: principle, physical parameters versus cell fate and perspectives in tissue engineering.

Nanomedicine. 5(3):507–515.

Gulsen, D., Chauhan, A. (2006). Effect of water content on transparency, swelling, lidocaine diffusion in p-HEMA gels. *Journal of Membrane Science*. 269(1):35–48.

Gunatillake, P. A., Adhikari, R., Gadegaard, N. (2003). Biodegradable synthetic polymers for tissue engineering. *European Cells and Materials*. 20;5:1-16

Guo, X., Hutcheon, A. E. K., Melotti, S. A., et al. (2007). Morphologic characterization of organized extracellular matrix deposition by ascorbic acid-stimulated human corneal fibroblasts. *Investigative Ophthalmology and Visual Science*. 48:4050–4060.

Guvendiren, M., Molde, J., Soares, R. M. D. et al. (2016). Designing Biomaterials for 3D Printing. *ACS Biomaterials Science & Engineering*. 2(10):1679–1693.

Hao, J. L., Nagano, T., Nakamura, M., et al. (1999). Galardin inhibits collagen degradation by rabbit keratocytes by inhibiting the activation of pro-matrix metalloproteinases. *Experimental eye research*. 68:565–572.

Hashimoto, Y., Funamoto, S., Sasaki, S., et al. (2010). Preparation and characterization of decellularized cornea using high-hydrostatic pressurization for corneal tissue engineering. *Biomaterials*. 31(14):3941–3948.

Hasirci, N., Kilic, C., Kömez, A., et al. (2016). "Hydrogels in Regenerative Medicine" in *Gels Handbook* (ed. Demirci, Utkan; Khademhosseini, Ali).1–52. World Scientific

Hasirci, V., Lewandrowski, K., Gresser, J. D., et al. (2001). Versatility of biodegradable biopolymers: degradability and an in vivo application. *Journal of biotechnology*. 86(2):135–50.

Hassell, J. R., Birk, D. E. (2010). The molecular basis of corneal transparency. *Experimental Eye Research*. 91(3):326-35.

Hatou, S., Yoshida, S., Higa, K., et al. (2013). Functional Corneal Endothelium Derived from Corneal Stroma Stem Cells of Neural Crest Origin by Retinoic Acid

and Wnt/ β -Catenin Signaling. *Stem Cells and Development*. 22:828–839.

Hazra, S., Nandi, S., Naskar, D., et al. (2016). Non-mulberry Silk Fibroin Biomaterial for Corneal Regeneration. *Scientific reports*. 6:21840.

Hellio-Serughetti, D., Djabourov, M. (2006). Gelatin Hydrogels Cross-Linked with Bisvinyl Sulfonemethyl. 2. The Physical and Chemical Networks', *Langmuir*. American Chemical Society, 22(20):8516–8522.

Henderson, T. M. A., Ladewig, K., Haylock, D. N., et al. (2013). Cryogels for biomedical applications', *Journal of Materials Chemistry B*. 1:2682-2695

Hoch, E., Schuh, C., Hirth, T., et al. (2012). Stiff gelatin hydrogels can be photochemically synthesized from low viscous gelatin solutions using molecularly functionalized gelatin with a high degree of methacrylation. *Journal of Materials Science: Materials in Medicine*. 23(11):2607–2617.

Hoeltzel, D. a, Altman, P., Buzard, K. et al. (1992). Strip extensiometry for comparison of the mechanical response of bovine, rabbit, and human corneas. *Journal of biomechanical engineering*. 114:202–215.

Hoffmann, B., Schäfer, C. (2010). Filopodial focal complexes direct adhesion and force generation towards filopodia outgrowth. *Cell Adhesion & Migration*. Landes Bioscience, 4(2):190–193.

Homsy, C. a (1970). Bio-Compatibility in selection of materials for implantation. *Journal of Biomedical Materials Research*. 4(3):341–356.

Hong, S., Yun, J. H., Kim, E.-S., et al. (2018). Human Conjunctival Epithelial Sheets Grown on Poly(Lactic-Co-Glycolic) Acid Membranes and Cocultured With Human Tenon's Fibroblasts for Corneal Repair. *Investigative Ophthalmology & Visual Science*. 59(3):1475–1485.

Hongshan, L., Jianhua, Z., Chia-Yang, L., et al. (2011). Bone marrow mesenchymal stem cells can differentiate and assume corneal keratocyte phenotype. *Journal of Cellular and Molecular Medicine*. 16(5):1114–1124.

- Hu, W.-J., Eaton, J. W., Ugarova, T. P. et al. (2001). Molecular basis of biomaterial-mediated foreign body reactions. *Blood*. 98(4):1231-1238.
- Hu, X., Lui, W., Cui, L., et al. (2005). Tissue engineering of nearly transparent corneal stroma. *Tissue engineering*. 11(11–12):1710–1717.
- Hutson, C. B., Nichol, J. W., Aubin, H., et al. (2011). Synthesis and Characterization of Tunable Poly(Ethylene Glycol): Gelatin Methacrylate Composite Hydrogels. *Tissue Engineering. Part A*. 17(13–14):1713–1723.
- Ifkovits, J. L., Burdick, J. A. (2007). Review: Photopolymerizable and Degradable Biomaterials for Tissue Engineering Applications. *Tissue Engineering*. 13(10):2369-85
- Isaacson, A., Swioklo, S., Connon, C. J. (2018). 3D bioprinting of a corneal stroma equivalent. *Experimental Eye Research*. 173:188–193.
- Jacob, S., Naveen, P. (2016). Anatomy of the Cornea', in *Mastering Endothelial Keratoplasty*. 1-11. Springer.
- Jacobsen, I. E., Jensen, O. A., Prause, J. U. (1984). Structure And Composition of Bowman's Membrane: Study by frozen resin cracking. *Acta Ophthalmologica*. 62(1):39-53
- Jeong, B., Kim, S. W., Bae, Y. H. (2012). Thermosensitive sol–gel reversible hydrogels. *Advanced Drug Delivery Reviews*. 64:154–162.
- Jester, J. V, Barry-Lane, P. A., Cavanagh, H. D. et al. (1996). Induction of alpha-smooth muscle actin expression and myofibroblast transformation in cultured corneal keratocytes. *Cornea*. 15(5):505–516.
- Jester, J. V, Petroll, W. M., Barry, P. A. et al. (1995). Expression of alpha-smooth muscle (alpha-SM) actin during corneal stromal wound healing. *Investigative Ophthalmology & Visual Science*. 36(5):809–819.
- Johnson, B., Niedermaier, D. J., Crone, W. C., et al. (2002). Mechanical properties of a pH sensitive hydrogel. in *Proceedings of the 2002 Annual Conference of Society*

for Experimental Mechanics.

Joung, D., Truong, V., Neitzke, C. C., et al. (2018). 3D Printed Stem-Cell Derived Neural Progenitors Generate Spinal Cord Scaffolds. *Advanced Functional Materials*. 28:1801850.

Jue, B., Maurice, D. M. (1986). The mechanical properties of the rabbit and human cornea. *Journal of Biomechanics*. 19(10):847–853.

Kawakita, T., Higa, K., Shimmura, S., et al. (2014). A gelatin hydrogel for corneal stromal transplantation in rabbit. *Investigative Ophthalmology & Visual Science*. 55(13):5156.

Kaye, G. I., Pappas, G. D. (1962). Studies on the Cornea. *The Journal of Cell Biology*. 12(3):457-479.

Kilic Bektas, C., Hasirci, V. (2018). Mimicking corneal stroma using keratocyte-loaded photopolymerizable methacrylated gelatin hydrogels. *Journal of Tissue Engineering and Regenerative Medicine*. 12(4):e1899-e1910

Kilic, C., Girotti, A., Rodriguez-Cabello, J. C. et al. (2014). A collagen-based corneal stroma substitute with micro-designed architecture. *Biomaterials Science*. 2(3):318-329.

Kolesky, D. B., Truby, R. L., Gladman, A. S., et al. (2014). 3D bioprinting of vascularized, heterogeneous cell-laden tissue constructs. *Advanced Materials*. 26(19):3124–3130.

Komez, A., Baran, E. T., Erdem, U., et al. (2016). Construction of a patterned hydrogel-fibrous mat bilayer structure to mimic choroid and Bruch's membrane layers of retina. *Journal of Biomedical Materials Research- Part A*. 104(9):2166-7

Kong, B., Sun, W., Chen, G., et al. (2017). Tissue-engineered cornea constructed with compressed collagen and laser-perforated electrospun mat. *Scientific Reports*. 7(1):970.

Kubinová, Š., Horák, D., Syková, E. (2009). Cholesterol-modified superporous

- poly(2-hydroxyethyl methacrylate) scaffolds for tissue engineering. *Biomaterials*. 30(27):4601–4609.
- Laattala, K., Huhtinen, R., Puska, M., et al. (2011). Bioactive composite for keratoprosthesis skirt. *Journal of the Mechanical Behavior of Biomedical Materials*. 4:1700–1708.
- Lam, H. J., Patel, S., Wang, A., et al. (2010). In vitro regulation of neural differentiation and axon growth by growth factors and bioactive nanofibers. *Tissue engineering. Part A*. 16(8):2641–2648.
- Langer, R. and Vacanti, J. P. (1993). Tissue engineering. *Science*. 5110:920-926
- Lee, H., Han, W., Kim, H., et al. (2017). Development of Liver Decellularized Extracellular Matrix Bioink for Three-Dimensional Cell Printing-Based Liver Tissue Engineering. *Biomacromolecules*. 18:1229–1237.
- Lee, K. Y., Mooney, D. J. (2001). Hydrogels for tissue engineering. *Chemical Reviews*. 101(7):1869-1880
- Li, C., Liu, S., Zheng, Y. et al. (2013). Collagen modified porous pHEMA–TiO₂ composite hydrogels for tissue engineering. *Journal of Controlled Release*. 172:e143–e143.
- Li, J., Chen, M., Fan, X. et al. (2016). Recent advances in bioprinting techniques: approaches, applications and future prospects. *Journal of translational medicine*. 14:271.
- Liao, C.-J., Chen, C.-F., Chen, J.-H., et al. (2001). Fabrication of porous biodegradable polymer scaffolds using a solvent merging/particulate leaching method. *Journal of Biomedical Materials Research*. 59(4):676–681.
- Lin, L., Jin, X. (2018). The development of tissue engineering corneal scaffold: which one the history will choose?. *Annals of Eye Science; January 2018*. 3(6):1–8.
- Liu, C., Paul, B., Tandon, R., et al. (2005). The Osteo-Odonto-Keratoprosthesis (OOKP). *Seminars in Ophthalmology*. 20(2):113–128.

- Liu, W., Merrett, K., Griffith, M., et al. (2008). Recombinant human collagen for tissue engineered corneal substitutes. *Biomaterials*. 29(9):1147–1158.
- Liu, Y., Ren, L., Wang, Y. (2013). Crosslinked collagen-gelatin-hyaluronic acid biomimetic film for cornea tissue engineering applications. *Materials Science and Engineering C*. 33:196–201.
- Loftsson, T., Stefánsson, E. (2003). Cyclodextrins in eye drop formulations: enhanced topical delivery of corticosteroids to the eye. *Acta Ophthalmologica Scandinavica*. 80(2):144–150.
- Long, Y., Zhao, X., Liu, S., et al. (2018). Collagen–Hydroxypropyl Methylcellulose Membranes for Corneal Regeneration. *ACS Omega*. 3(1):1269–1275.
- Lozinsky, V. I., Galaev, I. Y., Plieva, F. M., et al. (2003). Polymeric cryogels as promising materials of biotechnological interest. *Trends in Biotechnology*. 21(10):445-51.
- Ludwig, P. E., Dulebohn, S. C. (2017). Anatomy, Head, Eye, Cornea. StatPearls Publishing. Available from: <https://www.ncbi.nlm.nih.gov/books/NBK470340/>
- Luo, L. J., Lai, J. Y., Chou, S. F., et al. (2018). Development of gelatin/ascorbic acid cryogels for potential use in corneal stromal tissue engineering. *Acta Biomaterialia*. 65:123-136
- Madden, L. R., Mortisen, D. J., Sussman, E. M., et al. (2010). Proangiogenic scaffolds as functional templates for cardiac tissue engineering. *Proceedings of the National Academy of Sciences*. 107(34):15211-15216.
- Malafaya, P. B., Silva, G. A., Reis, R. L. (2007). Natural-origin polymers as carriers and scaffolds for biomolecules and cell delivery in tissue engineering applications. *Advanced Drug Delivery Reviews*. 59:207–233.
- Mallet, J. D., Rochette, P. J. (2013). Wavelength-dependent ultraviolet induction of cyclobutane pyrimidine dimers in the human cornea. *Photochemical & Photobiological Sciences*. 12(8):1310–1318.

- Mandrycky, C., Wang, Z., Kim, K. et al. (2016). 3D bioprinting for engineering complex tissues. *Biotechnology Advances*. 34(4):422-434.
- Mano, J. F., Silva, G. A., Azevedo, H. S. et al. (2007). Natural origin biodegradable systems in tissue engineering and regenerative medicine: present status and some moving trends. *Journal of The Royal Society Interface*. 4(17):999 LP-1030.
- Marco, S., Javier, N., P., F. J. (2018). Micro- and Macrobioprinting: Current Trends in Tissue Modeling and Organ Fabrication. *Small Methods*. 2(3):1700318.
- Maurice, D. M. (1957). The structure and transparency of the cornea. *The Journal of Physiology*. 136(2):263–286.
- McLaughlin, C. R., Osborne, R., Hyatt, A., et al. (2009). Tissue engineered models for in vitro studies. in *Fundamentals of Tissue Engineering and Regenerative Medicine*. (ed. Meyer, Ulrich; Handschel, Jörg; Wiesmann, Hans P.; Meyer, Thomas). 759–772. Springer
- Meek, K. M., Fullwood, N. J. (2001). Corneal and scleral collagens- A microscopist's perspective. *Micron*. 32(3):261-72
- Meek, K. M., Knupp, C. (2015). Corneal structure and transparency. *Progress in Retinal and Eye Research*. 49:1-16.
- Merrett, K., Griffith, C. M., Deslandes, Y., et al. (2001). Adhesion of corneal epithelial cells to cell adhesion peptide modified pHEMA surfaces. *Journal of Biomaterials Science, Polymer Edition*. 12(6):647–671.
- Mimura, T., Amano, S., Yokoo, S., et al. (2008). Tissue engineering of corneal stroma with rabbit fibroblast precursors and gelatin hydrogels. *Molecular vision*. 14:1819–1828.
- Mirazul Islam, M., Cèpla, V., He, C., et al. (2015). Functional fabrication of recombinant human collagen–phosphorylcholine hydrogels for regenerative medicine applications. *Acta Biomaterialia*. 12:70–80.
- Murphy, S. V., Atala, A. (2014). 3D bioprinting of tissues and organs. *Nature*

Biotechnology. 32:773–785.

Muthusubramaniam, L., Peng, L., Zaitseva, T., et al. (2012). Collagen fibril diameter and alignment promote the quiescent keratocyte phenotype. *Journal of Biomedical Materials Research - Part A*. 100(3):613-621.

Nair, L. S., Laurencin, C. T. (2007). Biodegradable polymers as biomaterials. *Progress in Polymer Science (Oxford)*. 32(8-9):762–798.

Nakamura, T., Yokoo, S., Bentley, A. J., et al. (2016). Development of functional human oral mucosal epithelial stem/progenitor cell sheets using a feeder-free and serum-free culture system for ocular surface reconstruction. *Scientific Reports*. 6:37173.

Nguyen, K. T., West, J. L. (2002). Photopolymerizable hydrogels for tissue engineering applications. *Biomaterials*. 23(22):4307-4314.

Nichol, J. W., Koshy, S. T., Bae, H., et al. (2010). Cell-laden microengineered gelatin methacrylate hydrogels. *Biomaterials*. 31(21):5536–5544.

Nishi, O., Nishi, K. (1991). Fibrin reaction and its cause. *Dev Ophthalmology*. 22:126-31.

O'Brien, F. J. (2011). Biomaterials & scaffolds for tissue engineering. *Materials Today*. 14(3):88–95.

Oliva, M., Gulati, M., Schottman, T. (2012). Turning the tide of corneal blindness. *Indian Journal of Ophthalmology*. 60(5):423-7

Ozbolat, I. T., Hospodiuk, M. (2016). Current advances and future perspectives in extrusion-based bioprinting. *Biomaterials*. 76:321–343.

Ozcelik, B., Brown, K. D., Blencowe, A., et al. (2013). Ultrathin chitosan-poly(ethylene glycol) hydrogel films for corneal tissue engineering. *Acta Biomaterialia*. 9(5):6594–6605.

Peppas, N. A., Hilt, J. Z., Khademhosseini, A. et al. (2006). Hydrogels in biology and medicine: From molecular principles to bionanotechnology. *Advanced*

Materials. 18:1345–1360.

Peppas, N., Moynihan, H. J., Lucht, L. M. (1985). The structure of highly crosslinked poly(2-hydroxyethyl methacrylate) hydrogels. *Journal of biomedical materials research*. 19:397–411.

Perova, T. S., Vij, J. K., Xu, H. (1997). Fourier transform infrared study of poly (2-hydroxyethyl methacrylate) PHEMA. *Colloid and Polymer Science*. 275(4):323–332.

Phu, D., Wray, L. S., Warren, R. V. et al. (2010). Effect of Substrate Composition and Alignment on Corneal Cell Phenotype. *Tissue Engineering Part A*. 17(5–6):799–807.

Pianini, V., Passani, A., Rossi, G. C. M. et al. (2010). Efficacy and safety of netilmycin/dexamethasone preservative-free and tobramycin/dexamethasone-preserved fixed combination in patients after cataract surgery. *Journal of Association for Ocular Pharmacology and Therapeutics*. 26(6):617–621.

Pinnamaneni, N., Funderburgh, J. L. (2012). Concise review: Stem cells in the corneal stroma. *Stem Cells*. 30:1059–1063.

Pradhan, E. (2017). Ocular trauma: prevention. *Nepalese Journal of Ophthalmology*. 8(16):07–109.

Rafat, M., Li, F., Fagerholm, P., et al. (2008). PEG-stabilized carbodiimide crosslinked collagen-chitosan hydrogels for corneal tissue engineering. *Biomaterials*. 29:3960–3972.

Ratner, B. D., Miller, I. F. (1973). Transport through Crosslinked Poly(2-Hydroxyethyl Methacrylate) Hydrogel Membranes. *Journal of Biomedical Materials Research*. 7(4):353–367.

Rengier, F., Mehndiratta, A., von Tengg-Kobligk, H., et al. (2010). 3D printing based on imaging data: review of medical applications. *International Journal of Computer Assisted Radiology and Surgery*. 5(4):335–341.

- Riley, G. P., Harrall, R. L., Watson, P. G., et al. (1995). Collagenase (MMP-1) and TIMP-1 in destructive corneal disease associated with rheumatoid arthritis. *Eye (Lond)*. 9:703–718.
- Ringvold, A. (1998). Corneal epithelium and UV-protection of the eye. *Acta Ophthalmologica Scandinavica*. 76(2):149–153.
- Rizwan, M., Peh, G. S. L., Ang, H. P., et al. (2017). Sequentially-crosslinked bioactive hydrogels as nano-patterned substrates with customizable stiffness and degradation for corneal tissue engineering applications. *Biomaterials*. 120:139-154.
- Ruberti, J. W., Zieske, J. D. (2008). Prelude to corneal tissue engineering- Gaining control of collagen organization. *Progress in Retinal and Eye Research*. 27:549–577.
- Ruberti, J. W., Zieske, J. D., Trinkaus-Randall, V. (2007). Chapter Sixty Eight- Corneal Tissue Replacement. in *Principles of Tissue Engineering* (ed. Lanza, Robert; Langer, Robert; Vacanti, Joseph P.). 1025–1047. Academic Press.
- Salvador-Culla, B., Kolovou, E. P. (2016). Keratoprosthesis: A Review of Recent Advances in the Field. *Journal of Functional Biomaterials*. 7(2):13
- Schuurman, W., Levett, P., Pot, M. W., et al. (2013). Gelatin-methacrylamide hydrogels as potential biomaterials for fabrication of tissue-engineered cartilage constructs. *Macromolecular bioscience*. 13(5):551-561.
- Schwartz, N. J., Mackay, R. S., Sackman, J. L. (1966). A theoretical and experimental study of the mechanical behavior of the cornea with application to the measurement of intraocular pressure. *The bulletin of mathematical biophysics*. 28(4):585–643.
- Seo, E., Kumar, S., Lee, J., et al. (2017). Modified hydrogels based on poly(2-hydroxyethyl methacrylate) (pHEMA) with higher surface wettability and mechanical properties. *Macromolecular Research*. 25(7):704–711.
- Sivak, J. M. and Fini, M. E. (2002). MMPs in the eye: emerging roles for matrix metalloproteinases in ocular physiology. *Progress in Retinal and Eye Research*.

21(1):1–14.

Sorkio, A., Koch, L., Koivusalo, L., et al. (2018). Human stem cell based corneal tissue mimicking structures using laser-assisted 3D bioprinting and functional bioinks. *Biomaterials*. 171:57–71.

Srinivasan, M. (2017). Prevention of traumatic corneal ulcer in South East Asia. *Community Eye Health*. 30(99):S15–S17.

Stock, U. A., Vacanti, J. P. (2001). Tissue Engineering: Current State and Prospects. *Annual Review of Medicine*. 52:443–451.

Suntornnond, R., Tan, E. Y. S., An, J. et al. (2017). A highly printable and biocompatible hydrogel composite for direct printing of soft and perfusable vasculature-like structures. *Scientific Reports*. 7(1):16902.

Takeda, Y. S. and Xu, Q. (2014). Fabrication of 2D and 3D constructs from reconstituted decellularized tissue extracellular matrices. *Journal of biomedical nanotechnology*. 10(12):3631–3637.

Tan, D. T. H., Dart, J. K. G., Holland, E. J. et al. (2012). Ophthalmology 3 Corneal transplantation. *The Lancet*. 379:1749–1761.

Tang, Q., Luo, C., Lu, B., et al. (2017). Thermosensitive chitosan-based hydrogels releasing stromal cell derived factor-1 alpha recruit MSC for corneal epithelium regeneration. *Acta Biomaterialia*. 61:103–113.

Tonsomboon, K. and Oyen, M. L. (2013). Composite electrospun gelatin fiber-alginate gel scaffolds for mechanically robust tissue engineered cornea. *Journal of the Mechanical Behavior of Biomedical Materials*. 21:185–194.

Torbet, J., Malbouyres, M., Builles, N., et al. (2007). Orthogonal scaffold of magnetically aligned collagen lamellae for corneal stroma reconstruction. *Biomaterials*. 28:4268–4276.

Toricelli, A. A. M., Santhanam, A., Wu, J., et al. (2016). The corneal fibrosis response to epithelial–stromal injury. *Experimental Eye Research*. 142:110–118.

- Trindade, R., Albrektsson, T., Tengvall, P. et al. (2014). Foreign Body Reaction to Biomaterials: On Mechanisms for Buildup and Breakdown of Osseointegration. *Clinical Implant Dentistry and Related Research*. 18(1):192–203.
- Viitala, R., Franklin, V., Green, D., et al. (2009). Towards a synthetic osteo-odonto-keratoprosthesis. *Acta Biomaterialia*. 5:438–452.
- Vrana, N. E., Builles, N., Justin, V., et al. (2008). Development of a Reconstructed Cornea from Collagen–Chondroitin Sulfate Foams and Human Cell Cultures. *Investigative Ophthalmology & Visual Science*. 49(12):5325–5331.
- Vrana, N. E., Elsheikh, A., Builles, N., et al. (2007). Effect of human corneal keratocytes and retinal pigment epithelial cells on the mechanical properties of micropatterned collagen films. *Biomaterials*. 28(29):4303–4310.
- Wang, L., Lu, C., Liu, H., et al. (2016). A double network strategy to improve epithelization of a poly (2-hydroxyethyl methacrylate) hydrogel for corneal repair application. *RSC Advances*. 6(2):1194–1202.
- Wang, S., Ghezzi, C. E., Gomes, R., et al. (2017). In vitro 3D corneal tissue model with epithelium, stroma, and innervation. *Biomaterials*. 112:1–9.
- Waring, G. O., Bourne, W. M., Edelhauser, H. F. et al. (1982). The corneal endothelium. Normal and pathologic structure and function. *Ophthalmology*. 89(6):531-90.
- West-Mays, J. A., Dwivedi, D. J. (2006). The keratocyte: corneal stromal cell with variable repair phenotypes. *The international journal of biochemistry & cell biology*. 38(10):1625–31.
- Whitcher, J. P., Srinivasan, M., Upadhyay, M. P. (2001). Corneal blindness: A global perspective. *Bulletin of the World Health Organization*. 79(3):214–271.
- Wichterle, O., Lím, D. (1960). Hydrophilic Gels for Biological Use. *Nature*. 185:117–118.
- Williams, S. F., Martin, D. P., Horowitz, D. M. et al. (1999). PHA applications:

Addressing the price performance issue: I. Tissue engineering. *International Journal of Biological Macromolecules*. 25(1-3):111–121.

Wong, K. H., Kam, K. W., Chen, L. J. et al. (2017). Corneal blindness and current major treatment concern-graft scarcity. *International Journal of Ophthalmology*. 10(7):1154–1162.

Wray, L. S., Orwin, E. J. (2009). Recreating the Microenvironment of the Native Cornea for Tissue Engineering Applications. *Tissue Engineering Part A*. 15(7):1463-1472.

Wu, J., Du, Y., Mann, M. M., et al. (2013). Bioengineering organized, multilamellar human corneal stromal tissue by growth factor supplementation on highly aligned synthetic substrates. *Tissue engineering. Part A*. 19(17–18):2063–75.

Xiao, J., Duan, H., Liu, Z., et al. (2011). Construction of the recellularized corneal stroma using porous acellular corneal scaffold. *Biomaterials*. 32(29):6962–6971.

Xu, T., Rodriguez-Devora, J. I., Reyna-Soriano, D., et al. (2014). Chapter 6 - Principles of Bioprinting Technology', (ed. Orlando, Giuseppe; Lerut, Jan; Soker, Shay; Stratta, Robert J.) in *Regenerative Medicine Applications in Organ Transplantation*. 67–79. Academic Press.

Yang, S., Leong, K.-F., Du, Z. et al. (2001). The Design of Scaffolds for Use in Tissue Engineering. Part I. Traditional Factors. *Tissue Engineering*. 7(6):679–689.

Yin, J., Yan, M., Wang, Y., et al. (2018). 3D Bioprinting of Low-Concentration Cell-Laden Gelatin Methacrylate (GelMA) Bioinks with a Two-Step Cross-linking Strategy. *ACS Applied Materials & Interfaces*. 10(8):6849–6857.

Zhang, Y. S., Yue, K., Aleman, J., et al. (2017). 3D Bioprinting for Tissue and Organ Fabrication. *Annals of Biomedical Engineering*. 45(1):148–163.

Zhou, L., Tan, G., Tan, Y., et al. (2014). Biomimetic mineralization of anionic gelatin hydrogels: effect of degree of methacrylation. *RSC Advances*. 4(42):21997.

Zorlutuna, P., Builles, N., Damour, O., et al. (2007). Influence of keratocytes and

retinal pigment epithelial cells on the mechanical properties of polyester-based tissue engineering micropatterned films. *Biomaterials*. 28(24):3489–3496.

Zorlutuna, P., Tezcaner, A., Kiyat, I., et al. (2006). Cornea engineering on polyester carriers. *Journal of Biomedical Materials Research - Part A*. 79(1):104–113.

APPENDIX A

STRESS STRAIN CURVE OF A VISCOELASTIC MATERIAL

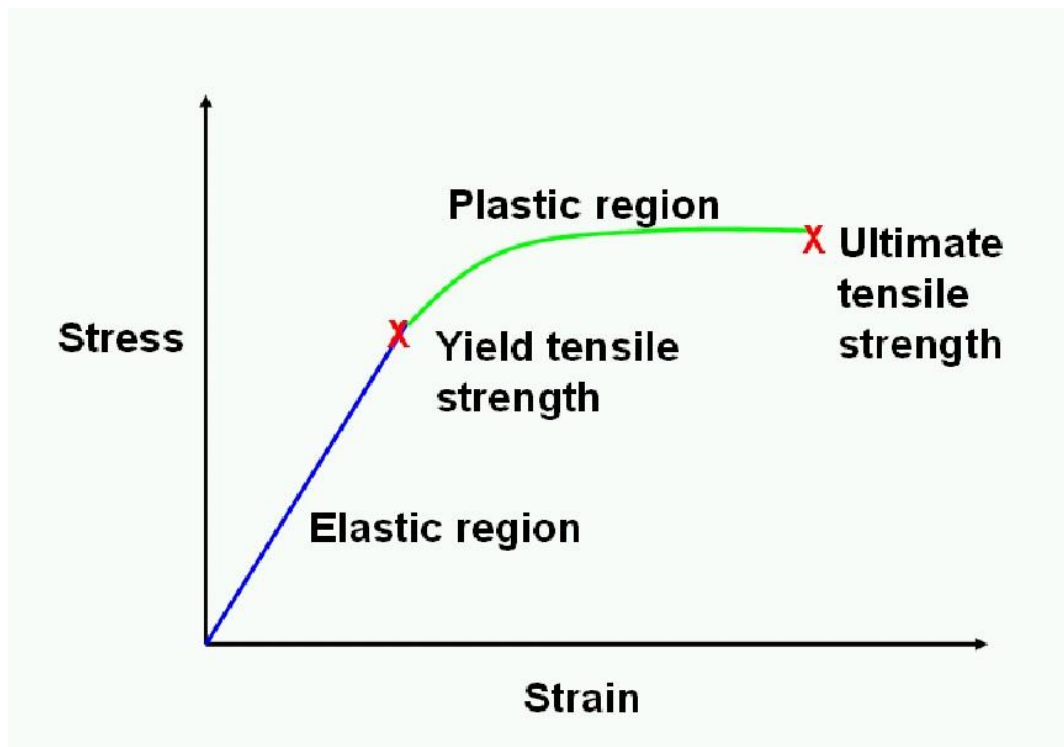


Figure A.1: A typical stress strain curve for viscoelastic materials. Compressive moduli of the scaffolds are calculated from the slope of the very first linear region.

APPENDIX B

ALAMAR BLUE CALIBRATION CURVE

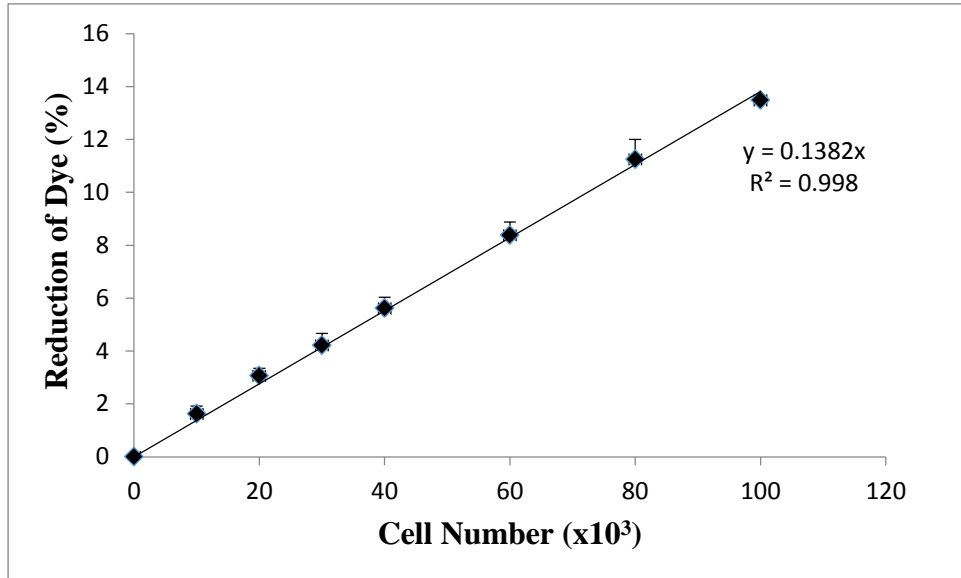


Figure A.2: Alamar Blue Assay calibration curve for human corneal keratocytes

APPENDIX C

5-FAM-Pro-Leu-OH CALIBRATION CURVE

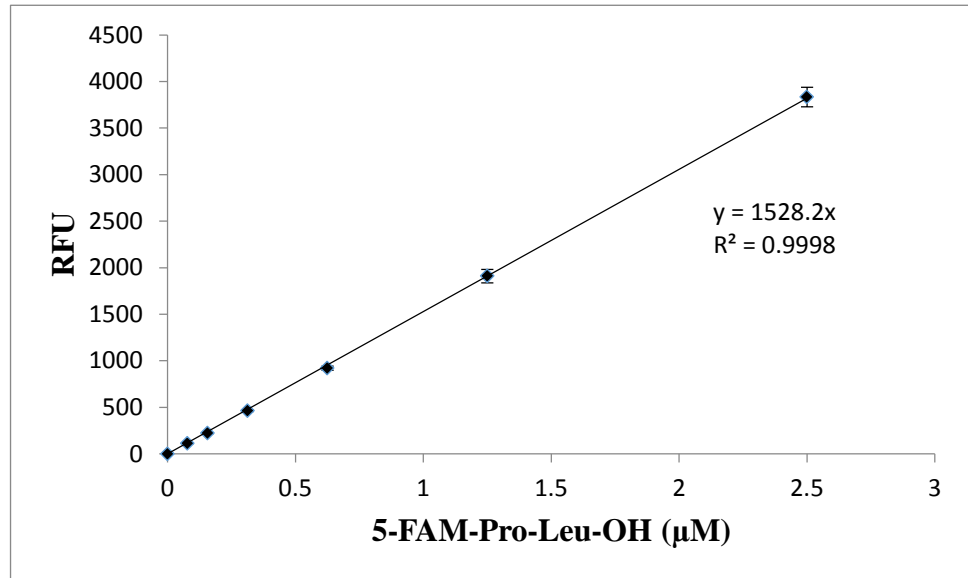


Figure A.3: 5-FAM-Pro-Leu-OH Calibration Curve for MMP Activity

APPENDIX D

COOMASSIE PLUS (BRADFORD) ASSAY CALIBRATION CURVE

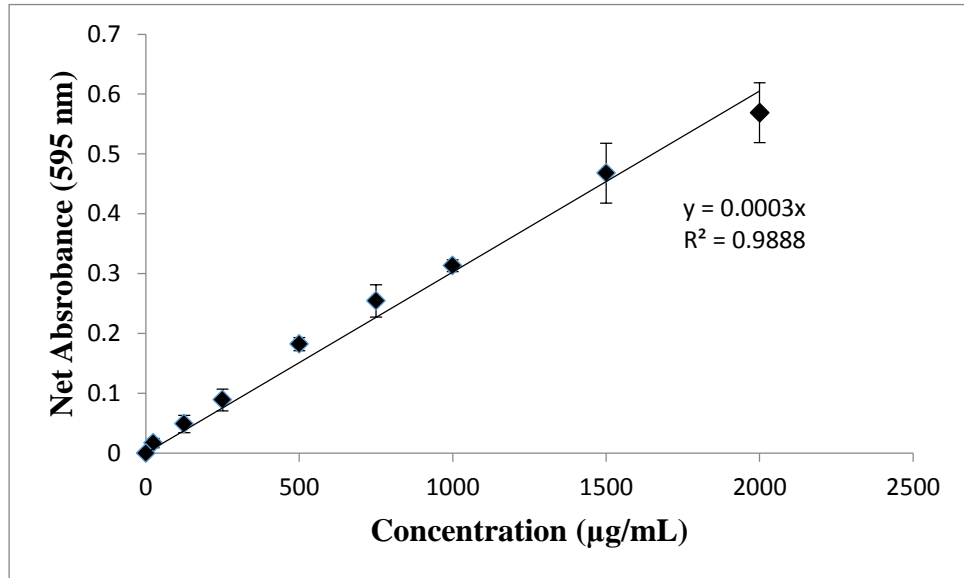


Figure A.4: Coomassie Plus (Bradford) Assay calibration curve for total protein determination.

APPENDIX E

ETHICS COMMITTEE REPORT



T.C.
Sağlık Bakanlığı
Ankara Eğitim ve Araştırma Hastanesi
“Hayvan Deneyleri Yerel Etik Kurulu Karar Defteri”

Toplantı No: 0045

01.03.2018

PROJENİN ADI (Varsa Kodu): Kornea stroma implantı olarak metakrile jelatin (GelMA) hidrojellerinin kullanılması.

SORUMLU ARAŞTIRMACI : Dr.Hande Hüsniye Telek. Araştırma Projesi

T.C.Ankara Eğitim ve Araştırma Hastanesi **Göz Kliniği**

(Arş.Gör.Cemile Bektaş, Dr.Hande Hüsniye Telek, Prof.Dr.Ayşe Burcu, Dr.Firdevs Örnek, Prof.Dr.Gökhan Gedikoğlu, Prof.Dr.Vasıf Hasırcı)

ARAŞTIRMAYI DESTEKLEYEN KURULUŞ(LAR): Onay aldıktan sonra TÜBİTAK

KARAR:

509.Çalışmanın Protokol, usul, yaklaşım ve yöntem yönünden “**ETİK**” değerlendirmesinde “**UYGUN**” “**OLDUĞUNA**”/“**OLMADIĞINA**” “**OYBİRLİĞİ**” / “**OYÇOKLUĞU**” ile karar verilmiş ve araştırma için belirlenen tüm hayvan, uygulama, tetkik ve girişimlerin bedellerinin araştırma grubunca karşılanması kaydı ile çalışmanın yapılmasına ve Hastanemiz arşiv bilgi ve belgelerinin ve Hayvan Deneyleri Laboratuvarı'nın kullanılmasına “**İZİN**” “**VERİLMİŞTİR**” / “**VERİLMEMİŞTİR**”.


Prof.Dr.Uğur KOÇER

Doç.Dr.Nezih SUNGUR



Doç.Dr.Kemal KİSMET
(Raportör)

Veteriner Hek. Cengiz YALCIN
(Raportör ve Kurul Seretarı)



Ahmet Zeki GÜLER
(Sivil Toplum Örgütü Üyesi)

Gülcan BAŞEĞMEZ
(Sivil Üye)

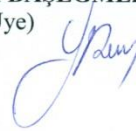


Figure A.5: Ethical permission was granted by Ankara Education and Research Hospital, Animal Experiments Local Ethics Committee.

CURRICULUM VITAE

CEMILE KILIC BEKTAS

Contact Adress METU, Center of Excellence in Biomaterials and Tissue Engineering (BIOMATEN), 06800, Ankara/Turkey

e-mail cemile.kilic@metu.edu.tr

Nationality Turkish

Date of Birth January 28, 1987

Gender Female

Status Married w/ 1 daughter (19 mo)

WORK

2011- Present Teaching Assistant at METU Biological Sciences Dept.

2010-Present Full Time Researcher at METU, Center of Excellence in Biomaterials and Tissue Engineering (BIOMATEN)

EDUCATION

2013- 2018 PhD Studies
Thesis Title: “3D Printed, Cell Carrying GelMA Hydrogels in Corneal Stroma Engineering”
METU Graduate School of Natural and Applied Sciences
Department of Biotechnology
CGPA: 3.93/4.00

2010- 2013

MSc

Thesis Title: “Study of Patterned, Multilayered, Collagen-Based Scaffolds Designed to Serve as a Corneal Stroma”

Middle East Technical University

Graduate School of Natural and Applied Sciences

Department of Biological Sciences

CGPA: 3.79/4.00

2005– 2010

BSc

Middle East Technical University

Faculty of Arts and Sciences

Department of Molecular Biology and Genetics

CGPA: 3.67 / 4.00

WORK EXPERIENCE

August, 2011- September, 2011 (Erasmus Summer Practice Program)

Prof. Dr. Philippe Lavalle and Dr. Nihal Engin Vrana

Strasbourg University, France

In vitro and in vivo studies of the trachea tissue engineering

June, 2011- August, 2011 (Erasmus Summer Practice Program)

Prof. Dr. J. Carlos Cabello

University of Valladolid, Spain

Production and purification of Elastin Like Recombinamers (YIGSR) to be used in corneal tissue engineering

February, 2010- June, 2010

Prof. Dr. Vasif Hasirci

METU Biotechnology Research Unit, Turkey

Special project to develop biodegradable biomaterials for corneal tissue engineering

January, 2010-February, 2010

Prof. Dr. Emin Erdal

Mersin University, Turkey

Polymorphism (RFLP) and routine molecular biology studies

July, 2009-August, 2009

Prof. Beard's Lab

Ecole Polytechnique Fédérale de Lausanne (EPFL), Switzerland

Possible interactions between viral proteins and sub-nuclear structures

March- June,2008

Prof. Dr. Vasif Hasirci

METU, Turkey

Drug Delivery With Small Vesicles (liposomes)

ACADEMIC INTERESTS

- Tissue Engineering and Regenerative Medicine
- Hydrogels and 3D Bioprinting
- Micro-chips, Microfluidics

PUBLICATIONS

1. **C. Kilic Bektas**, Tugba Dursun Usal, Nesrin Hasirci, Vasif Hasirci. Engineered Hydrogels, in Biological Soft Matter Textbook, John Wiley & Sons Publishing, 2018 (Submitted)
2. Tugba Dursun Usal, **C. Kilic Bektas**, Nesrin Hasirci, Vasif Hasirci. Engineered Biopolymers, in Biological Soft Matter Textbook, John Wiley & Sons Publishing, 2018 (Submitted)
3. **C. Kilic Bektas**, Ilgin Kimiz, Aylin Sendemir-Urkmez, Vasif Hasirci, Nesrin Hasirci. A Bilayer Scaffold Prepared from Collagen and Carboxymethyl Cellulose for Skin Tissue Engineering Applications. Journal of Biomaterials Science, Polymer Edition, 2018, doi: 10.1080/09205063.2018.1498718

4. **C. Kilic Bektas**, V. Hasirci. Mimicking Corneal Stroma Using Keratocyte Loaded Photopolymerizable Methacrylated Gelatin Hydrogels. *Journal of Tissue Engineering and Regenerative Medicine*, 2018, 12(4):e1899-e1910. doi: 10.1002/term.2621.
5. N. Hasirci, **C. Kilic**, A. Komez, G. Bahcecioglu, V. Hasirci. Hydrogels in Regenerative Medicine, in Gels Handbook Fundamentals, Properties and Applications. U. Demirci, A. Khademhosseini (ed), World Scientific Publishing, Singapore, 2016.
6. **C. Kilic**, A. Girotti, J. Rodriguez-Cabello, V. Hasirci. A collagen-based corneal stroma substitute with micro-designed architecture. *Biomaterials Science*, 2014, 2(3), 318-329. doi:10.1039/C3BM60194C

PUBLICATIONS (In Preparation)

1. An in vivo study of GelMA Hydrogels as a Corneal Stroma Substitute: Case Report. **Cemile Kilic Bektas**, Ayse Burcu, Gokhan Gedikoglu, Hande Husniye Telek, Firdevs Ornek, Vasif Hasirci.
2. 3D Printed Cell-laden GelMA Hydrogels in Corneal Stroma Engineering. **Cemile Kilic Bektas** and Vasif Hasirci.
3. Cell Loaded GelMA-HEMA Hydrogels for Corneal Stroma Engineering. **Cemile Kilic Bektas** and Vasif Hasirci.

CONFERENCE PRESENTATIONS

1. **C. Kilic Bektas** and V. Hasirci. 3D Printed, Cell Carrying GelMA Hydrogels in Corneal Stroma Engineering. 23th National Biomedical Science and Technology Symposium (BIOMED2018-TR), pg. 97, 15-16 December, İstanbul- Turkey (Poster Presentation).
2. **C. Kilic Bektas**, Ayse Burcu, Gokhan Gedikoglu, Hande Karaguzel, Firdevs Ornek, Vasif Hasirci. Methacrylated Gelatin Hydrogels as Corneal Stroma Substitutes: An In Vivo Study. 2nd International Biomedical Engineering Congress (IBMEC'2018), pg. 99, 24-27 May, 2018, Lefkosa-Cyprus (Oral Presentation).

3. **C. Kilic Bektas** and V. Hasirci. Human Corneal Keratocytes Loaded Methacrylated Gelatin Hydrogels as a Model Corneal Stroma. 28th European Conference on Biomaterials (ESB2017), pg. 409, 4-8 September, 2017, Athens-Greece (Rapid Fire Presentation).
4. **C. Kilic Bektas** and V. Hasirci. GelMA-HEMA IPN Hydrogels for Corneal Stroma Engineering. 22nd International Biomedical Science and Technology Symposium, P-028, 12-14 May, 2017, Ankara-Turkey. (Poster Presentation- Presented by V. Hasirci)
5. **C. Kilic Bektas** and V. Hasirci. Cell incorporated methacrylated gelatin (GelMA) hydrogels for corneal stroma tissue engineering. 10th World Biomaterials Congress, 17-22 May, 2016, Montreal-Canada. *Front. Bioeng. Biotechnol. Conference Abstract*: doi: 10.3389/conf.FBIOE.2016.01.02297 (Poster Presentation)
6. Kimiz, B. Zeybek, **C. Kilic Bektas**, V. Hasirci, N. Hasirci and A. Sendemir Urkmez. Collagen/Chondroitin Sulfate and Carboxymethyl Cellulose Bilayered Scaffolds for Skin Tissue Engineering Applications. 7th Bioengineering Congress (BEC2015), 19-21 November, 2015, İzmir- Turkey (Poster Presentation- Presented by I. Kimiz).
7. **C. Kilic Bektas**, I. Kimiz, A. Sendemir Urkmez, N. Hasirci, V. Hasirci. NaCMC and Collagen Bilayer Scaffolds for Skin Tissue Engineering. 21st International Biomedical Science and Technology Symposium, pg. 184, 22-24 October, 2015, Antalya- Turkey. (Poster Presentation)
8. **C. Kilic Bektas**, I. Kimiz, A. Sendemir Urkmez, N. Hasirci, V. Hasirci. NaCMC and Collagen Bilayer Scaffolds for Skin Tissue Engineering. East West Asia Biomaterials Symposium (EWAB2015), pg. 17, 21 October 2015, Antalya- Turkey. (Oral Presentation)
9. V. Hasirci, S.Alagoz, T.Dursun, **C. Kilic Bektas**, N. Hasirci. Biopolymers in Tissue Engineering and Regenerative Medicine. 8th European Symposium on Biopolymers (ESBP2015), pg 46, 15-18 September 2015, Rome- Italy. (Invited Oral Presentation- Presented by V. Hasirci).

10. **C. Kilic Bektas**, I. Kimiz, A. Sendemir Urkmez, V. Hasirci, N. Hasirci. Collagen and Carboxymethyl Cellulose Bilayers for Skin Tissue Repair. 27th European Conference on Biomaterials (ESB2015), pg. 161, 30 August-3 September 2015, Krakow- Poland. (Poster Presentation)
11. **C. Kilic Bektas** and V. Hasirci. Patterned Thermoresponsive NIPAM-pHEMA Hydrogels for Corneal Repair. 27th European Conference on Biomaterials (ESB2015), pg. 733, 30 August-3 September 2015, Krakow-Poland. (Oral Presentation)
12. V. Hasirci, N. Hasirci and **C. Kilic**. Biodegradable Polymers in Tissue Engineering. The 2nd International Symposium on Polymer Ecomaterials (PEM 2014), 22- 26 August 2014, Kuming- China (Invited Oral Presentation- Presented by V. Hasirci).
13. **C. Kilic**, V. Hasirci. Characterization of Micropatterned Collagen Films for Corneal Stroma Engineering. 19th International Biomedical Science and Technology Symposium (BIOMED), pg. 48, 12-15 November 2013, Kusadası- Turkey. (Oral Presentation)
14. B. Zeybek, **C. Kilic**, A. Sendemir-Urkmez, N. Hasirci, and V. Hasirci. Three Dimensional Cross-linked Collagen Skin Equivalent Model. 19th International Biomedical Science and Technology Symposium (BIOMED), pg. 77, 12-15 November 2013, Kusadası- Turkey. (Poster Presentation- Presented by B. Zeybek)
15. **C. Kilic**, J. Carlos Rodriguez Cabello, and V. Hasirci. Multilayer Col and Col:ELR Constructs for Corneal Stroma Equivalent. The European Society for Biomaterials (ESB), 8-12 September 2013, Madrid- Spain. (Oral Presentation)
16. **C. Kilic**, V. Hasirci. A Multilayer Collagen Scaffold for Corneal Stroma Tissue Engineering. The European Chapter Meeting of the Tissue Engineering and Regenerative Medicine International Society (TERMIS-EU 2013), pg. 312, 17-20 June 2013, İstanbul- Turkey. (Oral- Poster Presentation)